UNIVERSITY OF CALIFORNIA SAN DIEGO

Emergent patterns of bronchoconstriction: What can the healthy lung teach us about asthma?

A dissertation submitted in partial satisfaction of the requirements for the degree Doctor of Philosophy

in

Biomedical Sciences

by

Eric Geier

Committee in charge:

Professor G. Kim Prisk, Chair
Professor Frank Powell, Co-Chair
Professor Rick Buxton
Professor Hemal Patel
Professor Tony Yaksh

2018

This dissertation of Eric Geier is approved, and it is acceptable in quality and form for publication on microfilm and electronically:

Co-Chair

Chair

University of California San Diego

2018

DEDICATION

For everyone who takes the next exit instead of barging in.

EPIGRAPH

All you can do is hope for a pattern to emerge, and sometimes it never does.
Still, with a plan, you only get the best you can imagine.
I'd always hoped for something better than that.

-Chuck Palahniuk, Lullaby

TABLE OF CONTENTS

LIST OF ABBREVIATIONS

BTP – Bronchial Thermoplasty

COM – Center of Mass

CT – Computed Tomography

FEV_1 – Forced expiratory volume in 1 second

FiO_2 – Fraction of inspired oxygen

FRC – Functional Residual Capacity

FWHM – Full-width at half maximum

MBW – Multiple Breath Washout

MIGET – Multiple Inert Gas Elimination Technique

MR – Magnetic Resonance

MRI – Magnetic Resonance Imaging

PET – Positron Emission Tomography

SPECT – Single-photon emission computed tomography

SV – Specific Ventilation

SVI – Specific Ventilation Imaging

LIST OF FIGURES

LIST OF TABLES

ACKNOWLEDGEMENTS

I was lucky to have Dr. G. Kim Prisk and Dr. Rui Carlos Sá as research mentors for the last four and a half years. Fully describing their impact feels too daunting, so I'll leave it with this: Kim taught me how to say what I mean, and Rui taught me how to question what I say.

The pulmonary imaging laboratory includes some of the kindest and smartest people I've met. People so experienced aren't usually so generous with their time. I should have been the one buying coffee.

The following figures have been reproduced with permission: 1-1, 1-2, 1-3, 1-4.

Chapter 2, in full, is a reprint of Geier ET, Neuhart I, Theilmann RJ, Prisk GK, Sá RC.. Journal of Applied Physiology 2018, volume 124, pages 1222-1232. The dissertation author was the primary investigator and author of this paper.

Chapter 3, in full, is a reprint of Geier ET, Kubo K, Theilmann RJ, Prisk GK, Sá RC. This article was published online by the Journal of Applied Physiology on Sept. 6 2018, ahead of print. The dissertation author was the primary investigator and author of this paper.

Chapter 4, in full, was submitted for publication in the Journal of Applied Physiology on October 15, 2018, by Geier ET, Theilmann RJ, Prisk GK, Sá RC. It is presented as it may appear online. The dissertation author was the primary investigator and author of this paper.

Appendix A, in full, is part of a future submission to the Journal of Visualized Experiments, by Geier ET, Theilmann RJ, Darquenne C, Prisk GK, Sa SC. The dissertation author was the first author of this paper.

Appendix B, in full, is a reprint of Cook FR, Geier ET, Asadi AK, Sá RC, Prisk GK. The article was published by 3D Printing and Additive Manufacturing, Volume 2, 2015. The dissertation author was the second author of this paper.

VITA

2011 Bachelor of Science, Indiana University, Bloomington

2018 Doctor of Philosophy, University of California San Diego

PUBLICATIONS

Geier E.T, Kubo, K. Theilmann, R., Prisk, G.K., Sá, R.C. The spatial pattern of methacholine bronchoconstriction recurs when supine, independently of posture during provocation, but does not recur between postures. *Journal of Applied Physiology.* Article in Press. Published online 6 September 2018

Geier E.T, Neuhart, I., Theilmann, R., Prisk, G.K., Sá, R.C. Spatial persistence of reduced specific ventilation following methacholine challenge in the healthy human lung. *Journal of Applied Physiology.* 2018, 124(5): 1222-1232

Kang, W., Tawhai, M.H., Clark, A.R., Sá, R.C, Geier, E.T., Prisk, G.K., Burrowes, K.S. *In silico* modeling of oxygen-enhanced MRI of specific ventilation. *Physiological Reports*, 2018, 6(7): e13659

Cook F, Geier E.T., Asadi, A., Sá R.C, Prisk, G.K. Rapid prototyping of inspired gas delivery system for pulmonary MRI research. *3D Printing and Additive Manufacturing* 2(4): 197-203

Zapol, W.M., Cecil, C.H., Martin, A.R., Sá R.C., Yu, B., Ichinose, F., MacIntryre, N., Mammarappallil, J., Moon, R., Chen, J.Z., Geier, E.T., Darquenne, C., Prisk, G.K., Katz, I. Pulmonary Delivery of Therapeutic and Diagnostic Gases. *Journal of Aerosol Medicine and Pulmonary Drug Delivery.* 2018, 31(2): 78-87

Geier, E.T., Kubo, K., Neuhart, I., Theilmann, R.J., Prisk, G.K., Sá, R.C. Methacholine bronchoconstriction is spatially persistent and independent of posture during drug inhalation. Invited talk, International Society for Aerosols in Medicine 2018 Symposium. May 2018

Geier, E.T., Neuhart, I., Theilmann, R.J., Prisk, G.K. Sá, R.C. Healthy Lung Units Which Constrict During One Methacholine Challenge are More Likely To Do So Again in the Next. Poster presentation. American Thoracic Society 2018 Conference

Geier, E.T., Sá, R.C., Cook, F.R., Bird, E.M., Prisk, G.K. Proton MRI suggests that the spatial pattern of methacholine bronchoconstriction may be non-random. Oral presentation. International Workshop on Pulmonary Imaging 2017

ABSTRACT OF THE DISSERTATION

Emergent patterns of bronchoconstriction: What can the healthy lung teach us about asthma?

by

Eric Geier

Doctor of Philosophy in Biomedical Sciences

University of California San Diego 2018

Professor G. Kim Prisk, Chair
Professor Frank Powell, Co-Chair

Asthma is defined by its intermittence. Periods of normal function are interrupted by intermittent bouts of airflow obstruction, and the severity and frequency of these bouts define the severity of the disease. Asthma also varies in space just as it does in time. Patches of the lung become compromised during an asthma attack, while the rest of the lung continues to function normally. This dissertation explores the intersection of these two modes of variation – what causes bronchoconstriction to occur in patches, and will it cause the same patches to emerge time after time?

A seminal modeling study predicted that lung units under smooth muscle stress exhibit a type of emergent behavior; self-organized patches of constriction can arise from the small airways because of the interdependence of airflow through the airway tree. In a sense, airways "communicate" with each other through flow patterns in a way that allows large-scale patterns to emerge.

One goal of this dissertation work was to empirically verify the findings of this model. We chose to perform studies in healthy normal subjects to ensure that the patterns of constriction we observed were due to interdependence and not to underlying inflammation or remodeling. The results of our first study (Chapter 2) found that bronchoconstriction – provoked with methacholine – in healthy subjects did indeed occur in a spatially patchy pattern.

Further, we found that this patchy pattern was recurrent in challenges weeks to months apart. We showed that, although subjects each had a characteristic pattern of constriction, there was an overall tendency for the dependent lung to constrict when supine. Our second study (Chapter 3) showed that this was due to the interaction between gravitational compression of tissue and the underlying topography of the airway tree structure.

Our final study (Chapter 4) showed that healthy subjects did not recover from constriction immediately after albuterol inhalation, even though traditional metrics of lung function indicated that they had. We interpreted this as evidence for the power and utility of functional imaging in detecting and characterizing pathologic function.

CHAPTER ONE

Introduction

The oldest historical record of asthma is the most dramatic.

Hector, the greatest defender of Troy, fled from the Achaens. He was not having a great day. His javelin, infamous in its own right after ten years of war, had just been swatted out of the air by the man-giant Ajax.

Hector's day did not get better from there. His colossal enemy found a ballast stone, and made a (probably quite lucky) throw. Hector was sent spinning to the ground by the force of the stone, and Homer describes Hector lying on the ground, "gripped by difficult asthma, vomiting up blood" (56).

Granted, Homer's meaning was different from our current understanding of asthma - it's more likely that he used the greek term 'azein' to refer to panting or wheezing (41). But by the time of Hippocrates (460-360 BC), azein was already being used in a more familiar context. Hippocrates and his contemporaries recognized asthma as a clinical syndrome that was prevalent in areas exposed to warm winds, especially in the summer and fall (41, 56).

Millenia later, we still think about asthma; the reasons for which it emerges, the ways in which it affects us, and the ways in which we can best alleviate its symptoms. In the last year for which we have data, asthma afflicted 8% of Americans, caused more than 400,000 hospital admissions, and killed more than 3,500 people (73).

The focus of this dissertation is on asthma's most trademark characteristic - its variability within a given subject. As the Greeks first recognized, asthma's severity varies with time - patients experience long intervals without symptoms that are punctuated by acute or subacute exacerbations, which can be mild or severe. But it also varies in space - some areas of the lung are obstructed during an attack while nearby areas are barely affected. My research focused on how these two forms of variability interact: do the affected areas recur over time?

The answer to this question has the potential to affect how we diagnose, prognosticate, and treat asthma. Areas of spatially recurrent bronchoconstriction could be targets for localized therapy with bronchial thermoplasty, and their presence and size could be a biomarker for disease severity or treatment response. As several high-cost monoclonal antibodies become approved to treat refractory cases of asthma (42), these types of biomarkers may become crucial for patient selection and measurement of efficacy in order to maintain an appropriate cost-benefit ratio for treatment.

Asthma etiology, in brief

Asthma attacks can be triggered by cold, exercise, allergens, stress, a warm breeze coming off the Aegean in the summer, or nothing at all. For one patient, an attack may a nuisance; for another, a life-threatening emergency.

The common thread amongst all patients is wheezing and shortness of breath that comes and goes. This wheezing is due to a decrease in the caliber of the patient's airways that causes increased airflow resistance.

This decrease in caliber can be broadly attributed to three causes, which each may exist to varying degrees in any given patient: 1) Infiltration of cells or mucus into the airspace, 2)

Contraction of airway smooth muscle to decrease the airway radius, and 3) Changes to the airway wall thickness.

****

Asthma, due to its intermittent nature, was originally considered an entirely reversible disorder that was due to intrinsic abnormalities in airway smooth muscle (11). However, the realization that steroids (an anti-inflammatory medication) provided a benefit for asthmatics, and the discovery of eosinophils in post-mortem asthmatic lungs made it clear that inflammation must also play a role (11). This was reaffirmed by bronchial biopsies that showed inflammatory changes in both the central and the peripheral airways of the asthmatic lung (19, 29). Now, asthma is thought to be an inflammatory syndrome at its core (44).

The reason that this syndrome arises in some people but not others is becoming more evident. There is a genetic component; asthma is strongly associated with atopy (8, 46, 48). Environmental exposure to viruses and allergens have also been shown to play a role in the emergence of disease (20, 61, 71).

Two hallmark characteristics of inflammation – edema and mucus hypersecretion (37) – can directly lead to airflow obstruction by their products taking up space within the airway lumen. But the majority of disease burden comes from a byproduct of pulmonary inflammation – that it causes airway smooth muscle to become hyperreactive to stimuli (16, 44, 72). Julian Solway, a professor of pulmonary medicine at the University of Chicago, once said that "if airway inflammation didn't cause bronchospasm, asthma might be a tolerable disease" (58).

The mechanism by which inflammation leads to smooth muscle hyperreactivity is unclear. Originally, it was thought that the increase in smooth muscle bulk associated with asthma might be the cause of bronchial hyperreactivity (24). But when hypersensitive airways

were removed from the lung, they were found to lose their hypersensitivity *in vitro* (4), and even in some cases become *hypo*sensitive (14, 70). Therefore, smooth muscle hypersensitivity is caused by the microenvironment of the smooth muscle *in vivo*. The specific contributors to this microenvironment are a matter of active investigation; immune cells (57), inflammatory cytokines (49), changes in airway elastance (5, 6), or structural changes in neighboring, non-muscle tissue (39, 40) may each play a role.

The fact that airway smooth muscle exists at all is a bit of a mystery. Wayne Mitzner called it "the appendix of the lung" for its apparent lack of physiological purpose (43). At least 10 functions for airway smooth muscle have been proposed, but Mitzner, for one, is not convinced by the evidence for any (43). His opinion is that the null hypothesis is the most apt: airway smooth muscle is a vestigial structure that exists due to the lung's shared origin with the foregut (58).

Like the appendix, the only manifestation of airway smooth muscle is malfunction. Smooth muscle constriction is always undesirable. For this reason, scientific studies thus far have been focused on understanding why constriction turns on, and, if possible, understanding how to turn it off (58).

Disease progression

The two causes of airflow obstruction that have already been discussed - inflammation and smooth muscle contraction - are both reversible with pharmacotherapy, so they both fit into a model of asthma as a fully reversible disease process. This reversible model, however, was contradicted by evidence from the Copenhagen Heart Study. In this longitudinal study of 17,506 people over 15 years, it was demonstrated that the respiratory function of the 1,095 asthmatics

deteriorated more rapidly than it did in the rest of the cohort (33). This meant that asthma must lead to permanent damage that accumulates over time.

This damage comes in the form of airway wall thickening and can be understood in terms of repeated injury and healing (11). Just as the skin is altered by repeated wounds, so is the airway changed by repeated bouts of inflammation. All components of the airway are thickened, by 10-100% in non-fatal asthma and 50-300% in fatal asthma (11).

Permanent increases in thickness occur in both the smooth muscle and the connective tissue (11, 65, 66). Hypertrophy (increase in muscle size) and hyperplasia (increase in muscle cell count) of smooth muscle have been shown to occur in patients with asthma, though hyperplasia was only observed in the fatal cases (25). The connective tissue layer is thickened by deposition of proteoglycans and collagen types I, III, and V (50).

As the changes wrought by airway remodeling are structural, they are not reversible with anti-inflammatory or bronchodilator treatment, though adequate control with these drugs may slow the remodeling process. The Copenhagen Heart Study provided evidence that this type of damage accumulates over time, so its presence or absence may be an indicator of disease severity or progression.

The spatial and temporal heterogeneity of asthma

It has been well documented by necropsy (9) and various imaging modalities - PET (23, 67), CT (3, 15), SPECT (26), MRI (62, 63) - that asthma does not affect all regions of the lung equally. Relatively large patches of the lung have drastically reduced ventilation while the rest of the lung continues to ventilate normally (67). This spatially patchy pattern of constriction was originally considered to be evidence that asthmatic constriction occurs primarily in large,

conducting airways (28, 55). This deduction, however, was at odds with other studies, which showed that asthma has a more profound effect in the peripheral airways than in the central airways (3, 21, 22, 38).

If asthma primarily effects small airways, why do some airways become partially or completely obstructed during an attack while others continue to ventilate as if nothing had happened? And why are the affected airways arranged together in clusters?

****

Anafi and Wilson addressed the first question (why do some airway close while other stay open?) by constructing a model of a single terminal airway under stress from activated smooth muscle (1).

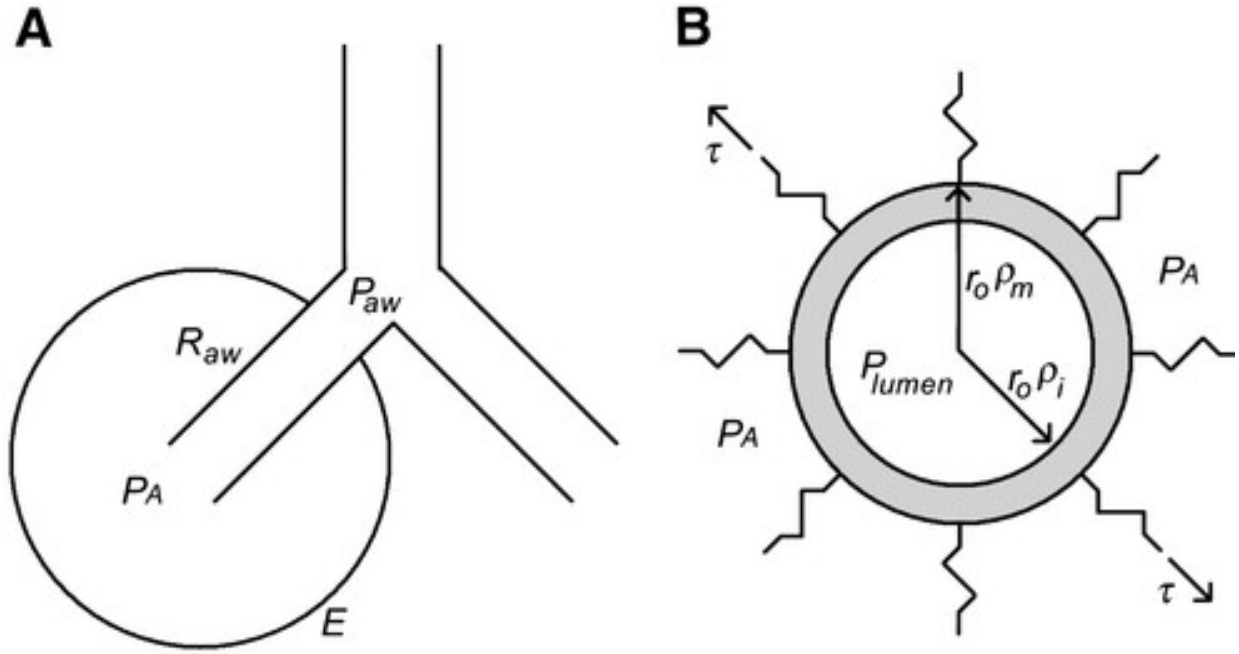

Figure 1-1 Depiction of an airway, as modeled by Anafi and Wilson in (1). **A.** Flow is driven by a difference in pressure between the airway opening (P_{aw}) and the alveolus (P_A). The airway has resistance R_{aw} and the alveolus has elastance E. **B.** Inner and outer radii of the airway are expressed as a factor of baseline airway radius (r_o). P_{lumen} acts on the inner surface of the airway to keep it open. The pressure in the alveolus (P_A) and the tethering force (τ) together act on the outside of the airway. Reproduced with permission from the *Journal of Applied Physiology.*

In the Anafi-Wilson model (Figure 1-1) the airway is assumed to be completely immersed in the parenchyma it supplies. This assumption allowed Anafi and Wilson to model all forces acting on the airway to be from one of two sources, the airway or the tissue with which it communicates. The two communicating compartments have pressures that vary in time sinusoidally - with a phase lag between them - due to respiration. The magnitudes of the two pressures are related by the physical properties of the airway - the length, elastance, and inner radius.

The length and elastance of an airway, in this model, are assumed to remain constant, but the inner radius varies based on the balance of forces applied to it. These forces are:

1) The transmural pressure - the difference between the pressure inside (P_{lumen}) and outside (P_A) of the airway.

2) The tethering forces of the surrounding airway parenchyma (τ) that act to keep the airway open.

3) Hoop stress due to constriction of the smooth muscle, which acts to close the airway.

Anafi and Wilson used the Lai-Fook equation (30) to express the tethering force in terms of the pressure outside of the airway (P_A), which simplified the system of equations by one factor (1). To model the hoop stress applied by the activated smooth muscle, they used previous experimental results (12, 17, 59) which showed that the tension of the smooth muscle is related to the length of the fibers (which, in a circular smooth muscle, is related to the radius of the airway).

This allowed Anafi and Wilson to express both peak transmural pressure and hoop stress as a function of airway radius (Figure 1-2). For the radius of an airway to be stable, these two forces must be equal. If they are not equal, the radius of the airway would shrink due to excess

force generated by hoop stress or expand due to excess force generated transmural pressure. Thus, the intersections in Figure 1-2 between the light and dark lines represent the stable airway radii for each peak airway pressure.

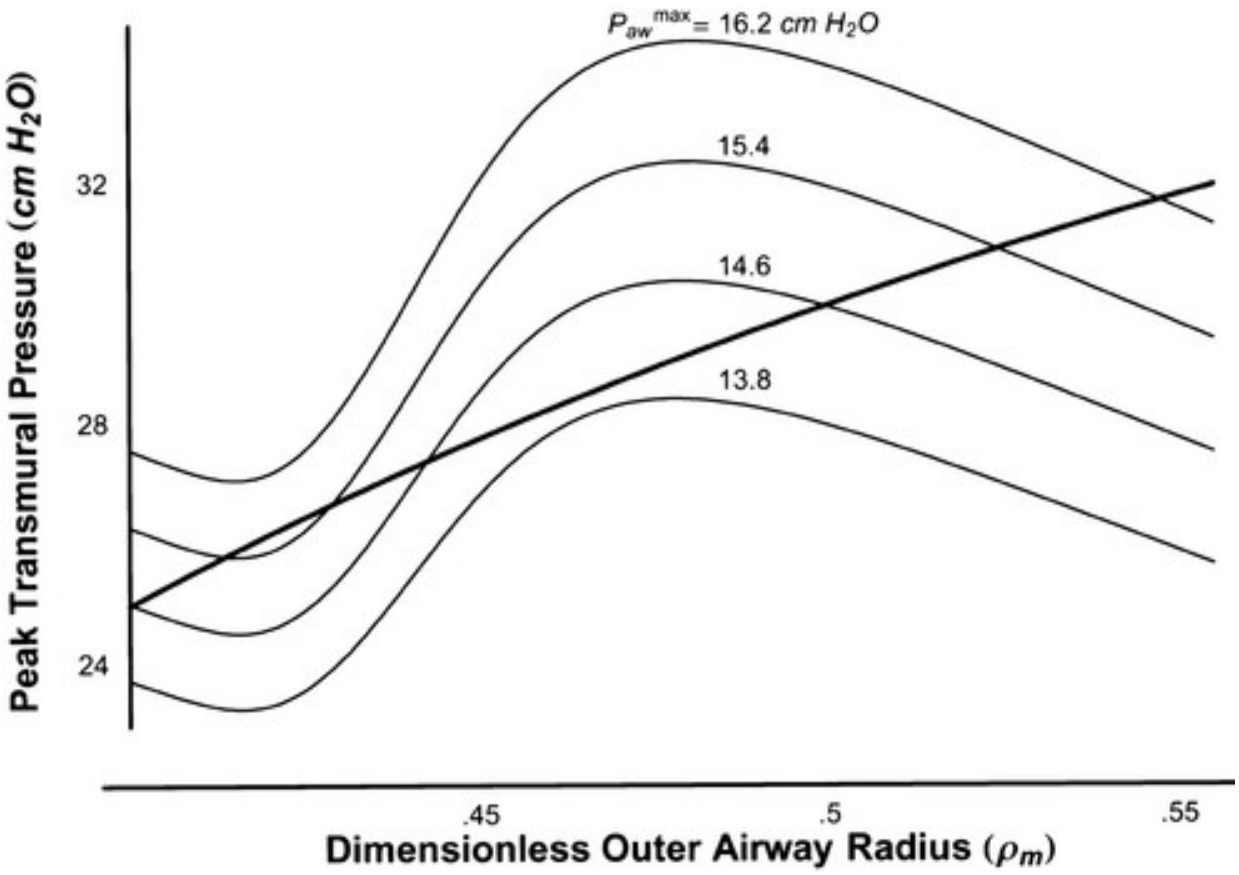

Figure 1-2: Modeling results from (1) show the transmural pressure as a function of airway radius (semi-sinusoidal, light lines) for four different maximum peak airway entrance pressures (P_{aw}^{max}). The dark, roughly linear relationship shows the hoop stress exerted by smooth muscle as a function of airway radius. The intersections between dark and light lines represent stable radii for airways with each peak entrance pressure. Reproduced with permission from the *Journal of Applied Physiology*.

The novel finding of this study was that many airways have more than one possible steady-state radius. This is displayed in Figure 1-2 in which some of the light, semi-sinusoidal lines have 2-3 intersections with the dark line. Anafi and Wilson hypothesized that this multi-steady-state characteristic of terminal airways is what causes a spatially heterogeneous pattern of

airflow limitation. At a given peak airway pressure, some airways find their low-radius steady-state and some find their high-radius steady-state.

Furthermore, this result implied that more terminal airways would "pop open" to their high-radius steady state if peak airway pressure was increased. Thus, they predicted that deep inspirations (which require a higher peak airway pressure) should cause airways to pop open and airflow limitation to be ameliorated. Subsequent experimental studies have confirmed this predicted bronchodilatory effect of deep inspirations (60, 69).

****

The Anafi-Wilson model, however, is a picture of only a single airway. While it explained the observed bimodal distribution of airway responses to stress – some closed airways and some open airways – it did not explain why the closed airways are found clustered together in the lung.

Jose Venegas and Tilo Winkler proposed a solution to this question, though, four years later in a letter to *Nature* (67). The letter presented both experimental evidence of patchy bronchoconstriction, imaged with PET, and an explanation for this patchiness that came from of a model of a 12-generation airway tree, built from 4,096 Anafi-Wilson terminal units (67).

The radii of the airways in the modeled tree were representative of the 4^{th} through 16^{th} generations of airways in a human lung. Each generation of airways came from a nearly symmetric bifurcation of the airways in the previous generation, but very small asymmetries in airway wall thickness (1% coefficient of variation) were introduced to break the computational symmetry of the system. The results were conspicuous. Above a certain level of smooth muscle activation, a highly patchy pattern of bronchoconstriction emerged.

This patchy pattern emerged because of "propagation of constriction up and down the tree as a result of airway-tissue interactions that magnify small regional heterogeneities in the tree and contribute to break the symmetry of the system" (67). For example, if a slightly higher than average number of terminal bronchioles in a small region fed by a common conducting airway find their Anafi-Wilson constricted state, the common conducting airway that feeds them will have reduced flow. The reduced flow in that common branch will result in less tissue expansion during respiration. The absence of periodic stretch in an airway promotes constriction (13, 18, 27) so that common branch will now constrict more than its neighbors within its own generation. Viciously, this effect then will feed back in the distal direction. The relative constriction of the common branch will result in even more reduced flow to the distal terminal bronchioles (the ones that caused the problem in the first place). By the same principles, the reduced stretch in these bronchioles will cause them to constrict even further. This positive feedback loop provides a mechanism by which small inhomogeneities can be quickly amplified to create large-scale spatial heterogeneity.

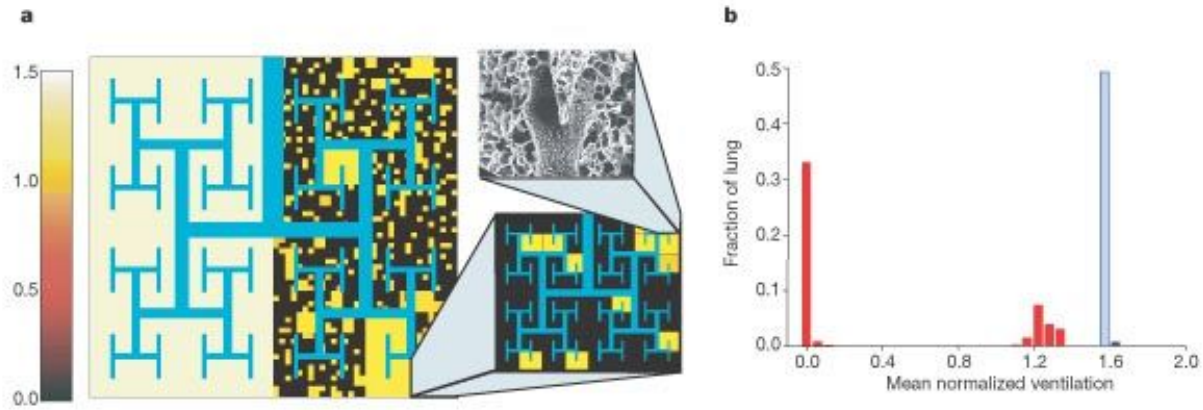

Figure 1-3: Modeling results from (67). **a.** Depicts the symmetrically bifurcating "Mandelbrot-like" airway tree, with mean normalized ventilation indicated by a color scale. **b.** A histogram of mean normalized ventilation shows a dramatically bimodal distribution. Within patches of bronchoconstriction, mean normalized ventilation is either 0 or essentially normal. Outside of patches of bronchoconstriction, mean normalized ventilation is increased. Reproduced with Permission from *Nature*.

Thus, Venegas and Winkler showed that smooth muscle action in the terminal bronchioles can result in self-organized patches of bronchoconstriction. But the model lead to as many questions as it answered. Venegas and Winkler's model was a chaotic system; its ventilatory fate could be drastically altered by minor changes in its initial conditions. But their system was built upon a nearly (with only 1% coefficient of variation) symmetric version of the lung. How relevant are these minor fluctuations in initial conditions in the setting of an actual human lung, which we know is far from symmetric?

****

Answering this question required a volumetric rendering of the lung upon which to project the functional model. Meryn Tawhai and her associates at the University of Auckland had accomplished that in order to answer questions about how the lung deforms under gravity (64). The lung model she and her associates created was based on high-resolution CT images from the Human Lung Atlas - an ongoing project led by Eric Hoffman at the University of Iowa.

With this anatomically realistic model in hand, Del Leary and colleagues were able to build an Anafi-Wilson based functional model of an airway tree in which the lengths and radii of the airways were based on CT images of actual human subjects. They found that, in contrast to the symmetric model in which bronchoconstriction was spatially chaotic and variable from one episode to the next, bronchoconstriction in the anatomically asymmetric lung was highly deterministic and reproducible from one episode to the next.

This result could have been predicted, given the original findings of Venegas and Winkler (67). Venegas and Winkler showed that the effect of airway interdependence under smooth muscle stress was to amplify inhomogeneities. In their initial study, these inhomogeneities were small (<1% coefficient of variation) and random, which means that when

amplified they resulted in a spatially random distribution of bronchoconstriction that varied between events.

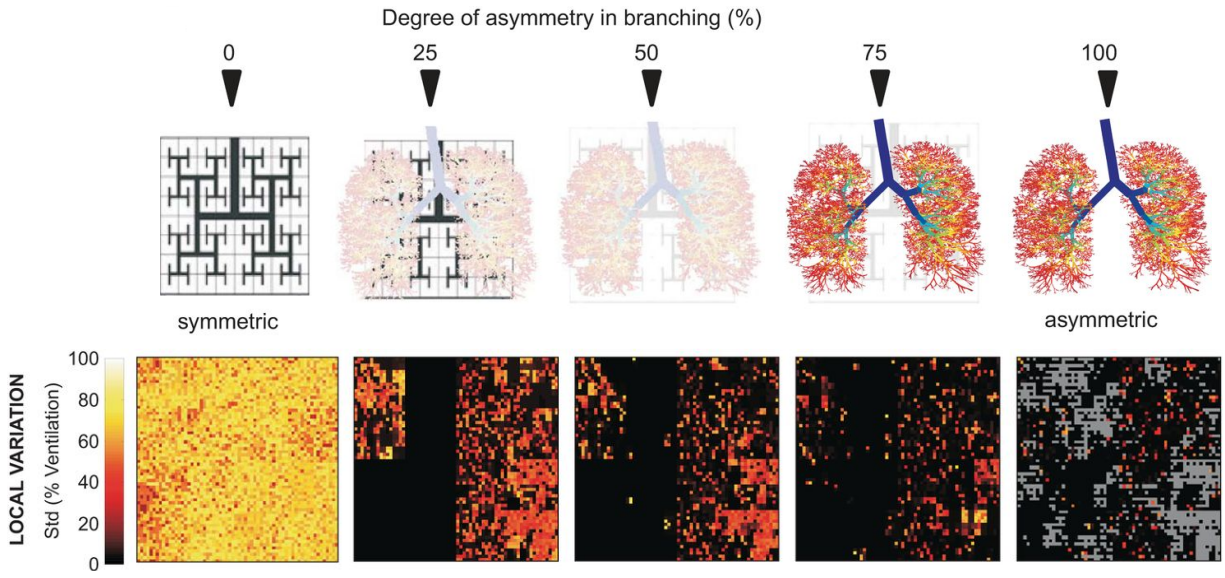

Figure 1-4: Modeling results from (34). As the lung becomes more anatomically asymmetric (top row) the pattern of bronchoconstriction becomes less variable (bottom row) between constriction events. The color scale in the bottom row depicts the % of variation between constriction events in each lung unit. In the anatomically asymmetric case (far right), the average variation is less than 3%.

In the anatomical lung, however, these small (1%), random inhomogeneities were insignificant when superimposed on the much larger, anatomical inhomogeneities in airway radius and length. Thus, the spatial pattern of bronchoconstriction was determined almost entirely by innate airway geometry, and almost not at all by the superimposed perturbations. Since airway geometry does not vary between exacerbations, neither did the pattern of constriction the model predicted.

The lung under smooth muscle duress acts like a guitar amplifier. When the only input is small, random perturbations (when the guitar is unplugged) and smooth muscle action (the volume knob) is increased, the output signal is random. Introducing structural inhomogeneity

into the system is like plugging in the guitar. The random signal is still present, but its influence on the output is barely (if at all) detectable when superimposed on the melody played by the guitar.

Leary's work predicted that, at least to the degree that each individual has their own airway tree structure, each individual should have their own "fingerprint" pattern of bronchoconstriction. And, like a fingerprint, each individual's pattern of bronchoconstriction should be relatively consistent from constriction event to the next.

Granted, the fingerprint analogy may be a bit of a hyperbole. The lung is a more dynamic organ than the skin on our fingers. But multiple imaging studies of asthmatics have confirmed that a subject's spatial pattern of bronchoconstriction is reproducible in repeat studies (31, 32, 45).

The fact that these studies were performed in asthmatics, however, makes it uncertain whether the areas of recurrent bronchoconstriction are due to Anafi-Wilson interdependence (as Leary predicted) or to other factors. It cannot be ruled out that the spatially recurrent ventilation defects reported by De Lange (31, 32) and Niles (45) were actually due to persistent mucus plugging or airway remodeling from chronic inflammation.

This gap in our knowledge was the target of our first experiment. Is the spatial pattern of bronchoconstriction resulting from smooth muscle action *alone* spatially recurrent with time? We chose to study young, non-asthmatic individuals to eliminate the possibility that current or recent inflammation could influence the spatial pattern of bronchoconstriction. To elicit bronchoconstriction in these individuals - who do not have hypersensitive airway smooth muscle – we used methacholine, a cholinergic agonist. The concentrations of methacholine we used

were much higher than the dose that would have been required to elicit bronchoconstriction in asthmatics.

In our first published article, we reported that young, non-asthmatic individuals have a highly spatially recurrent pattern of bronchoconstriction after provocation with methacholine. Although the patterns are subject-specific (as we would predict from Leary's model), they do share common spatial features. We speculate about the cause(s) of these features in the Discussion session.

Our second article was designed to directly investigate the speculations outlined in the first. We re-studied the individuals from the first paper, this time varying their posture during the methacholine and imaging phases of the experiment. We observed how prone vs. supine posture during methacholine administration and imaging changed the resulting spatial pattern of bronchoconstriction. The observed differences between postures allowed us to understand why certain regions of the lung, in all subjects, are more likely than others to constrict.

The third article focused on recovery from methacholine bronchoconstriction. Subjects were given two puffs of albuterol, a short-acting beta agonist that is ubiquitously prescribed as a rescue drug for asthmatics, after their post-methacholine imaging session. We compared their regional ventilatory function after albuterol with their function at baseline and after methacholine. This third paper showed that, even though forced expiratory volume in 1 second (FEV_1) - the most commonly used marker of ventilatory function - returned to normal, a significant portion of the lung was still compromised following albuterol rescue.

Our experimental technique: Specific Ventilation Imaging

Each of the articles in this dissertation relies on a proton MR imaging technique called specific ventilation imaging (SVI). SVI allows us to spatially sample specific ventilation across 80% of the right lung.

SVI exploits the fact that oxygen is paramagnetic and thus decreases the T1 relaxation time of the tissue in which it is dissolved. O_2 has two unpaired electrons, which each have a potent (relative to protons) magnetic field. When oxygen diffuses in solution, these two unpaired electrons create a relatively strong fluctuating magnetic field. T1 relaxation (the time it takes for inverted spins to realign with the magnetic field in the scanner bore) depends on the transfer of energy from molecules that have been excited by an inversion pulse to nearby fluctuating fields. Thus, if more oxygen is present in the nearby lattice, the excited molecules return more quickly to their baseline state, and T1 is reduced.

A decrease in T1, given an appropriately timed pulse sequence, can be translated into an increase in MR signal. Thus, by using appropriate MR scanning parameters, we can read out tissue oxygenation as signal intensity.

This was the basis for the first wave of oxygen-enhanced pulmonary functional imaging. Edelman and colleagues published a *Nature Medicine* paper showing that, when T1 images were acquired breathing room air and, subsequently, 100% oxygen, some areas of the lung got brighter and some areas did not (10) The areas that did not get brighter were called ventilation defects and assumed to be regions of pathological lung function.

Rui Sá and colleagues would later expand oxygen-enhanced pulmonary imaging from a binary classifier (normal or defect) to a quantitative measurement of specific ventilation (52). They did so by realizing that, if a change in intensity indicates the presence of ventilation, then the *rate of that change* must represent the rate of ventilation. Their 2010 paper (52), in which

they measured the vertical gradient of specific ventilation in a cohort of healthy subjects, demonstrated that this was possible.

Since this original application, SVI has been validated (2, 51) and combined with regional perfusion measurements to make spatial maps of the ventilation/perfusion (V/Q) ratio (53). It has also been used to study high-altitude pulmonary edema (47) and to characterize the way in which regional ventilation affects the deposition of coarse aerosol particles (54).

Over time, the specific ventilation imaging protocol has evolved. The series of three articles included in this dissertation represent the first time that SVI maps have been simultaneously acquired in parallel imaging planes. This expansion from imaging one slice to imaging four (~20% to ~80% lung coverage) became necessary in order to study asthma, as it is known to be a spatially heterogeneous disease and therefore a single imaging slice might fail to detect a representative pattern of regional abnormalities.

Several data collection and processing steps have recently been improved to make the protocol more streamlined and robust. One of these improvements was a custom 3D-printed flow-bypass device that allowed for rapid switching between inspired gases while eliminating the need for reservoir bags and rebreathing valves (7). Appendix A is an article recently submitted to the Journal of Visualized Experiments, in which we give a step-by-step description of the updated SVI protocol. Brief descriptions of SVI are also included in each of the three following articles.

Other ways to measure regional ventilation

Specific Ventilation Imaging (SVI) is not the only way to quantify lung function. Two gas elimination techniques - the multiple inert gas elimination technique (MIGET) and the

multiple breath washout (MBW) test - have been since the 1970s to measure the functional heterogeneity of the entire lung (35, 36, 68). However, neither of these techniques allow visualization of ventilation. Regions of abnormal ventilation can be detected but not localized.

More recently, a plethora of imaging-based techniques – PET (23, 67), CT (3, 15), SPECT (26), and MRI (62, 63) – have been developed to allow for functional ventilation mapping across the lung. SVI is the latest example of this type of technique.

References

1. **Anafi RC**, **Wilson TA**. Airway stability and heterogeneity in the constricted lung. American Physiological SocietyBethesda, MD.

2. **Arai TJ**, **Horn FC**, **Sá RC**, **Rao MR**, **Collier GJ**, **Theilmann RJ**, **Prisk GK**, **Wild JM**. Comparison of Quantitative Multiple Breath Specific Ventilation Imaging Using Co-localized 2D Oxygen Enhanced MRI and Hyperpolarized ^{3} He MRI. *J. Appl. Physiol.* (August 30, 2018). doi: 10.1152/japplphysiol.00500.2017.

3. **Beigelman-Aubry C**, **Capderou A**, **Grenier PA**, **Straus C**, **Becquemin MH**, **Similowski T**, **Zelter M**. Mild intermittent asthma: CT assessment of bronchial cross-sectional area and lung attenuation at controlled lung volume. *Radiology* (2002). doi: 10.1148/radiol.2231010779.

4. **Bottino G**, **Carbone R**. Hyperresponsiveness of airway muscle to acetylcholine in asthmatic and non-asthmatic subjects. [Online]. *Eur Rev Med Pharmacol Sci* 4: 33–42, [date unknown]. http://www.ncbi.nlm.nih.gov/pubmed/11409187 [16 Oct. 2018].

5. **Bramley AM**, **Roberts CR**, **Schellenberg RR**. Collagenase increases shortening of human bronchial smooth muscle in vitro. *Am J Respir Crit Care Med* 152: 1513–7, 1995.

6. **Bramley AM**, **Thomson RJ**, **Roberts CR**, **Schellenberg RR**. Hypothesis: excessive bronchoconstriction in asthma is due to decreased airway elastance. [Online]. *Eur Respir J* 7: 337–41, 1994. http://www.ncbi.nlm.nih.gov/pubmed/8162988 [19 Oct. 2018].

7. **Cook FR**, **Geier ET**, **Asadi AK**, **Sá RC**, **Prisk GK**. Rapid prototyping of inspired gas delivery system for pulmonary MRI research. *3D Print Addit Manuf* 2, 2015.

8. **Cookson W**. The alliance of genes and environment in asthma and allergy. *Nature* 402: 5–11, 1999.

9. **Dunnill MS**. The pathology of asthma, with special reference to changes in the bronchial mucosa. *J Clin Pathol* 13: 27–33, 1960.

10. **Edelman RR**, **Hatabu H**, **Tadamura E**, **Li W**, **Prasad P V**. Noninvasive assessment of regional ventilation in the human lung using oxygen-enhanced magnetic resonance imaging. [Online]. *Nat Med* 2: 1236–9, 1996. http://www.ncbi.nlm.nih.gov/pubmed/8898751 [22 Oct. 2018].

11. **Elias JA**, **Zhu Z**, **Chupp G**, **Homer RJ**. Airway remodeling in asthma. *J Clin Invest* 104: 1001–6, 1999.

12. **Fredberg JJ**, **Inouye D**, **Miller B**, **Nathan M**, **Jafari S**, **Raboudi SH**, **Butler JP**, **Shore SA**. Airway smooth muscle, tidal stretches, and dynamically determined contractile states. *Am J Respir Crit Care Med* 156: 1752–9, 1997.

13. **Fredberg JJ**, **Inouye DS**, **Mijailovich SM**, **P. BJ**. Perturbed Equilibrium of Myosin Binding in Airway Smooth Muscle and Its Implications in Bronchospasm. *Am J Respir Crit Care Med* 159: 959–967, 1999.

14. **Goldie R**, **Spina D**, **Henry P**, **Lulich K**, **Paterson J**. In vitro responsiveness of human asthmatic bronchus to carbachol, histamine, beta-adrenoceptor agonists and theophylline. *Br J Clin Pharmacol* 22: 669–676, 1986.

15. **Goldin JG**, **Mcnitt-Gray MF**, **Sorenson SM**, **Johnson TD**, **Dauphinee B**, **Kleerup EC**, **Tashkin DP**, **Aberle DR**, **Medicine N**. Thoracic Imaging Airway Hyperreactivity: Assessment with Helical Thin-Section CT1 [Online]. https://pubs.rsna.org/doi/pdf/10.1148/radiology.208.2.9680554 [11 Apr. 2018].

16. **Grootendorst DC**, **Rabe KF**. Mechanisms of Bronchial Hyperreactivity in Asthma and Chronic Obstructive Pulmonary Disease. *Proc Am Thorac Soc* 1: 77–87, 2004.

17. **Gunst SJ**. Contractile force of canine airway smooth muscle during cyclical length changes. *J Appl Physiol* 55: 759–769, 1983.

18. **Gunst SJ**, **Meiss RA**, **Wu MF**, **Rowe M**. Mechanisms for the mechanical plasticity of tracheal smooth muscle. *Am J Physiol* 268: C1267-76, 1995.

19. **Haley KJ**, **Sunday ME**, **R. WB**, **Kozakewich HP**, **Reilly JJ**, **Mentzner SJ**, **Sugarbaker DJ**, **Doerschuk CM**, **Drazen JM**. Inflammatory Cell Distribution within and along Asthmatic Airways. *Am J Respir Crit Care Med* 158: 565–572, 1998.

20. **Halonen M**, **Stern DA**, **Lohman C**, **Wright AL**, **Brown MA**, **Martinez FD**. Two Subphenotypes of Childhood Asthma That Differ in Maternal and Paternal Influences on Asthma Risk. *Am J Respir Crit Care Med* 160: 564–570, 1999.

21. **Hamid Q**, **Song Y**, **Kotsimbos TC**, **Minshall E**, **Bai TR**, **Hegele RG**, **Hogg JC**. Inflammation of small airways in asthma. *J Allergy Clin Immunol* 100: 44–51, 1997.

22. **Hamid QA**. Peripheral inflammation is more important than central inflammation [Online]. https://core.ac.uk/download/pdf/82673172.pdf [26 Sep. 2018].

23. **Harris RS**, **Winkler T**, **Tgavalekos N**, **Musch G**, **Vidal Melo MF**, **Schroeder T**, **Chang Y**, **Venegas JG**. Regional pulmonary perfusion, inflation, and ventilation defects in bronchoconstricted patients with asthma. *Am J Respir Crit Care Med* 174: 245–253, 2006.

24. **Huber HL**, **Koessler KK**. The Pathology of Bronchial Asthma. *Arch Intern Med* 30: 689, 1922.

25. **James AL**, **Elliot JG**, **Jones RL**, **Carroll ML**, **Mauad T**, **Bai TR**, **Abramson MJ**, **McKay KO**, **Green FH**. Airway Smooth Muscle Hypertrophy and Hyperplasia in Asthma. *Am J Respir Crit Care Med* 185: 1058–1064, 2012.

26. **King GG**, **Eberl S**, **Salome CM**, **Meikle SR**, **Woolcock AJ**. Airway closure measured by a technegas bolus and SPECT. *Am J Respir Crit Care Med* 155: 682–688, 1997.

27. **King GG**, **Paré PD**, **Seow CY**. The mechanics of exaggerated airway narrowing in asthma: the role of smooth muscle. *Respir Physiol* 118: 1–13, 1999.

28. **Klarreich E**. Take a deep breath. *Nature* 424: 873–874, 2003.

29. **Kraft M**, **Djukanovic R**, **Wilson S**, **Holgate ST**, **Martin RJ**. Alveolar tissue inflammation in asthma. *Am J Respir Crit Care Med* 154: 1505–10, 1996.

30. **Lai-Fook SJ**. A continuum mechanics analysis of pulmonary vascular interdependence in isolated dog lobes. *J Appl Physiol* 46: 419–429, 1979.

31. **de Lange EE**, **Altes TA**, **Patrie JT**, **Battiston JJ**, **Juersivich AP**, **Mugler JP**, **Platts-Mills TA**. Changes in Regional Airflow Obstruction over Time in the Lungs of Patients with Asthma: Evaluation with ^{3} He MR Imaging. *Radiology* 250: 567–575, 2009.

32. **de Lange EE**, **Altes TA**, **Patrie JT**, **Parmar J**, **Brookeman JR**, **Mugler JP**, **Platts-Mills TAE**. The variability of regional airflow obstruction within the lungs of patients with asthma: Assessment with hyperpolarized helium-3 magnetic resonance imaging. *J. Allergy Clin. Immunol.* (2007). doi: 10.1016/j.jaci.2006.12.659.

33. **Lange P**, **Parner J**, **Vestbo J**, **Schnohr P**, **Jensen G**. A 15-Year Follow-up Study of Ventilatory Function in Adults with Asthma. *N Engl J Med* 339: 1194–1200, 1998.

34. **Leary D**, **Winkler T**, **Braune A**, **Maksym GN**. Effects of airway tree asymmetry on the emergence and spatial persistence of ventilation defects. *J Appl Physiol* 117: 353–362, 2014.

35. **Lewis SM**. Emptying patterns of the lung studied by multiple-breath N2 washout. *J Appl Physiol* 44: 424–430, 1978.

36. **Lewis SM**, **Evans JW**, **Jalowayski AA**. Continuous distributions of specific ventilation recovered from inert gas washout. *J Appl Physiol* 44: 416–23, 1978.

37. **Lundgren JD**, **Baraniuk JN**. Mucus secretion and inflammation. *Pulm Pharmacol* 5: 81–96, 1992.

38. **Lutchen KR**, **Jensen A**, **Atileh H**, **Kaczka DW**, **Israel E**, **Suki B**, **Ingenito EP**. Airway Constriction Pattern Is a Central Component of Asthma Severity. *Am J Respir Crit Care Med* 164: 207–215, 2001.

39. **Macklem PT**. Mechanical factors determining maximum bronchoconstriction. [Online]. *Eur Respir J Suppl* 6: 516s–519s, 1989. http://www.ncbi.nlm.nih.gov/pubmed/2803407 [19 Oct. 2018].

40. **Macklem PT**. A theoretical analysis of the effect of airway smooth muscle load on airway narrowing. *Am J Respir Crit Care Med* 153: 83–9, 1996.

41. **Marketos SG**, **Ballas CN**. Bronchial asthma in the medical literature of Greek antiquity. [Online]. *J Asthma* 19: 263–9, 1982. http://www.ncbi.nlm.nih.gov/pubmed/6757243 [4 Sep. 2018].

42. **McCracken JL**, **Tripple JW**, **Calhoun WJ**. Biologic therapy in the management of asthma. *Curr Opin Allergy Clin Immunol* 16: 375–82, 2016.

43. **Mitzner W**. Airway Smooth Muscle. *Am J Respir Crit Care Med* 169: 787–790, 2004.

44. **Nhlbi**. National Heart, Lung, and Blood Institute National Asthma Education and Prevention Program Expert Panel Report 3: Guidelines for the Diagnosis and Management of Asthma Full Report 2007 [Online]. https://www.nhlbi.nih.gov/files/docs/guidelines/asthgdln.pdf [30 Aug. 2018].

45. **Niles DJ**, **Kruger SJ**, **Dardzinski BJ**, **Harman A**, **Jarjour NN**, **Ruddy M**, **Nagle SK**, **François CJ**, **Fain SB**. He MR Imaging 1. *Radiol n Radiol* 266, 2013.

46. **Ober C**, **Cox NJ**, **Abney M**, **Di Rienzo A**, **Lander ES**, **Changyaleket B**, **Gidley H**, **Kurtz B**, **Lee J**, **Nance M**, **Pettersson A**, **Prescott J**, **Richardson A**, **Schlenker E**, **Summerhill E**, **Willadsen S**, **Parry R**. Genome-wide search for asthma susceptibility loci in a founder population. The Collaborative Study on the Genetics of Asthma. [Online]. *Hum Mol Genet* 7: 1393–8, 1998. http://www.ncbi.nlm.nih.gov/pubmed/9700192 [19 Oct. 2018].

47. **Patz MD**, **Sá RC**, **Darquenne C**, **Elliott AR**, **Asadi AK**, **Theilmann RJ**, **Dubowitz DJ**, **Swenson ER**, **Prisk GK**, **Hopkins SR**. Susceptibility to high-altitude pulmonary edema is associated with a more uniform distribution of regional specific ventilation. *J Appl Physiol* 122: 844–852, 2017.

48. **Prescott SL**, **Macaubas C**, **Smallacombe T**, **Holt BJ**, **Sly PD**, **Holt PG**. Development of allergen-specific T-cell memory in atopic and normal children. *Lancet* 353: 196–200, 1999.

49. **Riffo-Vasquez Y**, **Spina D**. Role of cytokines and chemokines in bronchial hyperresponsiveness and airway inflammation. *Pharmacol Ther* 94: 185–211, 2002.

50. **Roberts CR**. Is asthma a fibrotic disease? [Online]. *Chest* 107: 111S–117S, 1995. http://www.ncbi.nlm.nih.gov/pubmed/7874987 [18 Oct. 2018].

51. **Sá RC**, **Asadi AK**, **Theilmann RJ**, **Hopkins SR**, **Prisk GK**, **Darquenne C**. Validating the distribution of specific ventilation in healthy humans measured using proton MR imaging. *J Appl Physiol* 116: 1048–1056, 2014.

52. **Sá RC**, **Cronin M V.**, **Cortney Henderson A**, **Holverda S**, **Theilmann RJ**, **Arai TJ**, **Dubowitz DJ**, **Hopkins SR**, **Buxton RB**, **Kim Prisk G**. Vertical distribution of specific ventilation in normal supine humans measured by oxygen-enhanced proton MRI. *J Appl Physiol* 109: 1950–1959, 2010.

53. **Sá RC**, **Henderson AC**, **Simonson T**, **Arai TJ**, **Wagner H**, **Theilmann RJ**, **Wagner PD**, **Prisk GK**, **Hopkins SR**. Measurement of the distribution of ventilation-perfusion ratios in the human lung with proton MRI: comparison with the multiple inert-gas elimination technique. *J Appl Physiol* 123: 136–146, 2017.

54. **Sá RC**, **Zeman KL**, **Bennett WD**, **Prisk GK**, **Darquenne C**. Regional Ventilation Is the Main Determinant of Alveolar Deposition of Coarse Particles in the Supine Healthy Human Lung During Tidal Breathing. *J Aerosol Med Pulm Drug Deliv* 30: 322–331, 2017.

55. **Samee S**, **Altes T**, **Powers P**, **de Lange EE**, **Knight-Scott J**, **Rakes G**, **Mugler III JP**, **Ciambotti JM**, **Alford BA**, **Brookeman JR**, **Platts-Mills TAE**. Imaging the lungs in asthmatic patients by using hyperpolarized helium-3 magnetic resonance: Assessment of response to methacholine and exercise challenge. *J Allergy Clin Immunol* 111: 1205–1211, 2003.

56. **Saunders K**. Origin of the word “asthma” [Online]. *Thorax* 48: 647, 1993. https://www.ncbi.nlm.nih.gov/pmc/articles/PMC464596/ [19 Oct. 2018].

57. **Schmidt D**, **Rabe KF**. Immune mechanisms of smooth muscle hyperreactivity in asthma. *J Allergy Clin Immunol* 105: 673–682, 2000.

58. **Seow CY**, **Fredberg JJ**. Historical perspective on airway smooth muscle: the saga of a frustrated cell. *J Appl Physiol* 91: 938–952, 2001.

59. **Shen X**, **Wu MF**, **Tepper RS**, **Gunst SJ**. Mechanisms for the mechanical response of airway smooth muscle to length oscillation. *J Appl Physiol* 83: 731–738, 1997.

60. **Skloot G**, **Togias A**. Bronchodilation and Bronchoprotection by Deep Inspiration and Their Relationship to Bronchial Hyperresponsiveness. *Clin Rev Allergy Immunol* 24: 55–72, 2003.

61. **Stein RT**, **Sherrill D**, **Morgan WJ**, **Holberg CJ**, **Halonen M**, **Taussig LM**, **Wright AL**, **Martinez FD**. Respiratory syncytial virus in early life and risk of wheeze and allergy by age 13 years. *Lancet* 354: 541–545, 1999.

62. **Svenningsen S**, **Guo F**, **Kirby M**, **Choy S**, **Wheatley A**, **McCormack DG**, **Parraga G**. Pulmonary functional magnetic resonance imaging: Asthma temporal-spatial maps. *Acad. Radiol.* (2014). doi: 10.1016/j.acra.2014.08.002.

63. **Svenningsen S**, **Kirby M**, **Starr D**, **Leary D**, **Wheatley A**, **Maksym GN**, **McCormack DG**, **Parraga G**. Hyperpolarized ^{3}He and ^{129}Xe MRI: Differences in asthma before bronchodilation. *J Magn Reson Imaging* 38: 1521–1530, 2013.

64. **Tawhai MH**, **Nash MP**, **Lin C-L**, **Hoffman EA**. Supine and prone differences in regional lung density and pleural pressure gradients in the human lung with constant shape. *J Appl Physiol* 107: 912–920, 2009.

65. **Tiddens HA**, **Paré PD**, **Hogg JC**, **Hop WC**, **Lambert R**, **de Jongste JC**. Cartilaginous airway dimensions and airflow obstruction in human lungs. *Am J Respir Crit Care Med* 152: 260–266, 1995.

66. **Tiddens HAWM**, **de Jongste JC**. Airflow Obstruction in Asthma: There is More than Smooth Muscle. In: *Intensive Care in Childhood: A Challenge to the Future*, p. 337–343.

67. **Venegas JG**, **Winkler T**, **Musch G**, **Melo MFV**, **Layfield D**, **Tgavalekos N**, **Fischman AJ**, **Callahan RJ**, **Bellani G**, **Harris RS**. Self-organized patchiness in asthma as a prelude to catastrophic shifts. *Nature* 434: 777–782, 2005.

68. **Wagner PD**. The multiple inert gas elimination technique (MIGET). *Intensive Care Med* 34: 994–1001, 2008.

69. **V. Wasilewski N**, **Fisher T**, **Turcotte SE**, **Fisher JT**, **Lougheed MD**. Bronchodilating effect of deep inspirations in asthma and chronic cough. *J Appl Physiol* 120: 1018–1028, 2016.

70. **Whicker SD**, **Armour CL**, **Black JL**. Responsiveness of bronchial smooth muscle from asthmatic patients to relaxant and contractile agonists. [Online]. *Pulm Pharmacol* 1: 25–31, 1988. http://www.ncbi.nlm.nih.gov/pubmed/2980284 [19 Oct. 2018].

71. **Wickens K**, **Pearce N**, **Siebers R**, **Ellis I**, **Patchett K**, **Sawyer G**, **Stone L**, **Tohill S**, **Kennedy J**, **Slater T**, **Lewis S**, **Fitzharris P**, **Crane J**. Indoor environment, atopy and the risk of the asthma in children in New Zealand. [Online]. *Pediatr Allergy Immunol* 10: 199–208, 1999. http://www.ncbi.nlm.nih.gov/pubmed/10565561 [19 Oct. 2018].

72. **Yarova PL**, **Stewart AL**, **Sathish V**, **Britt RD**, **Thompson MA**, **Lowe APP**, **Freeman M**, **Aravamudan B**, **Kita H**, **Brennan SC**, **Schepelmann M**, **Davies T**, **Yung S**, **Cholisoh Z**, **Kidd EJ**, **Ford WR**, **Broadley KJ**, **Rietdorf K**, **Chang W**, **Bin Khayat ME**, **Ward DT**, **Corrigan CJ**, **Ward JPT**, **Kemp PJ**, **Pabelick CM**, **Prakash YS**, **Riccardi D**. Calcium-sensing receptor antagonists abrogate airway hyperresponsiveness and inflammation in allergic asthma [Online]. www.ScienceTranslationalMedicine.org [24 Sep. 2018].

73. CDC - Asthma - Most Recent Asthma Data [Online]. 2018. https://www.cdc.gov/asthma/most_recent_data.htm [19 Oct. 2018].

CHAPTER TWO

Spatial persistence of reduced specific ventilation following methacholine challenge in the healthy human lung

J Appl Physiol 124: 1222–1232, 2018.
First published February 8, 2018; doi:10.1152/japplphysiol.01032.2017.

RESEARCH ARTICLE

Spatial persistence of reduced specific ventilation following methacholine challenge in the healthy human lung

E. T. Geier,[1] I. Neuhart,[2] R. J. Theilmann,[1] G. K. Prisk,[1] and R. C. Sá[1]

[1]*Department of Medicine, University of California San Diego, San Diego, California; and* [2]*The Ohio State University, Columbus, Ohio*

Submitted 19 November 2017; accepted in final form 1 February 2018

Geier ET, Neuhart I, Theilmann RJ, Prisk GK, Sá RC. Spatial persistence of reduced specific ventilation following methacholine challenge in the healthy human lung. *J Appl Physiol* 124: 1222–1232, 2018. First published February 8, 2018; doi:10.1152/japplphysiol.01032.2017.—Specific ventilation imaging was used to identify regions of the healthy lung (6 supine subjects, ages 21–41 yr, 3 men) that experienced a fall in specific ventilation following inhalation of methacholine. This test was repeated 1 wk later and 3 mo later to test for spatial recurrence. Our data showed that 53% confidence interval (CI; 46%, 59%) of volume elements that constricted during one methacholine challenge did so again in another and that this quantity did not vary with time; 46% CI (28%, 64%) recurred 1 wk later, and 56% CI (51%, 61%) recurred 3 mo later. Previous constriction was a strong predictor for future constriction. Volume elements that constricted during one challenge were 7.7 CI (5.2, 10.2) times more likely than nonconstricted elements to constrict in a second challenge, regardless of whether the second episode was 1 wk [7.7 CI (2.9, 12.4)] or 3 mo [7.7 CI (4.6, 10.8)] later. Furthermore, posterior lung elements were more likely to constrict following methacholine than anterior lung elements (volume fraction 0.43 ± 0.22 posterior vs. 0.10 ± 0.03 anterior; $P = 0.005$), and basal elements that constricted were more likely than their apical counterparts to do so persistently through all three trials (volume fraction 0.14 ± 0.04 basal vs. 0.04 ± 0.04 apical; $P = 0.003$). Taken together, this evidence suggests a physiological predisposition toward constriction in some lung elements, especially those located in the posterior and basal lung when the subject is supine.

NEW & NOTEWORTHY The spatial pattern of bronchoconstriction following methacholine is persistent over time in healthy individuals, in whom chronic inflammation and airway remodeling are assumed to be absent. This suggests that regional lung inflation and airway structure may play dominant roles in determining the spatial pattern of methacholine bronchoconstriction.

bronchoconstriction; methacholine; specific ventilation

INTRODUCTION

Asthma is a disease characterized by airflow obstruction that varies both temporally and spatially in the lung. The temporal variability is a hallmark of the disease: many patients experience long, symptom-free intervals punctuated by acute exacerbations that vary in severity between and within individuals. The spatial variability of the disease is displayed in the uneven, patchy distribution of affected lung tissue during an asthma exacerbation. This was first demonstrated in postmortem histology of subjects who died from an acute asthma attack (9) and has since been corroborated by imaging studies spanning a range of modalities: γ-scintigraphy (10, 11), single-photon emission computed tomography (19), positron emission tomography (15, 37), high-resolution computed tomography (2, 12, 25), and hyperpolarized gas MRI (1, 23, 32). This spatially heterogeneous obstruction results in regions of markedly low ventilation. Perfusion is actively regulated within these ventilation defects, by both hypoxia-mediated and non-hypoxia-mediated mechanisms (12, 18), to compensate for this low ventilation, but ventilation-to-perfusion ratio mismatch still occurs. This mismatch remains the most significant cause of hypoxemia in these patients (28).

Recently, imaging studies have begun to explore the interaction of the spatial and temporal modes of variation. Specifically, they seek to determine whether the spatial distribution of airway obstruction is a pattern that repeats throughout the natural history of the disease or whether it varies between exacerbations. Magnetic resonance imaging techniques have been most useful so far in addressing this question, as the lack of ionizing radiation makes the techniques amenable to repeated experiments. In hyperpolarized helium studies of young, moderate asthmatics given methacholine, de Lange et al. (6) showed 69% of postmethacholine defects recurred at the same location in studies performed 2 days apart. In a subsequent study in asthmatics (this time with exercise instead of methacholine to elicit bronchoconstriction), it was shown that the number of defects that recur in the same place decreases with time: from 67 to 38% for time intervals spanning 31–85 days, respectively (5). Another hyperpolarized helium study estimated the rate of spatial recurrence to be lower; in an experiment performed on patients with exercise-induced bronchoconstriction, Niles et al. (24) found that 20% of baseline defects and 29% of postexercise defects recur on separate days.

This study adds to the ongoing discourse regarding the spatial-temporal variability of repeat bronchoconstriction by studying the phenomena in healthy, nonasthmatic adults. We chose to study healthy nonasthmatics to examine the repeatability of bronchoconstriction in isolation from the possible underlying effects of chronic asthmatic inflammation and hypersensitivity. This insight into how the normal lung functions under abnormal conditions will both further our understanding of the healthy lung and act as a point of comparison for studies of pathological lung function.

Based on modeling (21) and empirical (13, 14) work, we hypothesized that the spatial pattern of bronchoconstriction

Address for reprint requests and other correspondence: E. T. Geier, UCSD Dept. of Medicine, 9500 Gilman Dr., MC 0852, La Jolla, CA 92093 (e-mail: egeier@ucsd.edu).

Table 1. *Subject demographic data and methacholine challenge results*

Subject	Sex	Age, yr	Height, m	Weight, kg	Seated FEV_1, l [%Predicted]	Methacholine PC_{20}*, mg/ml	Methacholine dose, mg/ml
S1	M	21	1.60	59	3.82 [100]	2.78	4
S2	F	27	1.57	45	3.05 [101]	6.32	8
S3	M	27	1.88	96	5.59 [110]	10.00	16
S4	F	28	1.70	77	3.54 [101]	5.15	8
S5	M	41	1.78	83	3.87 [92]	10.90	16
S6	F	27	1.64	66	3.25 [99]	3.27	4
Mean (SD)		29 (7)	1.70 (0.12)	71 (18)	3.85 (0.91) [101 (6)]	6.40 (3.40)	9 (5)

Three male (M) and three female (F) subjects were recruited by word of mouth. Average age was 29 yr, average height was 1.70 m, and average weight was 71 kg. Forced expiratory volume in 1 s (FEV_1) was measured seated as part of the subject-screening process to ensure normal lung function. Methacholine challenge testing to determine PC_{20} was performed supine so as to mimic the subjects' posture during future scanning visits. Methacholine dose for single-dose bronchoprovocations before scanning (far right column) was the final dose administered during the ascending-concentration challenge test. PC_{20}, concentration of methacholine that elicits 20% drop in FEV_1, determined by interpolation from an empirically determined dose-response curve. *Supine measurement.

would be mostly reproduced throughout multiple methacholine-induced constriction events. Modeling studies (21, 37, 39, 40) have predicted that lung regions are more likely to constrict due to local airway branching structure and/or regional lung inflation and that relatively small inhomogeneities in these properties can lead to largely deterministic patterns of bronchoconstriction (21). An imaging study by Harris et al. (13) confirmed that ventilation defects were indeed more likely to form in regions with a lower degree of lung inflation. Since airway structure and regional lung inflation are unlikely to change significantly with time in subjects without ongoing pulmonary disease, we theorized that the spatial pattern of bronchoconstriction in the healthy lung would be stable.

METHODS

Subjects and Study Sessions

This study was approved by the University of California San Diego Human Subjects Research Protection Program. Eight volunteers were recruited via advertisement and participated after giving written, informed consent. All subjects were MRI-compatible and had no history of significant pulmonary or cardiovascular disease. One subject was excluded from the study due to a methacholine challenge result that fell within the range characteristic of asthma (see below). One subject chose to withdraw from the study following the first study session. The remaining six subjects completed the entire study (for subject information, see Table 1).

Once enrolled into the study, subjects participated in four study sessions (Fig. 1). The first was a methacholine dose determination. The second session involved two MR scans, one at baseline and one postbronchoprovocation. The third session, 1 wk later, and fourth session, 3 mo later, involved one postbronchoprovocation MR scan.

Methacholine Bronchoconstriction

Methacholine dose determination was performed for each subject according to the procedures established by the American Thoracic Society (26) for methacholine challenge testing, with the modification that the subject was supine during all parts of the process to duplicate his or her position in the MR scanner. Provocholine (methacholine chloride United States Pharmacopeia; Methapharm, Brantford, Ontario, Canada) was administered in increasing doses via a KoKo dosimeter (nSpire Health, Longmont, CO) air nebulizer system. The drug was administered in stages of five breaths each, starting at 0.03125 mg/ml and doubling concentration every stage to a maximum dosage of 16 mg/ml. Before the first stage, a dose of nebulized saline diluent was given. Following each stage of saline and drug administration, spirometry was performed to determine forced expiratory volume in 1 s (FEV_1). The drug titration was terminated when the fall in FEV_1 exceeded 20% of the subject's postdiluent value. The concentration of methacholine that elicited a 20% drop in FEV_1 (PC_{20}) for each subject was determined from his or her dose-response curve. The dose chosen for the rest of the study (Table 1) was the final dose administered in the titration, the lowest dose that elicited a $>$20% reduction in FEV_1.

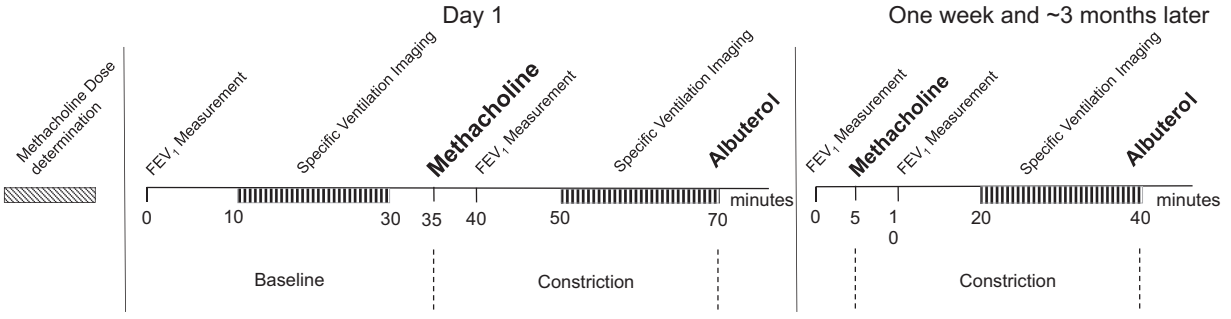

Fig. 1. Components of the 4 study sessions, with approximate time in minutes for the scanning sessions shown along the *x*-axis. During the 1st visit, methacholine dose (see Table 1) was determined by methacholine challenge testing performed in the supine posture per American Thoracic Society guidelines. The 2nd visit contained 2 forced expiratory volume in 1 s (FEV_1) measurements and specific ventilation imaging sessions: 1 at baseline without any drugs administered and a 2nd following single-dose administration of methacholine. All data were acquired within the ~75-min steady-state methacholine plateau (3). After the postmethacholine scan, return to baseline lung function was achieved with albuterol. The 3rd and 4th study sessions, which occurred 1 wk and ~3 mo later, contained only the postmethacholine specific ventilation imaging scan. During those visits, FEV_1 was measured before and after methacholine.

During each subsequent imaging session, bronchoconstriction was achieved via supine, single-dose administration of the final dose from the subject's PC_{20} determination. Provocholine was delivered using the same KoKo dosimeter nebulizer equipment from the dose determination, using the same five-breath procedure. The drug was administered while the subject lay supine and fully instrumented on the scan table, in the control room, to minimize the amount of time necessary between drug administration and MR imaging. FEV_1 determination was performed postbronchoconstriction and before MR scanning. Methacholine action peaks between 1 and 4 min after inhalation, plateaus for an average of 75 min, and then diminishes for an average of 57 min (3). The 20-min specific ventilation imaging (SVI) protocol took place 15–35 min after inhalation of the drug, during the plateau period in most subjects when smooth muscle activation would be in steady state. The SVI processing algorithm (described below) will report any non-steady-state behavior as a fitted temporal average of specific ventilation during the imaging period.

Imaging Sessions

Timeline. MR images were acquired at baseline and following three separate pharmaceutically induced bronchoconstriction episodes. Both proton density and specific ventilation images were acquired during each condition. An experimental timeline is shown in Fig. 1.

A detailed description of SVI is presented in Sá et al. (30). SVI as implemented in this study employs new hardware to streamline the experimental protocol (4) and a slightly altered stimulus block design to boost sensitivity to low specific ventilation units (see below). An overview of the protocol is presented here.

Experimental setup. Each subject lay supine on the scan table in the operator room and was fitted with a face mask (dead space 73–113 ml, depending on mask size; Hans Rudolph) attached to a three-dimensional-printed flow-bypass device (dead space 41 ml; Ref. 4). After bronchoconstriction and/or FEV_1 measurement, subjects were wheeled into the scan room and placed in the scanner. The input side of the flow-bypass system was attached to a tank of medical oxygen via 1/4-in. tubing and a three-way manual valve. When actuated, oxygen flowed through the flow-bypass face mask adapter at ~120 l/min. This rate was chosen to exceed maximal inspiratory flow rate and thus ensure that the subjects were breathing 100% oxygen while the valve was turned on. Actuation of the valve resulted in an abrupt switch from room air to oxygen, or vice versa, and occurred during expiration so that the concentration of inspired gas changed in a stepwise fashion between subsequent inspirations.

SVI air-oxygen stimulus. The physical basis of the SVI measurement (see Ref. 30 for full description) is that T_1-weighted signal intensity in the lung is dependent on the partial pressure of oxygen in the tissue and blood, which is in equilibrium with the alveolar gas (which itself provides no appreciable signal). Therefore, by changing the inspired concentration of oxygen, we change the blood and tissue oxygenation and the associated T_1-weighted signal intensity. Importantly, the rate of signal equilibration following an instantaneous change in inspired oxygen concentration is related to the rate at which fresh gas is replacing resident gas in that voxel. This rate of replenishment, when it is expressed as the change in volume of a voxel during inspiration divided by its previous end-expiratory volume, is termed specific ventilation. Thus rapid switches between inhaled air and 100% oxygen (and vice versa) act as stimuli for which we measure a response, MR signal intensity over time, which allows us to sample specific ventilation spatially. Before this study, an SVI experiment was implemented with 20 breaths between switches to allow for maximum sensitivity to the most physiologically relevant range of SV values, 0.08–0.5, and 1 40-breath interval to give sensitivity to lower SV voxels (specific ventilation values between 0.01 and 0.1).

For the purposes of this experiment, the 40-breath block of oxygen was delivered earlier in the experiment than has been described previously (30), this time during *breaths 21–60* instead of *breaths 181–220*. This choice was made to enhance sensitivity to lung regions with specific ventilation between 0.01 and 0.1 by equilibrating these slow-ventilated regions to a higher signal (and thus higher signal-to-noise-ratio) range early in the experiment. This alteration does not change the sensitivity to higher specific ventilation units, which are unaffected by the switch in block position.

SVI acquisition. Successive multiplanar image sets were acquired every 5 s. Subjects were trained to breathe between image acquisitions using the scanner noises as audible cues, each breath returning to a "relaxed" lung volume (functional residual capacity) and pausing postexpiration for the following image acquisition. Data were collected in the right lung to avoid cardiac motion artifacts. Four adjacent 15-mm sagittal slices were selected so that the imaging range included as little of the hilar vessels medially or the chest wall laterally as practical. The location of the vertebral spinous process at the level of the right hilar point was recorded and used as a landmark for future scans to ensure the same area was being imaged each time. With the use of a 1.5-T Excite HDx TwinSpeed MRI system (General Electric Medical Systems, Milwaukee, WI), four two-dimensional images were consecutively acquired with a single-shot fast spin-echo after a global inversion pulse during each breath hold. Consequently, each imaging slice had a unique inversion recovery time of 1,100, 1,335, 1,570, and 1,805 ms, respectively (medial to lateral). An eight-element torso coil was used to provide greater sensitivity than the built-in body coil. Each image in the multiplanar set had a 40×40 cm field of view acquired at 128×128 voxel resolution. Images were reconstructed by the scanner onto a 256×256 matrix.

Image Processing

Custom-written MATLAB (MathWorks, Natick, MA) code was used for image processing. Data from each scanning session were processed separately and compared during the analysis phase. The processing steps for each day were as follows.

For each of the 4 imaging slices, a time series of 220 images, each image corresponding to a separate postexpiratory breath hold, was assembled. A generalized dual-bootstrap iterative closest point algorithm (42) was used to register all images in the time series to a reference image chosen manually to be as close as possible to functional residual capacity. This publicly available algorithm identifies features based on edges and corners in the images to be registered and iteratively performs affine transformations based on features within a region that grows with each iteration. Multiple seed points are used to create multiple transformations via this region-growing approach, and only those that pass a set of decision criteria are accepted to compute a final transformation (42). Images in which the subject's postexpiratory lung volume required $>10\%$ correction (4 ± 2 images out of 220) to match the reference lung volume were removed from the time series and treated as missing data. This limit was chosen because we (1a) have shown that lung deformations within 10% can be accurately registered using an affine transformation.

A 220-image (breath) time course of signal intensity was constructed for every voxel within a manually drawn lung region of interest. The time course for each voxel was then correlated with 50 modeled theoretical time courses for specific ventilation values equally spaced in $\log_{10}$ from 0.01 to 10: these bin values were chosen to match the 50-compartment model employed by multiple-breath washout studies (29). The modeled time course with the maximum correlation coefficient was determined to be the specific ventilation of the voxel. The SV thus computed was only retained if the correlation was significant ($P < 0.05$) and the null hypothesis of no correlation rejected. Voxels failing to pass this test ($<1\%$) were treated as missing data.

For each of the 4 slices, a spatial map of specific ventilation and histogram of SV distribution was created. For further spatial analysis (intercondition/day comparison and identification of bronchocon-

stricted regions, described below), SV maps were smoothed using a geometric algorithm with a kernel size of 7 voxels (~1 cm^2).

Data Analysis

Specific ventilation heterogeneity. Maps of specific ventilation were used to construct distributions of SV for each subject at baseline and during the three episodes of bronchoprovocation. A log-Gaussian function was fit to each of these histograms, and the full-width half-maximum of the fitted distribution was reported as a measure of SV heterogeneity (29).

Identification of bronchoconstricted regions. To measure the change in specific ventilation maps between baseline and during methacholine challenge, we first normalized the maps so that the total imaged specific ventilation, the sum of all voxel specific ventilation values, of each multiplanar set was equal between conditions. Total imaged specific ventilation is a function of tidal volume, which can potentially change between conditions. An increase or decrease in tidal volume induces a global increase or decrease (respectively) in specific ventilation across the lung (27). Therefore, a decrease in tidal volume following methacholine-induced bronchoconstriction could cause "false-positive" indications of bronchoconstriction that are due to global but not regional changes in specific ventilation.

For the purposes of this study, we defined a bronchoconstriction event as a postnormalization 50% decrease in specific ventilation from baseline to a value below the center of the baseline distribution (e.g., 50% decrease to SV < 0.18 for *subject 2*; see Fig. 2). This imposed two conditions: *1*) that specific ventilation be significantly decreased and *2*) that the postmethacholine specific ventilation value of a constricted lung region implies that it is ventilating less than average. Importantly, these criteria effectively exclude two types of lung regions: *1*) regions with perpetually low specific ventilation that are not necessarily responding to methacholine and *2*) regions with high specific ventilation at baseline that are affected by the drug but not to the point that they could potentially generate regions with a low ventilation-to-perfusion ratio.

After normalization, the multiplanar image sets were spatially correlated. Because imaged thoracic cage volume varied between baseline and bronchoconstriction, on average by $18 \pm 10\%$, beyond the limit within which we can confidently register images accurately, 10% (1a), we did not perform image registration in the sense that we did within a 220-image temporal set (see above). Instead, we divided each multiplanar set into 12 (anterior-posterior) $\times$ 12 (apical-basal) $\times$ 4 (medial-lateral, defined by imaging plane) volume elements, the extent of which were redefined for each condition. Arithmetic mean specific ventilation of the voxels within each of these volume elements was measured, and comparisons were made between volume elements from different conditions with corresponding $12 \times 12 \times 4$ coordinates. Elements in which the specific ventilation fell to less than half of the baseline value and to less than the center of the baseline distribution were identified as constricted and used to create binary constriction masks (Fig. 3). The volume of each element (number of voxels inside the element) was taken into account, and all further processing was weighted by the volume of each element. For example, a constricted element in the middle of the lung containing 80 voxels would contribute more to the whole lung constriction fraction than would an element on the edge of the lung that contains only 30 voxels.

Spatial persistence of constriction between episodes of bronchoconstriction. Binary constriction masks were compared between conditions to determine *1*) the percentage of voxels that constrict in a subsequent methacholine challenge, given a prior constriction, and *2*) the predictive power of a prior constriction for a future constriction. These metrics were stratified for time between constrictions, 1 wk vs. ~3 mo, and for number of constrictions: one previous constriction predicting a second vs. two previous constrictions predicting a third. Odds ratios (exact usage defined in Fig. 4) were used as measures of predictive power. Volume elements that constricted following all three methacholine administrations were classified as "persistent."

Regional trends in bronchoconstriction across subjects. On each sagittal lung image, regions were defined by thirds in the apical-basal direction and thirds in the anterior-posterior direction. The 4 sagittal slices were grouped 2×2 to form a medial group and a lateral group. Thus 18 lung regions were defined, each with a unique spatial designation, e.g., apical-anterior-medial. In practice, this was done by resampling the $12 \times 12 \times 4$ grid of volume elements (from above) to a $3 \times 3 \times 2$ grid of regions. Regional tendency to bronchoconstrict following methacholine was characterized in our study by the average volume fraction of constriction in a region over the 3 study sessions. Likewise, tendency toward persistent constriction was characterized by the volume fraction of persistent (constricted in response to all 3

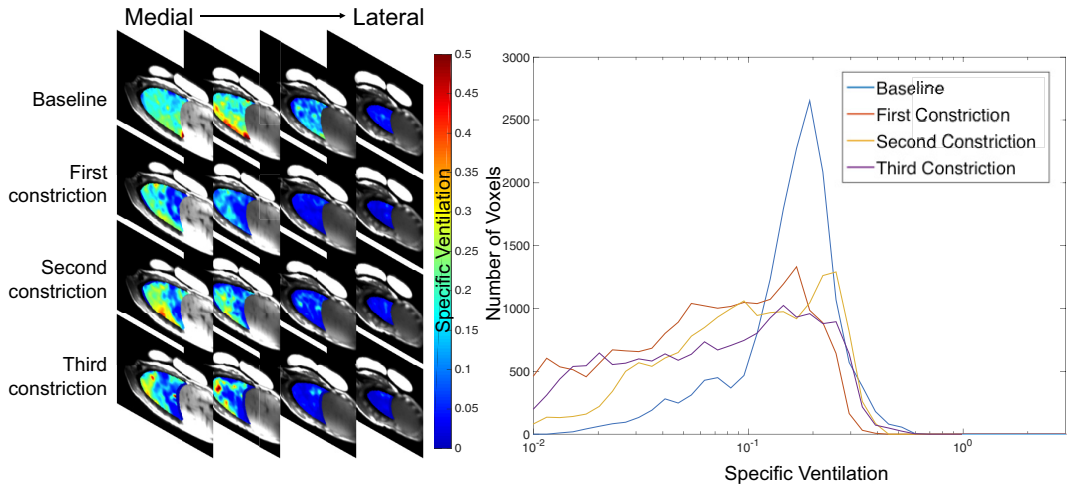

Fig. 2. *Left*: multiplanar specific ventilation (SV) maps for 1 subject (*S2*) from all 4 imaging sessions. Each row of images represents 1 day of imaging, and each column represents a sagittal slice of the subject's right lung. Rows are organized from medial on the left to lateral on the right. *Right*: SV histograms for *subject S2* from baseline (blue) and 3 constricted (red, yellow, and purple) imaging sessions. SV values from all 4 planar maps were combined into 1 histogram for each session.

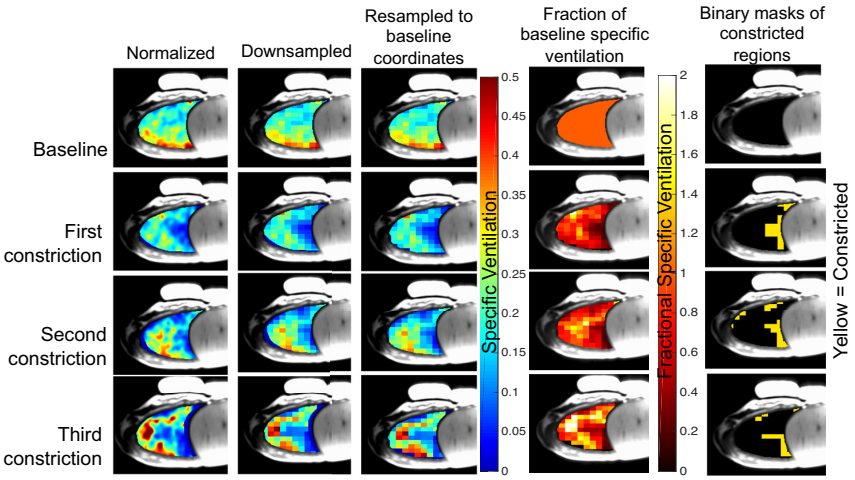

Fig. 3. Processing flow for *subject S2*'s midclavicular (*plane 2*) specific ventilation map, shown for baseline and each of the 3 constrictions. After normalization, maps were downsampled to a 12 × 12 grid of volume elements and then projected onto the baseline image frame for comparison. All further data processing steps were performed on these resampled maps. Volume elements with fractional specific ventilation (*column 4*) <0.5 were identified as constricted (*column 5*) if the end value of the element is less than the center of the baseline distribution (center of the blue histogram in Fig. 2, *right*). This process was repeated for all 4 planar maps.

methacholine administrations) voxels. Likelihood of a constricted region to persist over time, or persistence of constriction, was quantified as the ratio of the 2 fractions above, persistent to average constricted.

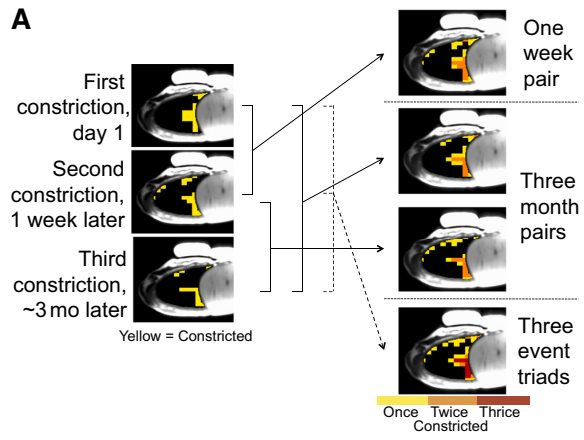

Fig. 4. *A*: pairs for interday comparison. Comparisons were always made going forward in time, i.e., the percentage of *day 1* constrictors (yellow regions in the 1st column) that constricted again 1 wk later (became orange in 2nd column) or the odds ratio for a 1-wk-later constrictor to constrict ~3 mo later. *B*: odds ratios for pairs were defined as the odds of a previous constrictor constricting again divided by the odds of a previous nonconstrictor constricting for the 1st time.

RESULTS

Demographic Data, Baseline Pulmonary Function Tests, and Methacholine Dose Determination

Subject demographic data, seated FEV_1 measurements, and methacholine challenge results are shown in Table 1. Average seated FEV_1 between subjects was 101 ± 6% of predicted (Table 1). Subsequent FEV_1 measurements were all made supine. Average supine FEV_1 at baseline (premethacholine) was 92 ± 5% of predicted (Table 2), which suggested that, as expected, supine posture significantly reduced FEV_1 (P = 0.002, paired t-test, 1-tailed).

Response to Methacholine Bronchoconstriction: Pulmonary Function Tests and Whole Lung Imaging Measures

Metrics of assessing bronchoconstriction are shown in Table 2. FEV_1, imaged thoracic cage value, and the width of the specific ventilation distribution all changed significantly between baseline and bronchoconstriction, both on average and for each individual episode ($P < 0.05$, paired t-tests). There were no statistically significant differences ($P > 0.05$, paired t-tests) between bronchoconstriction episodes in any of the four metrics.

Spatial Persistence of Constriction between Bronchoconstriction Episodes

On average, 53% CI (46%, 59%) of volume elements that constricted on a given day constricted again on a following day (Fig. 5). This finding was independent of the time between constrictions: 46% CI (28%, 64%) repeated 1 wk later and 56% CI (51%, 61%) repeated 3 mo later. Likewise, the odds ratio (Fig. 5) of a given constricted volume element constricting again during a later challenge was 7.7 CI (5.2, 10.2) and did not vary based on the time between challenges; odds ratios were 7.7 CI (2.9, 12.4) for 1 wk later and 7.7, CI (4.6, 10.8) for 3 mo later. The amount of constriction varied considerably between subjects (Fig. 6, Table 2).

Of volume elements that constricted during the first two methacholine administrations, 68% CI (57%, 79%) constricted

Table 2. *Lung-wide metrics of constriction for each study day*

Subject	Baseline, Supine FEV_1, l [%Predicted]	*Day 1* Constricted FEV_1, l [%Change]	One-Week-Later Constricted FEV_1, l [%Change]	Approximately-3 mo-Later Constricted FEV_1, l [%Change]	Average Constricted FEV_1, l [%Change]
S1	3.55 [93]	2.86 [−19]	2.91 [−18]	2.28 [−36]	2.68 [−25]
S2	2.91 [96]	2.53 [−13]	2.68 [−8]	2.51 [−14]	2.57 [−12]
S3	4.99 [99]	3.92 [−21]	3.42 [−32]	3.79 [−24]	3.71 [−26]
S4	3.05 [86]	2.34 [−22]	2.28 [−24]	2.62 [−13]	2.41 [−21]
S5	3.70 [88]	3.14 [−15]	2.90 [−22]	2.65 [−28]	2.90 [−22]
S6	3.11 [92]	2.38 [−24]	2.49 [−20]	2.03 [−35]	2.30 [−26]
Mean (SD)	3.56 (0.79) [92 (5)]	2.86 (0.60) [−20 (4)]	2.78 (0.40) [−21 (8)]	2.65 (0.61) [−26 (10)]	2.76 (0.51) [−22 (6)]

	Baseline Imaged Thoracic Cage Volume, cm^3	*Day 1* Constricted Imaged Thoracic Cage Volume, cm^3 [%Change]	One-Week-Later Constricted Imaged Thoracic Cage Volume, cm^3 [%Change]	Approximately-3 mo-Later Constricted Imaged Thoracic Cage Volume, cm^3 [%Change]	Average Constricted Imaged Thoracic Cage Volume, cm^3 [%Change]
S1	851	927 [9]	821 [−4]	905 [6]	884 [4]
S2	560	732 [31]	632 [13]	627 [12]	664 [19]
S3	930	1,206 [30]	1,221 [31]	1,198 [29]	1,208 [30]
S4	559	785 [40]	723 [29]	683 [22]	730 [31]
S5	509	518 [2]	544 [7]	649 [28]	570 [12]
S6	497	561 [13]	521 [5]	599 [21]	560 [13]
Mean (SD)	650 (190)	790 (250) [21 (15)]	740 (260) [26 (11)]	780 (230) [20 (9)]	770 (250) [18 (10)]

	Day 1 Volume Fraction of Constricted Elements	One-Week-Later Volume Fraction of Constricted Elements	Approximately-3 mo-Later Volume Fraction of Constricted Elements	Average Volume Fraction of Constricted Elements
S1	0.31	0.27	0.30	0.29
S2	0.25	0.14	0.26	0.22
S3	0.37	0.55	0.44	0.45
S4	0.33	0.27	0.18	0.26
S5	0.18	0.10	0.38	0.22
S6	0.26	0.13	0.25	0.21
Mean (SD)	0.28 (0.07)	0.24 (0.17)	0.30 (0.09)	0.28 (0.09)

	Baseline SV Distribution Width	*Day 1* SV Constricted FWHM [Change]	One-Week-Later Constricted SV FWHM [Change]	Approximately-3 mo-Later Constricted SV FWHM [Change]	Average Constricted SV FWHM [Change]
S1	0.43	0.92 [0.49]	0.95 [0.52]	0.75 [0.32]	0.87 [0.44]
S2	0.32	1.03 [0.71]	0.89 [0.58]	1.20 [0.32]	1.04 [0.72]
S3	0.43	0.91 [0.48]	1.81 [1.37]	1.02 [0.59]	1.25 [0.81]
S4	0.57	0.46 [−0.11]	1.19 [0.61]	0.4 [−0.13]	0.70 [0.12]
S5	0.61	0.55 [−0.06]	0.39 [−0.22]	1.15 [0.54]	0.69 [0.09]
S6	0.32	1.00 [0.68]	0.50 [0.18]	0.87 [0.54]	0.79 [0.47]
Mean (SD)	0.45 (0.12)	0.81 (0.25) [0.37 (0.36)]	0.95 (0.51) [0.51 (0.53)]	0.90 (0.28) [0.46 (0.34)]	0.89 (0.22) [0.44 (0.30)]

Data are presented as means (SD). Response to methacholine, quantified change in FEV_1, thoracic cage volume, or FWHM is expressed as percentage or absolute change. All measurements in this table were made in the supine posture. Supine forced expiratory volume in 1 s (FEV_1) was measured in all subjects before baseline scanning on *day 1*. FEV_1 was measured supine after methacholine administration on all 3 days to quantify response to the drug. Imaged thoracic cage volume is the size of the lung in MR images acquired at functional residual capacity. Volume fraction of constricted elements is the fraction of lung voxels that pass our 2 criteria for constriction [>50% decrease in specific ventilation (SV) from baseline to a value below the center of the baseline distribution]. Full-width half-maximum (FWHM) is the width of a log-Gaussian function fit to the specific ventilation distribution (see Fig. 2) acquired during each condition.

for a third time 90 days later (Fig. 5). This was significantly higher ($P = 0.01$, paired *t*-test, 1-tailed) than the 56% of volume elements in the 90-day pairs that repeated. The odds ratio of twice constrictors repeating a third time was 9.8 CI (4.1, 15.6). This odds ratio was higher than for the 90-day pairs, but this trend did not reach statistical significance ($P = 0.22$, paired *t*-test, 1-tailed).

Regional Trends in Bronchoconstriction across Subjects

Volume elements in the posterior lung were more likely to constrict than those in the anterior lung ($P = 0.005$, paired *t*-test, 1-tailed), and persistently constricting volume elements were more likely to be found in the posterior lung than the anterior lung ($P = 0.03$, paired *t*-test, 1-tailed). Although there was no statistically significant apical-basal gradient in overall constriction fraction ($P = 0.35$, paired *t*-test, 1-tailed), volume elements in the basal lung that do constrict were more likely than apical units to persist throughout all 3 challenges ($P = 0.01$, paired *t*-test, 1-tailed). There was no statistically significant medial-lateral bias toward constricted volume, persistent volume, or persistence of constriction in the healthy lungs we tested ($P = 0.63$, $P = 0.79$, and $P = 0.52$, respectively, paired *t*-tests, 2-tailed).

DISCUSSION

In healthy subjects, previous bronchoconstriction of a lung element following methacholine challenge is a strong predictor for future bronchoconstriction of that same element following methacholine challenge weeks or months later. The predictive value of a previous constriction does not diminish over 3 mo. There is a higher tendency toward bronchoconstriction in the posterior lung when supine and a tendency for basal lung units that constrict once to constrict persistently during each of three challenges given over 3 mo. These results are in agreement

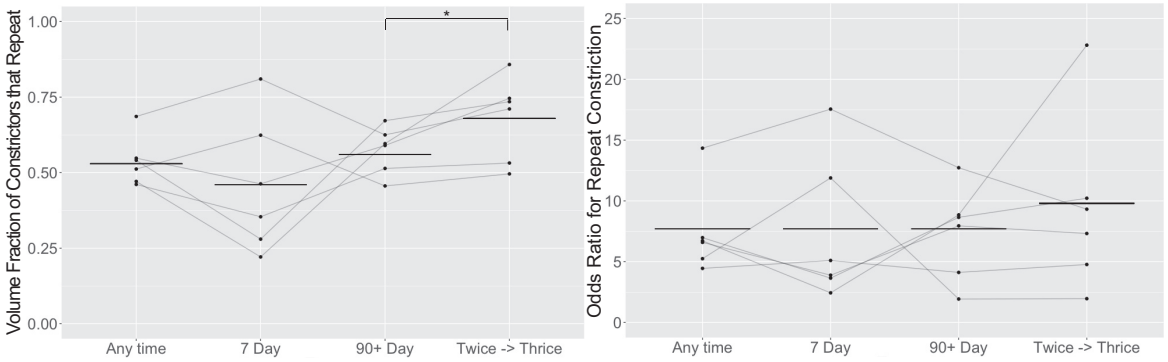

Fig. 5. *Left*: volume fraction of constricted elements that repeatedly constrict during a following methacholine challenge. *Right*: odds ratio for the likelihood of a constricted voxel to constrict again during a following challenge. In both cases, subject values are shown as dots and connected by gray lines, and group means are shown as solid black lines. Subject values may be the average of multiple measurements, i.e., "Any time" represents the average of all 3 pairs (Fig. 4) for a subject and ~3 mo later represents the average of the 2 3-mo pairs (Fig. 4). $*P = 0.038$, paired t-test, 1-tailed.

with previously published data from hyperpolarized He imaging (13, 14, 17, 41).

Airway smooth muscle activation following methacholine inhalation is counteracted, at the level of the airway, by tethering forces from surrounding lung tissue and by transmural pressure differences at the airway wall (41). Venegas et al. (37), with an integrative model of these forces acting on 12 generations of airways, showed that interdependence between serial and parallel airways gives rise to a self-organized patchy distribution of bronchoconstriction, even in a symmetric lung model (although in a symmetric lung model, the locations of the patches are random). Later, Leary et al. (21) showed that branching asymmetry in the model led to "local triggers" for this patchiness and found that when the degree of branching asymmetry of the simulated lung matched that of an anatomically realistic model (34), the spatial pattern of bronchoconstriction was highly persistent, with an average local variation between successive bronchoconstriction episodes of $<3\%$ (21).

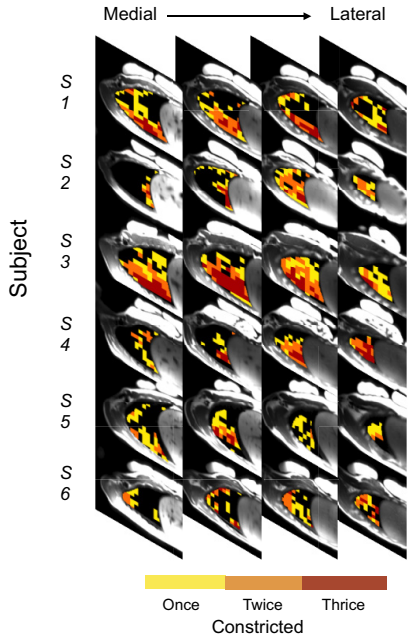

Fig. 6. Constriction frequency maps for all subjects. Imaging planes are arranged from medial on left to lateral on right, and subjects (S) are arranged vertically. The color of a lung region indicates the number of times the region constricted following methacholine challenge. Red volume elements constricted 3/3 times, orange constricted 2/3, yellow constricted 1/3, and black constricted 0/3. Red units, those that constricted during all 3 challenges, are classified in this study as "persistent constrictors."

This persistence due to branching asymmetry may help explain the spatial persistence of bronchoconstriction found in our study but likely is not the sole determining factor. Differences in regional lung inflation, or, rather, the differences in transmural pressure that are associated with differences in lung inflation, also cause lung regions to constrict persistently. Harris et al. (13) provided evidence for this effect in a PET study, which showed that ventilation defects were more likely to form in regions with a lower degree of lung inflation premethacholine. This principle is also supported by our data, which show that gravitationally dependent lung units are more likely to constrict than their nondependent counterparts. Since the dependent lung is compressed by the weight of the lung above it (16, 38), it is relatively less inflated. Thus the parenchymal forces holding open the airways and preventing airway collapse are less potent.

Since airway tree structure (absent remodeling from disease) and regional lung inflation (absent changes in posture or breathing) are not expected to change in healthy individuals between scanning sessions, we expected the forces driving regional tendency to bronchoconstrict following methacholine to be roughly the same and thus the pattern of constriction to be mostly persistent. This was borne out in the data.

However, there are potential factors other than innate airway asymmetry or regional inflation that could cause certain areas of the lung to be predisposed to constriction in our study, among which is that a reproducibly uneven pattern of methacholine deposition in the lung could lead to more drug response in regions receiving a higher dose. Indeed, the fact that posterior lung regions were more likely to constrict could be due to preferential deposition of methacholine in the posterior lung. It is well-known that the gravitationally dependent (in this case, posterior) lung ventilates more than the nondependent (in this

case, anterior) lung (22, 38). If methacholine simply followed the pattern of ventilation, one would expect more deposition in the posterior lung. Since the action of methacholine is mostly topical or local, this could have led to higher rates of constriction and persistence of constriction in the posterior lung.

Limitations

Our experiment is subject to certain factors that limit the scope of our conclusions. The most significant of these is that the supine posture in which all elements of the experiment were performed limits the interpretation of our findings. There are (at least) three factors that could lead to a persistent pattern of postmethacholine bronchoconstriction in healthy individuals: *1*) airway asymmetry acting as local triggers for constriction, *2*) lower inflation in the gravitationally dependent lung (and in other regions) predisposing these regions, and *3*) preferential deposition of methacholine and increased local action of the drug due to gravity and/or airflow at the time of administration. The repeatable pattern of constriction that we see in our subjects is likely influenced by all of these factors, but the degree to which each contributes is difficult to quantify. Since airway asymmetry is insensitive to posture and the other two factors are not, experiments in other postures may help give weight to the three factors.

A second limitation is that the four-slice imaging volume encompassed only 80% of one (the right) lung. It has been shown that specific ventilation imaging in a single, sagittal lung slice (~8% of total lung volume) accurately represents the heterogeneity of specific ventilation in a healthy lung (29). This is because *1*) in the healthy lung (without methacholine), no spatially localized heterogeneity is expected and *2*) gravity is a major source of specific ventilation heterogeneity in a healthy subject and a sagittal slice captures a cross-section of this gravitational gradient. However, in this study, in which we imposed an additional layer of SV heterogeneity, it is possible that the extent of that added effect could not have been captured by four imaging slices in one lung. However, the lack of a medial-lateral gradient in either constricted or persistent lung fraction suggests that exclusion of the most medial and lateral lung is unlikely to have biased our results. Any systematic difference between the behavior of the right lung and left lung (which was not imaged) postmethacholine was not captured by our experimental design.

Comparison with Other Studies

Although this was the first imaging study to probe the spatial reproducibility of methacholine bronchoconstriction in healthy individuals, other studies have done so in mild, moderate, and severe asthmatics. Direct comparison between those studies and ours is challenging, as the constriction metric used in previous studies, manual or semiautomated identification hypointense regions on hyperpolarized He scans, is not directly analogous to the constriction metric we have defined here, a 50% decrease in SV from baseline to a below average SV. However, some comparison is possible. Our finding, that 53% CI (46%, 59%) of voxels that constricted in one methacholine challenge did so in a second (Fig. 5), fits within a range previously reported by de Lange et al. (5). Those data showed that the rate of spatial recurrence of ventilation defects in asthmatics is between 38 and 67%, depending on the time between examinations. Unlike this previous result, the rate of recurrence in our study did not depend on the time between challenges. It is probable that there is a temporal disease process at work in the de Lange et al. (5) asthmatic study population that causes the spatial persistence of ventilation defects to decrease over time and that this process did not occur in our healthy individuals given methacholine.

Other studies on the recurrence of impaired ventilation during bronchoconstriction, using a variety of approaches and metrics, have reported a wide range of results: a separate study by de Lange et al. (6) showed that 69% of postmethacholine ventilation defects recur in the same place during a 2nd challenge; a study by Niles et al. (24) showed that 29% of postexercise defects recur in the same place during a 2nd exercise-induced exacerbation; and a study by Svenningsen et al. (33) showed that the ratio of intermittent to persistent ventilation defects in asthmatics postexercise was 20:1 (persistent defined as constricting in 3 out of 3 exercise challenges 5 ± 2 days apart). The discrepancy between our study and these is partially explainable by the different methods for eliciting, measuring, and quantifying bronchoconstriction and even more fundamentally by the wide spread in the results of the existing studies. The latter, which suggests a fundamental uncertainty in our understanding of the process and in the evidence to elucidate it, highlights the need for more studies of this type.

The spatial gradients of constriction and persistence (Fig. 7) that we report here directly corroborate previous reports by Svenningsen et al. (33) and Harris et al. (13, 14), both of which involved asthmatic (as opposed to healthy) subjects. In the study by Svenningsen et al. (33), in which asthmatics were imaged with hyperpolarized helium postexercise on three separate occasions, it was shown that both intermittent ventilation defect percentage (somewhat equivalent to our overall constricted fraction) and persistent ventilation defect percentage (somewhat equivalent to our persistently constricted fraction) increase from the anterior to the posterior lung and from the apical to the basal lung. This finding is reflected in our data. Importantly, both the methods of eliciting bronchoconstriction, exercise vs. supine methacholine administration, and the subject populations, asthmatics vs. healthy young volunteers, are different in the two studies, despite the similar results. This suggests that the pattern of methacholine distribution, and perhaps even underlying presence or lack of asthma, both play relatively minor roles in the spatial gradients of bronchoconstriction found in the studies. More likely, it is regional differences in airway structure or a predisposition due to differences in regional lung inflation that serve to drive the effect.

The 2009 (14) and 2012 (13) studies by Harris et al. (also corroborated by our data) lend support to the second of these possibilities, that the spatial pattern of bronchoconstriction is influenced by the systematically decreased inflation of the dependent lung compared with the nondependent lung. Harris et al. (14) showed that, whether the subject was prone or supine during imaging, bronchoconstriction following prone methacholine administration preferentially occurred in the gravitationally dependent lung. The group (13) went on to show that this gravitational dependence of constriction following methacholine existed both in mild asthmatics and healthy nonasthmatics, although the gravitational dependence was stronger in

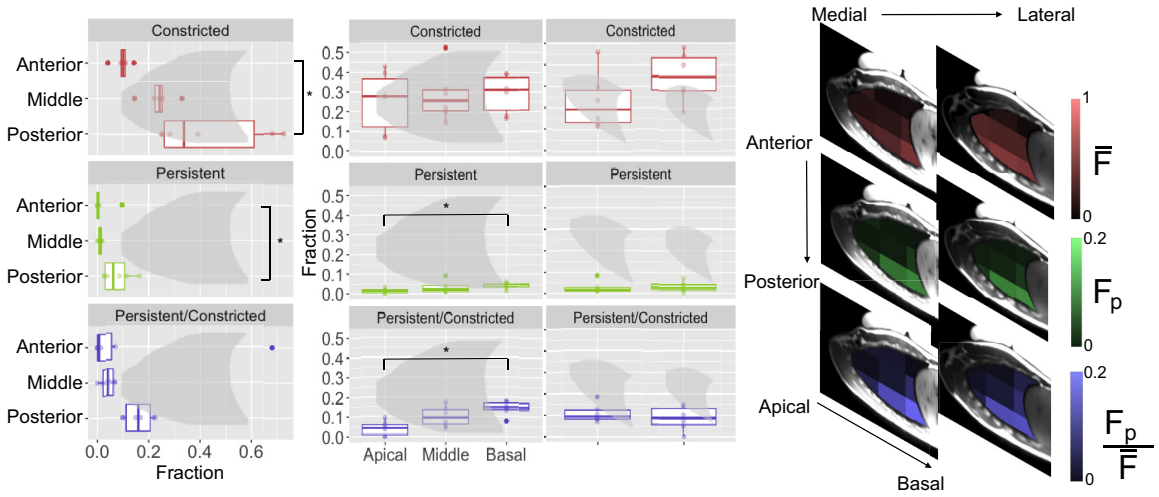

Fig. 7. *Top* row (red): the average fraction of voxels that constrict during each of the 3 challenges ($\bar{F}$) is shown as a function of anterior-posterior, apical-basal, and medial-lateral position. *Middle* row (green): the fraction of voxels that persistently constricted during all 3 methacholine challenges (F_p) is shown as a function of position. *Bottom* row (purple): the fraction of persistent voxels divided by the average fraction of voxels that constrict ($F_p/\bar{F}$) is shown as a function of position. Lines on box plots represent the median and 1st/3rd quartiles of the data, and dots represent subject values. Note that although the basal volume elements were no more or less likely to constrict than their apical counterparts, $P = 0.35$ by paired, 1-tailed *t*-test, those that do were more likely to persist through all 3 trials, $P = 0.01$ by paired, 1-tailed *t*-test. *Difference in regions that was significant with $P < 0.05$ by paired, 1-tailed *t*-test.

healthy nonasthmatics. This supports the conjecture above, that healthy individuals and mild asthmatics have spatial tendencies toward bronchoconstriction that are largely based on the same physiological phenomena. The caveat to this claim is that, in the mild asthmatics who were studied, the amount of airway remodeling from chronic inflammation is likely low and thus a minor factor governing constriction (13).

Potential Applications

With the emergence of new surgical and pharmaceutical treatments, quantification and localization of pathological lung regions is becoming important for informing treatment and evaluating efficacy. Surgical techniques that target specific regions of the lung, such as bronchial thermoplasty (8, 35), could potentially benefit from precise localization of airflow-obstructed regions before treatment, especially if these regions are shown to repeat between exacerbations. Furthermore, quantification of airflow deficits, both temporally repeatable and nonrepeatable, holds promise as a means of assessing disease progression and treatment response. Indeed, hyperpolarized imaging-derived ventilation defect volume has been shown to be more sensitive in some cases than standard pulmonary function tests for depicting short-term changes in chronic obstructive pulmonary disease (20). This work fits into the ongoing effort to transform functional MR imaging into a clinical tool for guiding therapy and for disease/treatment monitoring. The style of oxygen-enhanced imaging used in this study, specific ventilation imaging (SVI), has been validated (29), used to measure the gravitational gradient of ventilation in the lung (30), and recently integrated with blood flow measurements to map ventilation-to-perfusion ratio in the healthy lung (31). This study represented an extension of the technique in two regards: *1*) it was the first application of the technique to the study of pathological lung function, and *2*) it was the first study to implement a multislice form of SVI that extended the imaging volume from ~20 to ~80% of the right lung.

Conclusion

Specific ventilation imaging has shown that, in the healthy lung, an area of lung that undergoes a dramatic reduction in SV postmethacholine is much more likely to do so again in a successive challenge than is an area that resists the first challenge. This remains true whether considering challenges 1 wk apart or ~3 mo apart. Furthermore, it has shown that tissue in the posterior, in this case gravitationally dependent, lung is more likely to be susceptible to constriction and that tissue in the basal lung, although not necessarily more likely to constrict on average, is more likely to constrict persistently if it constricts at least once. Further studies involving changes in posture during drug administration and imaging are needed to determine whether regional vulnerability to constriction is driven by anatomy, drug delivery, or local transmural pressure due to regional lung inflation.

The overall repeatability and the spatial gradients of constriction in our study match previous hyperpolarized helium MR imaging work done in patients with asthma (5, 6, 13, 14, 33) despite the fact that our subjects have no history of asthma or any other pulmonary disease. This is evidence that methacholine constriction of healthy subjects may be a representative model for asthmatic bronchoconstriction, at least for the purposes of studying the spatial patterns of bronchoconstriction.

ACKNOWLEDGMENTS

Dr. Laura Crotty-Alexander was an invaluable resource as medical advisor and monitor for this study. We thank her, in particular, for her help in developing the human subject protocols. We benefited greatly from algorithms developed by Tatsuya J. Arai and Amran K. Asadi. Kent Kubo and Elizabeth M. Bird provided assistance during data collection. Finally, we owe a tremendous amount to our study participants, who were kind, patient, and endlessly game.

GRANTS

This work was supported by the National Heart, Lung, and Blood Institute (NHLBI) Grant R01-HL-119263. E. T. Geier's work was supported by NHLBI Grant F30-HL-127980-02.

DISCLOSURES

No conflicts of interest, financial or otherwise, are declared by the authors.

AUTHOR CONTRIBUTIONS

E.T.G., G.K.P., and R.C.S. conceived and designed research; E.T.G., I.N., and R.C.S. performed experiments; E.T.G., I.N., and R.C.S. analyzed data; E.T.G., R.J.T., G.K.P., and R.C.S. interpreted results of experiments; E.T.G. and I.N. prepared figures; E.T.G. drafted manuscript; E.T.G., R.J.T., G.K.P., and R.C.S. edited and revised manuscript; E.T.G., I.N., R.J.T., G.K.P., and R.C.S. approved final version of manuscript.

REFERENCES

1. **Altes TA, Powers PL, Knight-Scott J, Rakes G, Platts-Mills TA, de Lange EE, Alford BA, Mugler JP 3rd, Brookeman JR.** Hyperpolarized ^{3}He MR lung ventilation imaging in asthmatics: preliminary findings. *J Magn Reson Imaging* 13: 378–384, 2001. doi:10.1002/jmri.1054.

1a. **Arai TJ, Villongco CT, Villongco MT, Hopkins SR, Theilmann RJ.** Affine transformation registers small scale lung deformation. *Conf Proc IEEE Eng Med Biol Soc* 2012: 5298–5301, 2012. doi:10.1109/EMBC.2012.6347190.

2. **Beigelman-Aubry C, Capderou A, Grenier PA, Straus C, Becquemin MH, Similowski T, Zelter M.** Mild intermittent asthma: CT assessment of bronchial cross-sectional area and lung attenuation at controlled lung volume. *Radiology* 223: 181–187, 2002. doi:10.1148/radiol.2231010779.

3. **Cartier A, Malo JL, Bégin P, Sestier M, Martin RR.** Time course of the bronchoconstriction induced by inhaled histamine and methacholine. *J Appl Physiol Respir Environ Exerc Physiol* 54: 821–826, 1983. doi:10.1152/jappl.1983.54.3.821.

4. **Cook FR, Geier ET, Asadi AK, Sá RC, Prisk GK.** Rapid prototyping of inspired gas delivery system for pulmonary MRI research. *3D Print Addit Manuf* 2: 196–203, 2015. doi:10.1089/3dp.2015.0027.

5. **de Lange EE, Altes TA, Patrie JT, Battiston JJ, Juersivich AP, Mugler JP 3rd, Platts-Mills TA.** Changes in regional airflow obstruction over time in the lungs of patients with asthma: evaluation with ^{3}He MR imaging. *Radiology* 250: 567–575, 2009. doi:10.1148/radiol.2502080188.

6. **de Lange EE, Altes TA, Patrie JT, Parmar J, Brookeman JR, Mugler JP 3rd, Platts-Mills TA.** The variability of regional airflow obstruction within the lungs of patients with asthma: assessment with hyperpolarized helium-3 magnetic resonance imaging. *J Allergy Clin Immunol* 119: 1072–1078, 2007. doi:10.1016/j.jaci.2006.12.659.

8. **Dombret MC, Alagha K, Boulet LP, Brillet PY, Joos G, Laviolette M, Louis R, Rochat T, Soccal P, Aubier M, Chanez P.** Bronchial thermoplasty: a new therapeutic option for the treatment of severe, uncontrolled asthma in adults. *Eur Respir Rev* 23: 510–518, 2014. doi:10.1183/09059180.00005114.

9. **Dunnill MS.** The pathology of asthma, with special reference to changes in the bronchial mucosa. *J Clin Pathol* 13: 27–33, 1960. doi:10.1136/jcp.13.1.27.

10. **Engel LA, Landau L, Taussig L, Martin RR, Sybrecht G.** Influence of bronchomotor tone on regional ventilation distribution at residual volume. *J Appl Physiol* 40: 411–416, 1976. doi:10.1152/jappl.1976.40.3.411.

11. **Filuk RB, Berezanski DJ, Anthonisen NR.** Airway closure with methacholine-induced bronchoconstriction. *J Appl Physiol (1985)* 63: 2223–2230, 1987. doi:10.1152/jappl.1987.63.6.2223.

12. **Goldin JG, McNitt-Gray MF, Sorenson SM, Johnson TD, Dauphinee B, Kleerup EC, Tashkin DP, Aberle DR.** Airway hyperreactivity: assessment with helical thin-section CT. *Radiology* 208: 321–329, 1998. doi:10.1148/radiology.208.2.9680554.

13. **Harris RS, Fujii-Rios H, Winkler T, Musch G, Vidal Melo MF, Venegas JG.** Ventilation defect formation in healthy and asthma subjects is determined by lung inflation. *PLoS One* 7: e53216, 2012. [Erratum in *PLoS One* 9: doi:10.1371/annotation/0dafbfa4-2289-40ec-9f21-35b24a9302c3, 2014.] doi:10.1371/journal.pone.0053216.

14. **Harris RS, Winkler T, Musch G, Vidal Melo MF, Schroeder T, Tgavalekos N, Venegas JG.** The prone position results in smaller ventilation defects during bronchoconstriction in asthma. *J Appl Physiol (1985)* 107: 266–274, 2009. doi:10.1152/japplphysiol.91386.2008.

15. **Harris RS, Winkler T, Tgavalekos N, Musch G, Melo MF, Schroeder T, Chang Y, Venegas JG.** Regional pulmonary perfusion, inflation, and ventilation defects in bronchoconstricted patients with asthma. *Am J Respir Crit Care Med* 174: 245–253, 2006. doi:10.1164/rccm.200510-1634OC.

16. **Hopkins SR, Henderson AC, Levin DL, Yamada K, Arai T, Buxton RB, Prisk GK.** Vertical gradients in regional lung density and perfusion in the supine human lung: the Slinky effect. *J Appl Physiol (1985)* 103: 240–248, 2007. doi:10.1152/japplphysiol.01289.2006.

17. **Kaneko K, Milic-Emili J, Dolovich MB, Dawson A, Bates DV.** Regional distribution of ventilation and perfusion as a function of body position. *J Appl Physiol* 21: 767–777, 1966. doi:10.1152/jappl.1966.21.3.767.

18. **Kelly VJ, Hibbert KA, Kohli P, Kone M, Greenblatt EE, Venegas JG, Winkler T, Harris RS.** Hypoxic pulmonary vasoconstriction does not explain all regional perfusion redistribution in asthma. *Am J Respir Crit Care Med* 196: 834–844, 2017. doi:10.1164/rccm.201612-2438OC.

19. **King GG, Eberl S, Salome CM, Meikle SR, Woolcock AJ.** Airway closure measured by a technegas bolus and SPECT. *Am J Respir Crit Care Med* 155: 682–688, 1997. doi:10.1164/ajrccm.155.2.9032213.

20. **Kirby M, Mathew L, Wheatley A, Santyr GE, McCormack DG, Parraga G.** Chronic obstructive pulmonary disease: longitudinal hyperpolarized ^{3}He MR imaging. *Radiology* 256: 280–289, 2010. doi:10.1148/radiol.10091937.

21. **Leary D, Winkler T, Braune A, Maksym GN.** Effects of airway tree asymmetry on the emergence and spatial persistence of ventilation defects. *J Appl Physiol (1985)* 117: 353–362, 2014. doi:10.1152/japplphysiol.00881.2013.

22. **Lewis SM, Evans JW, Jalowayski AA.** Continuous distributions of specific ventilation recovered from inert gas washout. *J Appl Physiol Respir Environ Exerc Physiol* 44: 416–423, 1978. doi:10.1152/jappl.1978.44.3.416.

23. **Miller GW, Mugler JP 3rd, Altes TA, Cai J, Mata JF, de Lange EE, Tobias WA, Cates GD, Brookeman JR.** A short-breath-hold technique for lung pO_2 mapping with ^{3}He MRI. *Magn Reson Med* 63: 127–136, 2010. doi:10.1002/mrm.22181.

24. **Niles DJ, Kruger SJ, Dardzinski BJ, Harman A, Jarjour NN, Ruddy M, Nagle SK, François CJ, Fain SB.** Exercise-induced bronchoconstriction: reproducibility of hyperpolarized ^{3}He MR imaging. *Radiology* 266: 618–625, 2013. doi:10.1148/radiol.12111973.

25. **Park CS, Müller NL, Worthy SA, Kim JS, Awadh N, Fitzgerald M.** Airway obstruction in asthmatic and healthy individuals: inspiratory and expiratory thin-section CT findings. *Radiology* 203: 361–367, 1997. doi:10.1148/radiology.203.2.9114089.

26. **Popa V.** ATS guidelines for methacholine and exercise challenge testing. *Am J Respir Crit Care Med* 163: 292–293, 2001. doi:10.1164/ajrccm.163.1.16310b.

27. **Porra L, Monfraix S, Berruyer G, Le Duc G, Nemoz C, Thomlinson W, Suortti P, Sovijärvi AR, Bayat S.** Effect of tidal volume on distribution of ventilation assessed by synchrotron radiation CT in rabbit. *J Appl Physiol (1985)* 96: 1899–1908, 2004. doi:10.1152/japplphysiol.00866.2003.

28. **Rodriguez-Roisin R, Wagner PD.** Clinical relevance of ventilation-perfusion inequality determined by inert gas elimination. *Eur Respir J* 3: 469–482, 1990.

29. **Sá RC, Asadi AK, Theilmann RJ, Hopkins SR, Prisk GK, Darquenne C.** Validating the distribution of specific ventilation in healthy humans measured using proton MR imaging. *J Appl Physiol (1985)* 116: 1048–1056, 2014. doi:10.1152/japplphysiol.00982.2013.

30. **Sá RC, Cronin MV, Henderson AC, Holverda S, Theilmann RJ, Arai TJ, Dubowitz DJ, Hopkins SR, Buxton RB, Prisk GK.** Vertical distribution of specific ventilation in normal supine humans measured by oxygen-enhanced proton MRI. *J Appl Physiol (1985)* 109: 1950–1959, 2010. doi:10.1152/japplphysiol.00220.2010.

31. **Sá RC, Henderson AC, Simonson T, Arai TJ, Wagner H, Theilmann RJ, Wagner PD, Prisk GK, Hopkins SR.** Measurement of the distribution of ventilation-perfusion ratios in the human lung with proton MRI: comparison with the multiple inert-gas elimination technique. *J Appl Physiol (1985)* 123: 136–146, 2017. doi:10.1152/japplphysiol.00804.2016.

32. **Simon BA, Kaczka DW, Bankier AA, Parraga G.** What can computed tomography and magnetic resonance imaging tell us about ventilation? *J Appl Physiol* 113: 647–657, 2012. doi:10.1152/japplphysiol.00353.2012.

33. **Svenningsen S, Guo F, Kirby M, Choy S, Wheatley A, McCormack DG, Parraga G.** Pulmonary functional magnetic resonance imaging: asthma temporal-spatial maps. *Acad Radiol* 21: 1402–1410, 2014. doi:10.1016/j.acra.2014.08.002.
34. **Tawhai MH, Nash MP, Lin CL, Hoffman EA.** Supine and prone differences in regional lung density and pleural pressure gradients in the human lung with constant shape. *J Appl Physiol (1985)* 107: 912–920, 2009. doi:10.1152/japplphysiol.00324.2009.
35. **Thomen RP, Sheshadri A, Quirk JD, Kozlowski J, Ellison HD, Szczesniak RD, Castro M, Woods JC.** Regional ventilation changes in severe asthma after bronchial thermoplasty with ^{3}He MR imaging and CT. *Radiology* 274: 250–259, 2015. doi:10.1148/radiol.14140080.
37. **Venegas JG, Winkler T, Musch G, Vidal Melo MF, Layfield D, Tgavalekos N, Fischman AJ, Callahan RJ, Bellani G, Harris RS.** Self-organized patchiness in asthma as a prelude to catastrophic shifts. *Nature* 434: 777–782, 2005. doi:10.1038/nature03490.
38. **West JB.** *Respiratory Physiology: The Essentials*. Baltimore, MD: Lippincott Williams & Wilkins, 2012.
39. **Winkler T.** In silico modeling of airway mechanics. *Drug Discov Today Dis Models* 4: 125–129, 2007. doi:10.1016/j.ddmod.2007.12.002.
40. **Winkler T, Venegas JG.** Are all airways equal? *J Appl Physiol (1985)* 112: 1431–1432, 2012. doi:10.1152/japplphysiol.00253.2012.
41. **Winkler T, Venegas JG.** Complex airway behavior and paradoxical responses to bronchoprovocation. *J Appl Physiol (1985)* 103: 655–663, 2007. doi:10.1152/japplphysiol.00041.2007.
42. **Yang G, Stewart CV, Sofka M, Tsai CL.** Registration of challenging image pairs: initialization, estimation, and decision. *IEEE Trans Pattern Anal Mach Intell* 29: 1973–1989, 2007. doi:10.1109/TPAMI.2007.1116.

Chapter 2, in full, is a reprint of *Spatial persistence of reduced specific ventilation following methacholine challenge in the healthy human lung*, Geier ET, Neuhart I, Theilmann RJ, Prisk GK, Sá RC. This article appeared in the Journal of Applied Physiology 2018, volume 124 (5), pages 1222-1232. The dissertation author was the primary investigator and author of this paper.

CHAPTER THREE

The spatial pattern of methacholine bronchoconstriction recurs when supine, independently of posture during provocation, but does not recur between postures

J Appl Physiol 125: 1720–1730, 2018.
First published September 6, 2018; doi:10.1152/japplphysiol.00487.2018.

RESEARCH ARTICLE

The spatial pattern of methacholine bronchoconstriction recurs when supine independently of posture during provocation but does not recur between postures

Eric T. Geier,[1] Kent Kubo,[1] Rebecca J. Theilmann,[2] Gordon K. Prisk,[1] and Rui C. Sá[1]

[1]*Department of Medicine, University of California, San Diego, California; and* [2]*Department of Radiology University of California, San Diego, California*

Submitted 1 June 2018; accepted in final form 4 September 2018

Geier ET, Kubo K, Theilmann RJ, Prisk GK, Sá RC. The spatial pattern of methacholine bronchoconstriction recurs when supine independently of posture during provocation but does not recur between postures. *J Appl Physiol* 125: 1720–1730, 2018. First published September 6, 2018; doi:10.1152/japplphysiol.00487.2018.—The location of lung regions with compromised ventilation (often called ventilation defects) during a bronchoconstriction event may be influenced by posture. We aimed to determine the effect of prone versus supine posture on the spatial pattern of methacholine-induced bronchoconstriction in six healthy adults (ages 21–41, 3 women) using specific ventilation imaging. Three postural conditions were chosen to assign the effect of posture to the drug administration and/or imaging phase of the experiment: supine methacholine administration followed by supine imaging, prone methacholine administration followed by supine imaging, and prone methacholine administration followed by prone imaging. The two conditions in which imaging was performed supine had similar spatial patterns of bronchoconstriction despite a change in posture during methacholine administration; the odds ratio for recurrent constriction was mean (SD) = 7.4 (3.9). Conversely, dissimilar spatial patterns of bronchoconstriction emerged when posture during imaging was changed; the odds ratio for recurrent constriction between the prone methacholine/supine imaging condition and the prone methacholine/prone imaging condition was 1.2 (0.9). Logistic regression showed that height above the dependent lung border was a significant negative predictor of constriction in the two supine imaging conditions ($P < 0.001$ for each) but not in the prone imaging condition ($P = 0.20$). These results show that the spatial pattern of methacholine bronchoconstriction is recurrent in the supine posture, regardless of whether methacholine is given prone or supine but that prone posture during imaging eliminates that recurrent pattern and reduces its dependence on gravitational height.

NEW & NOTEWORTHY The spatial pattern of methacholine bronchoconstriction in the supine posture is recurrent and skewed toward the dependent lung, regardless of whether inhaled methacholine is administered while supine or while prone. However, both the recurrent pattern and the gravitational skew are eliminated if imaging is performed prone. These results suggest that gravitational influence on regional lung inflation and airway topography at the time of measurement play a role in determining regional bronchoconstriction in the healthy lung.

bronchoconstriction; methacholine; posture; specific ventilation

Address for reprint requests and other correspondence: E. Geier, Univ. of California, San Diego, Dept. of Medicine, 9500 Gilman Dr., La Jolla, CA 92093 (e-mail: egeier@ucsd.edu).

INTRODUCTION

Asthmatic bronchoconstriction is spatially heterogeneous (7, 12, 17, 29, 31). During a bronchoconstriction event, self-organized patches of very low ventilation form in some regions of the lung, whereas other regions continue to ventilate normally. The degree to which a patient's specific patchy pattern of low specific ventilation recurs between asthmatic episodes is a question of potential clinical importance.

In general, areas of slow space that recur over time can be understood as manifestations of local anatomical and/or functional properties of the lung. Modeling studies have shown that airway asymmetry can lead to spatially persistent foci of constriction and also that less inflated lung regions are more likely to constrict (21, 31, 32). At least one empirical study (10) has confirmed that less inflated lung regions are more likely to become ventilation defects than are more inflated regions.

In our previous work (8), we showed that many patches of ventilatory slow space resulting from methacholine inhalation recurred at the same spatial location in supine healthy subjects. There was a 46% (odds ratio 7.7) likelihood of bronchoconstricted regions recurring a week later and a 56% (odds ratio 7.7) likelihood of regions recurring 3 mo later. On average, 68% of regions that constricted in the first 2 challenges did so again in the third (odds ratio 9.8). Both recurrent and intermittent regions of bronchoconstriction were more likely to occur in the dependent lung than in the nondependent lung when supine; the volume fraction that constricted was 0.43 in the dependent lung versus 0.10 in the nondependent lung.

The relevance of the second finding (that the dependent lung was more likely to constrict than was the nondependent lung) was limited in our previous work because all elements of the experiment (methacholine administration and imaging) were performed supine. Thus, it was unclear whether the recurrent bronchoconstriction in the dependent lung was due to a gravitationally driven physiological effect or a fixed anatomical effect. In other words, we could not specify whether the data showed a predisposition in the dependent lung or a predisposition in the posterior lung, as these designations refer to the same region when supine. The goal of this study was to discern between these two alternatives by repeating the same experiment in the same subjects in two additional conditions: once with methacholine administered in the prone posture but imaging still performed in the supine posture and once with both

Table 1. *Subject characteristics and methacholine dosages used*

Subject	Sex	Age, yr	Height, m	Weight, kg	Seated FEV_1, liters (% predicted)	Methacholine PC_{20}, mg/ml	Methacholine dose, mg/ml
S1	M	21	1.60	59	3.82 (100)	2.8	4
S2	F	27	1.57	45	3.05 (101)	6.3	8
S3	M	27	1.88	96	5.59 (110)	10.0	16
S4	F	28	1.70	77	3.54 (101)	5.2	8
S5	M	41	1.78	83	3.87 (92)	10.9	16
S6	F	27	1.64	66	3.25 (99)	3.3	4
Means ± SD		29 ± 7	1.70 ± 0.12	71 ± 18	3.85 ± 0.91 (101 ± 6)	6.4 ± 3.4	9 ± 5

Three female and three male subjects were re-recruited from our previous study (8). Average age, height, and weight of the subjects are shown in the table as they were reported in the previous study (8). Average FEV_1, measured in the seated position, was 101 ± 6% predicted. Methacholine PC_{20} was determined through the standardized stepwise challenge (22), with the exception it was performed in the supine posture, as reported in the previous study (8). Each subject's methacholine dose was chosen to be the last in the stepwise challenge, i.e., the smallest that elicited a >20% drop in FEV_1. F, female; FEV_1, forced expiratory volume in one second; M, male; PC_{20}, concentration of methacholine that elicits 20% drop in FEV_1, determined by interpolation from an empirically determined dose-response curve.

methacholine administration and imaging performed in the prone posture. These data were then compared with the first set of results from the previously published data set (8), in which both methacholine administration and imaging were performed in the supine posture to look for a systematic difference in the corresponding spatial patterns of bronchoconstriction.

These two additional postural configurations (prone methacholine/supine imaging and prone methacholine/prone imaging) allowed us to address an additional question: if gravity skews the spatial pattern of methacholine constriction, is it gravity at the time of constriction or gravity at the time of imaging (or both) that matters? Skew introduced by gravitational orientation during drug inhalation would be expected to manifest similarly in the data sets in which posture during drug administration was the same (prone methacholine/supine imaging and prone methacholine/prone imaging) whereas skew introduced during imaging would be expected to manifest similarly in the conditions in which posture during imaging was the same (supine methacholine/supine imaging and prone methacholine/supine imaging). If the spatial pattern of constriction is determined primarily at the time of methacholine inhalation, we can infer that it is largely influenced by the pattern of methacholine deposition and that it is relatively static with time. On the other hand, if it is determined during imaging we may infer the opposite: that the spatial pattern of bronchoconstriction is due to factors other than methacholine deposition and that it can change to conform to a new gravitational condition.

METHODS

Human Subjects

The University of California, San Diego Human Research Protection Program reviewed and approved this study. Six subjects, the same from Geier et al. 2018 (8), were re-recruited, each passed a standard MRI safety screen, and all subjects denied any history of cardiopulmonary disease. Each subject provided written, informed consent to participate in the study. Forced expiratory volume in one second (FEV_1) measurements were made using an Easyone diagnostic Spirometer (ndd Medical Technologies, Inc., Andover, MA), and percent predicted values were obtained by comparison to National Health and Nutrition Examination Survey III reference values (9). Subjects had baseline FEV_1 values of 101% (6%). Two additional imaging sessions (prone methacholine/supine imaging and prone methacholine/prone imaging) were acquired; the subjects' concentration of methacholine that elicits 20% drop in FEV_1 (PC_{20}) values [6.4 mg/ml (SD 3.4)], methacholine doses [9 mg/ml (SD 5)] and imaging data from the supine baseline and first methacholine challenge (supine methacholine/supine imaging) from the previously published study were reused (8). Subject data as they were acquired for the previous study (8) are shown in Table 1. The time between study sessions, for each subject, is shown in Table 2. Although all subjects completed all sessions of the study, a technical issue discovered in postprocessing necessitated that the prone baseline and prone methacholine/prone imaging data for two subjects (S2 & S4) be excluded from the analysis (see *Experimental setup* below).

Table 2. *PC_{20} dose determination*

	Days from Study Enrollment for Each Study Session			
	Previous study		Current study	
	PC_{20} dose determination†	Supine baseline and supine Mch/supine imaging†	Prone Mch/supine imaging	Prone baseline and prone Mch/prone imaging
S1	0	86	442	536
S2	0	191	450	—
S3	0	327	567	571
S4	0	86	481	—
S5	0	1	312	319
S6	0	1	145	223
Mean ± SD	0 ± 0	115 ± 225	400 ± 149	464 ± 154

PC_{20} dose determination was performed for each subject on the day in which he or she was enrolled in the study. Time intervals, in days, between enrollment and each subsequent study session for each subject are shown. Only four of our six subjects had valid data for the last study, prone methacholine/prone imaging, because of an error in data acquisition (see METHODS). FEV_1, forced expiratory volume in one second; Mch, methacholine; PC_{20}, concentration of methacholine that elicits 20% drop in FEV_1. †Data from our previously published study (8). —Indicate the two sessions for which data had to be discarded following the discovery of a technical issue in data collection.

Methacholine Bronchoconstriction

In our previous study (8), each subject underwent a standard methacholine challenge test to determine the appropriate concentration of drug that could be used to elicit a moderate bronchoconstriction in the subsequent imaging sessions. Methacholine challenge testing was performed according to the standard procedures established by the American Thoracic Society (24) with the sole modification that the subject was supine during all parts of the challenge. Provocholine (methacholine chloride USP, Methapharm, Inc., Brantford, Canada) was nebulized and administered via a Koko Dosimeter (nSpire Health, Inc., Longmont, CO) in a stepwise fashion, starting at 0.03125 mg/ml and doubling each step until a 20% drop in FEV_1 was achieved. In these subjects, the maximum PC_{20} dose was 16 mg/ml.

For each subject, the methacholine concentration chosen for the rest of the study (Table 1) was the final concentration administered in the stepwise challenge, i.e., the lowest that elicited PC_{20}. Methacholine was administered via a Koko Dosimeter before imaging in either the prone or supine posture, depending on the specific imaging session (Table 2).

Methacholine action peaks between 1 and 4 min after inhalation, reaches a steady state that lasts for an average of 75 min, and then fades for an average of 57 min (5). In all three visits, the specific ventilation (SV) imaging (SVI) protocol took place 15–35 min after methacholine administration in the steady-state period of methacholine action so that SV was as constant as possible during the 20-min acquisition. Methacholine was administered to all subjects in all sessions by the same individual. Each subject was given the same instructions so that breathing during drug inhalation was as standardized as possible between subjects.

Imaging Sessions

MR imaging was performed twice at baseline, once while supine and once while prone, and three times following bronchoconstriction by methacholine. The subjects' posture was modified during methacholine administration and imaging as part of the experiment. The postural conditions were *1*) supine methacholine and supine imaging, *2*) prone methacholine and supine imaging, and *3*) prone methacholine and prone imaging. In the second condition, the subjects were turned from prone to supine directly before imaging, ~10 min after methacholine inhalation. The delay between administration and repositioning was included to ensure that the subjects had reached, while prone and before repositioning, the steady state phase of methacholine action (5). The data for supine baseline and supine methacholine/supine imaging condition were acquired in a previous study (8). The supine methacholine/supine imaging condition is the same as that from the first constriction (*day 1*) in that previous study.

FEV_1 measurements were made before imaging for the baseline scans and between methacholine inhalation (~2 min postadministration) and imaging for the bronchoconstricted scans. Supine baseline imaging was performed the same day as *condition 1*, and prone baseline imaging was performed the same day as *condition 3*. Imaging sessions were always performed in order of 1–3. The time intervals between study sessions are shown in Table 2. The long duration of the study reflects the fact that subjects were re-recruited from the prior study, and *day 1* of the previous study was treated as *day 1* of the current study.

SVI

SVI is described in detail in Sá et al. (27). This implementation of SVI was the same as in our previous work (8), with the sole exception that the subjects' posture during methacholine delivery and MR imaging was modified. A brief description of SVI is presented here.

Experimental setup. Methacholine was administered while the subject lay prone or supine (depending on the session) via a Koko Dosimeter (nSpire Health, Inc., Longmont, CO) and spirometry was performed to measure FEV_1. The subject was then fitted with a facemask (7600 Series Oro-nasal mask, Hans Rudolph). After a 10-min wait to ensure that methacholine had reached a steady-state plateau, the subject was placed into the scanner (for the condition in which subjects were imaged supine but given methacholine prone, the subjects were reoriented from prone to supine at this point). A flow-bypass device (6) was attached to the subject's facemask and medical oxygen, driven from a tank via 1/4-in. tubing, was supplied to the flow-bypass at a flow rate of ~120 l/min (chosen to exceed maximal inspiratory flow rate). Oxygen was switched on and off through actuation of a three-way valve, which occurred during subject expiration to produce a stepwise change in fraction of inspired oxygen between subsequent inspirations.

Abrupt switches in fraction of inspired oxygen, facilitated by the system above, cause a rise or fall in alveolar oxygen content. Oxygen diffuses rapidly into the tissue, and the concentration of oxygen dissolved in tissue manifests as a change in T_1-weighted signal. The rate of change from one steady state of oxygenation (and thus MR signal) to another is directly related to the rate at which resident alveolar gas is being replenished by inhaled gas. Expressed as a ratio of volumes, this is the volume of inspired gas that reaches the voxel during inspiration divided by its previous end expiratory volume ($\Delta V/V_o$) and is termed SV. Thus, SV was determined by T_1 imaging while subjects alternately breathed room air and 100% oxygen over 20 min.

The prone imaging data for two subjects (S2 & S4) had to be excluded from our analysis. These subjects laid with their arms over their heads, which obstructed the flow of gas away from the flow bypass system at the mouth. This meant that the subjects rebreathed a mixture of 100% oxygen and room air during the "room air" blocks. Because the precise mixture of gas they were breathing could not be estimated, the signal response for those imaging series could not be modeled.

Image acquisition. Using a 1.5T EXCITE HDx TwinSpeed MRI system (General Electric Medical Systems, Milwaukee, WI) and an eight-element torso coil, four two-dimensional, abutting 15-mm-thick sagittal slices of the right lung were acquired with a single-shot fast spin echo after a global inversion pulse. Inversion recovery times for each slice, respectively (medial to lateral), were 1,100, 1,335, 1,570, and 1,805 ms. Each image slice had a 40 cm $\times$ 40 cm field of view, was acquired at 128 $\times$ 128 resolution, and was reconstructed by the scanner onto a 256 $\times$ 256 matrix.

Image processing. Image processing was performed with custom-written Matlab (Mathworks, Natick, MA) code. Each scan was treated independently, and comparisons between conditions were performed after processing.

For each sagittal slice imaged (4 from each scan) a 220-image time series was created. A generalized dual-bootstrap iterative closest point algorithm (34), used in affine transformation mode, was applied to register images to a selected reference image. Images with a $>$10% change in imaged lung volume because of transformation were removed from the time series and treated as missing data, based on previous work that has shown that deformations up to 10% volume change can be accurately registered using an affine transformation (1).

Intensity time series were created for voxels within a manually drawn region of interest, and each voxel's time course was correlated with 50 modeled time courses for SV values equally spaced in $\log_{10}$ from 0.01 to 10. The modeled time course that shared the maximum correlation coefficient with the measured time course was selected as the voxel's SV. The spatial map of all voxel SV values was smoothed using a geometric algorithm with a kernel size of 7 voxels (~1 cm^2). Maps from the four sagittal slices in each scan were combined to create a histogram of voxel-SV values for the entire imaged right lung (Fig. 1).

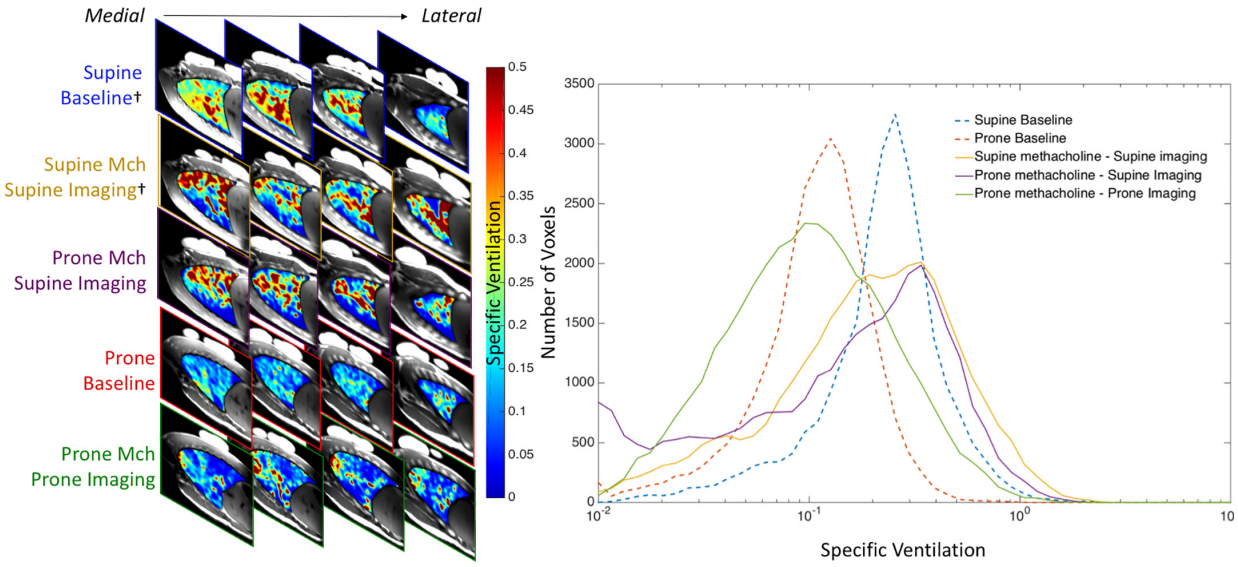

Fig. 1. *Left*: multislice SV maps for one subject (S3) from five imaging sessions. Each row of images represents a separate scanning session/condition. Slices are presented medial to lateral from left to right, with each column representing a sagittal slice of the subject's right lung in each of the sessions. Each map is oriented so that the gravitationally dependent lung is toward the bottom of the imaging frame. In the supine images the posterior lung is gravitationally dependent, whereas in the prone images the anterior lung is gravitationally dependent. *Right*: SV histograms from the same subject (S3) for both baseline (supine and prone) and all three constricted conditions. Baseline data are shown as dashed lines whereas constricted data are shown as solid lines. All histograms are constructed from a compilation of all four imaging slices for the respective condition. †Data from our previously published study (8). Mch, methacholine; SV, specific ventilation.

SV Heterogeneity

SV heterogeneity, as has been reported by our group previously (26), was taken as the full-width at half maximum of a log(Gaussian) function fit to the SV histogram of the entire imaged right lung (Fig. 1). This metric was computed for the two baseline scans and three bronchoconstricted scans for each subject.

Identification of bronchoconstricted regions. SV maps were normalized between conditions to account for changes in global SV, which can be the result of changes in tidal volume and/or FRC. Table 3 shows the prenormalized mean SV and imaged thoracic cage volumes for each condition.

Following normalization, bronchoconstricted maps were spatially correlated with their respective baseline maps, prone to prone and supine to supine. Because the average imaged lung volume during bronchoconstriction was 17% (SD 13) larger than at baseline, a difference that exceeded the 10% limit to which we can confidently register using an affine transformation, we could not use our standard image registration approach. Instead, we divided each multislice set of images into 12 (dependent-nondependent) × 12 (apical-basal) × 4 (medial-lateral, defined by slice) volume elements, the extent of which were based on the size of the lung, redefined for each condition. Comparisons were then made between volume elements in different conditions with the same 12 × 12 × 4 coordinate (Fig. 2). Each of the 12 × 12 × 4 volume elements contained typically between 25 and 100 voxels (depending on its location in the lung). Individual voxels were not compared between conditions.

For the purposes of this study, a volume element *i* was considered constricted if

$$SV^{i}_{challenge} < 0.5 * SV^{i}_{baseline} \quad \text{and} \quad SV^{i}_{challenge} < \overline{SV}_{baseline} \qquad (1)$$

where $\overline{SV}$ represented the center of the SV distribution.

This imposed two conditions for the constriction designation: *1*) SV must have decreased significantly from baseline and *2*) that a volume element labeled "constricted" was ventilating less than average. These criteria were designed to prevent two types of lung regions from being misclassified as constricted, *1*) regions with consistently low ventilation (even at baseline) that were not necessarily responding to methacholine and *2*) regions with unusually high SV at baseline that may have experienced a reduction in ventilation because of methacholine but not one severe enough to hamper gas exchange.

The constriction designation we use in this study is somewhat analogous to the ventilation defect designation that appears in other, similar studies (10–12, 21, 32, 33). Ventilation defects are clusters of voxels that represent ventilatory slow space. They can be identified through at least three different methods: manually by an experienced observer, through hierarchical k-means clustering (18), or by spatial fuzzy c-means clustering (15).The lung elements in our study that are designated as constricted certainly include voxels that would be designated as ventilation defect, but they also include others that strongly respond to methacholine, as indicated by their >50% drop in FEV_1 but not to the point that they would be considered "defects." For example, a lung element with a relatively high SV (say of 0.3 compared with a lungwide mean SV of 0.2) that fell to an SV of 0.14 (compared with a lungwide mean SV of 0.2) would be considered constricted but would probably not be considered to be part of a defect. Conversely, an element with extremely low SV (say 0.02 compared with a lung-wide mean of 0.2) at baseline that stayed the same after methacholine may be considered a defect in both conditions but would not be classified as constricted in our analysis.

Height from the dependent lung as a predictor of constriction. The vertical height of each 12 × 12 × 4 volume element from the dependent lung border was measured and, along with constriction outcome for each condition, concatenated for all subjects. For each postural condition, a logistic regression model was used to estimate the how the ln(odds) of constriction (our binary outcome variable) varied as a function of a volume element's height (Fig. 3).

Odds ratio for repeat constriction. Constriction maps were compared between days to determine the odds ratio for repeat constriction

Table 3. *Global metrics of constriction for all six subjects in all imaging conditions*

	FEV_1, l/s (% Change From Baseline)				
	Supine baseline†	Prone baseline	Supine Mch/supine imaging†	Prone Mch/supine imaging	Prone Mch/prone imaging
S1	3.55	3.80	2.86 (−19)	2.94 (−23)	3.40 (−11)
S2	2.91		2.53 (−13)	2.49 (−19)	
S3	4.99	5.01	3.92 (−21)	4.11 (−18)	4.10 (−18)
S4	3.05		2.34 (−22)	2.84 (−16)	
S5	3.70	3.56	3.14 (−15)	2.99 (−19)	2.54 (−29)
S6	3.11	2.95	2.38 (−22)	2.06 (−30)	2.59 (−12)
Mean ± SD	3.53 ± 0.78	3.83 ± 0.86	2.86 ± 0.60 (−19 ± 4)	2.91 ± 0.69 (−20 ± 6)	3.16 ± 0.74 (−17 ± 8)
	Mean Specific Ventilation, Prenormalization (% Change from Baseline)				
S1	0.25	0.10	0.10 (−61)	0.19 (−24)	0.12 (26)
S2	0.17		0.09 (−46)	0.08 (−53)	
S3	0.26	0.13	0.28 (5)	0.23 (−12)	0.15 (16)
S4	0.16		0.13 (−16)	0.20 (23)	
S5	0.33	0.24	0.33 (−2)	0.31 (−6)	0.14 (−43)
S6	0.37	0.13	0.21 (−42)	0.15 (−60)	0.16 (22)
Mean ± SD	0.26 ± 0.08	0.15 ± 0.07	0.19 ± 0.10 (−27 ± 27)	0.19 ± 0.08 (−22 ± 31)	0.14 ± 0.01 (5 ± 32)
	Imaged Thoracic Cage Volume, ml (% Change from Baseline)				
S1	851	844	927 (9)	831 (−2)	811 (−4)
S2	600		732 (22)	655 (9)	
S3	930	980	1,206 (30)	1,141 (23)	1,371 (40)
S4	559		785 (40)	698 (25)	
S5	509	736	518 (2)	556 (9)	827 (12)
S6	497	551	561 (13)	567 (14)	637 (16)
Mean ± SD	658 ± 186	778 ± 181	788 ± 254 (19 ± 14)	741 ± 220 (13 ± 10)	912 ± 318 (16 ± 18)
	FWHM of SV Distribution (% Change from Baseline)				
S1	0.44	0.47	0.92 (110)	0.79 (80)	0.43 (−9)
S2	0.32		1.03 (224)	0.79 (343)	
S3	0.43	0.48	0.91 (111)	0.99 (129)	0.93 (93)
S4	0.57		0.46 (−20)	0.49 (−15)	
S5	0.61	0.52	0.55 (−9)	1.12 (85)	0.92 (78)
S6	0.32	0.52	1.00 (210)	1.86 (475)	0.94 (80)
Mean ± SD	0.45 ± 0.12	0.50 ± 0.02	0.81 ± 0.25 (104 ± 104)	1.11 ± 0.48 (183 ± 186)	0.80 ± 0.25 (60 ± 47)
	Volume Fraction of Lung Constricted				
S1			0.32	0.27	0.06
S2			0.25	0.32	
S3			0.38	0.34	0.39
S4			0.34	0.20	
S5			0.19	0.19	0.29
S6			0.27	0.30	0.31
Mean ± SD			0.29 ± 0.07	0.27 ± 0.06	0.26 ± 0.14

The two left columns show the baseline (premethacholine) values of each metric measured in both the supine and prone postures. See text for details. Postmethacholine values are shown in the right three sets of columns with headings referring to their respective conditions. Relative changes from baseline are indicated as percentages. Only four of our six subjects had valid data for the last study, prone methacholine/prone imaging, because of an error in data acquisition (see METHODS). FEV_1, forced expiratory volume in one second; FWHM, full width half maximum; Mch, methacholine; SV, specific ventilation. †Indicates data from our previously published study (8).

of a 12 × 12 × 4 volume element in the second or third (prone methacholine/supine imaging or prone methacholine/prone imaging, respectively) conditions given a constriction in the first (supine methacholine/supine imaging) condition, and the odds ratio for repeat constriction in the third (prone methacholine/prone imaging) given a constriction in the second (prone methacholine/supine imaging). For the comparison between supine methacholine/supine imaging and prone methacholine/supine imaging, this process was straightforward because the imaging planes were in the same position and orientation. The comparisons between the supine imaging conditions, supine methacholine/supine imaging and prone methacholine/supine imaging, and the prone methacholine/prone imaging condition is less intuitive because of the flip in gravitational orientation. A volume element in the dependent lung while supine is now in the nondependent lung while prone, and vice versa. Because of the differences in lung container shape and gravitational stretch between the prone and supine postures, it is likely that each volume element encompasses a slightly different region of lung tissue after the flip (e.g., a basal/posterior unit was dependent and compressed while supine, but is now nondependent and stretched while prone, so it may now contain less tissue and/or some tissue from elements that were neighbors while supine). Thus, comparisons between the supine methacholine/supine imaging and prone methacholine/prone imaging conditions must be made with this limitation in mind.

Statistics

R (25) was used for all statistical analyses performed in this study. Paired *t*-tests were performed using the stats package (25) to determine how prone versus supine posture affected baseline measurements of FEV_1, SV heterogeneity, mean SV, and thoracic cage volume. Only data from subjects with both measurements were used for this last computation.

Linear mixed effects models were generated using the lme4 package (2) to investigate the dependence of metrics of constriction (Table 2, Fig. 4) on the postural condition of the experiment, given the missing measurements for two subjects. For each model, the postural condition of the experiment (supine methacholine/supine imaging, prone methacholine, supine imaging, etc.) or pair of experiments was taken as a fixed effect and subject was taken as a random effect. *P*

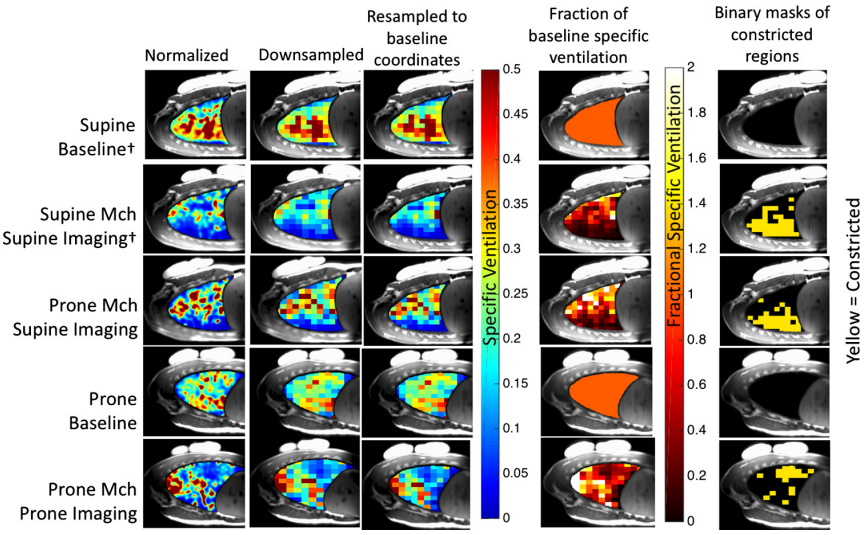

Fig. 2. Processing flow for subject S3's midclavicular (second slice) SV map in all five study conditions. The first column of each row shows the normalization based on the total SV (compiled from all four slices, only the midclavicular slice is shown) of the supine baseline condition. Maps from each slice were then downsampled (second column) to a 12 × 12 grid of volume elements and then projected onto the relevant baseline image (third column) for further analysis. Fractional SV (fourth column) was computed by dividing maps by the relevant baseline condition map. For baseline data this metric is, by definition, 1.0 everywhere. Elements were classified as constricted (fifth column) if their fractional SV was less than 0.5 and their normalized SV was less than the center of the baseline SV distribution. In each case, the gravitationally dependent lung is shown at the bottom of the image, as it was during imaging. †Data from our previously published study (8). Mch, methacholine; SV, specific ventilation.

values were obtained by a likelihood ratio test of the model with the fixed effect (postural condition) versus a null model with no fixed effect.

Logistic regression models were fit using the glm package (25) to characterize how the likelihood of constriction varied as a function of height above the dependent lung. McFadden's pseudo-R^2 was used to estimate the strength of the model fit (22). Formally, McFadden's $R^2 = 1 - \ln(L_M)/\ln(L_0)$ where L_M is the likelihood for the model with the chosen predictors and L_0 is the likelihood for a null model with no predictors. A higher value of McFadden's R^2 means that more of the variance in the data is being explained by the logistic regression model (14). The P value (Wald Test) for each model and the fit coefficient for height are also reported in Fig. 3. To characterize the uncertainty of our logistic regression models, we used a data-driven bootstrapping approach. For each postural condition, we resampled with replacement from our measured data set of height versus constriction (keeping the links between the two intact) until a set of equal size to the original was obtained. A logistic regression was then fit to this resampled data set, and the P value, fit coefficients, and McFadden's R^2 of the model were recorded. We repeated this process 1,000 times and took the standard deviation of each set of 1,000 outputs to be the uncertainty of our original fit.

A log transformation was applied to the odds ratios account for their intrinsic positive skew and thus make statistical testing possible

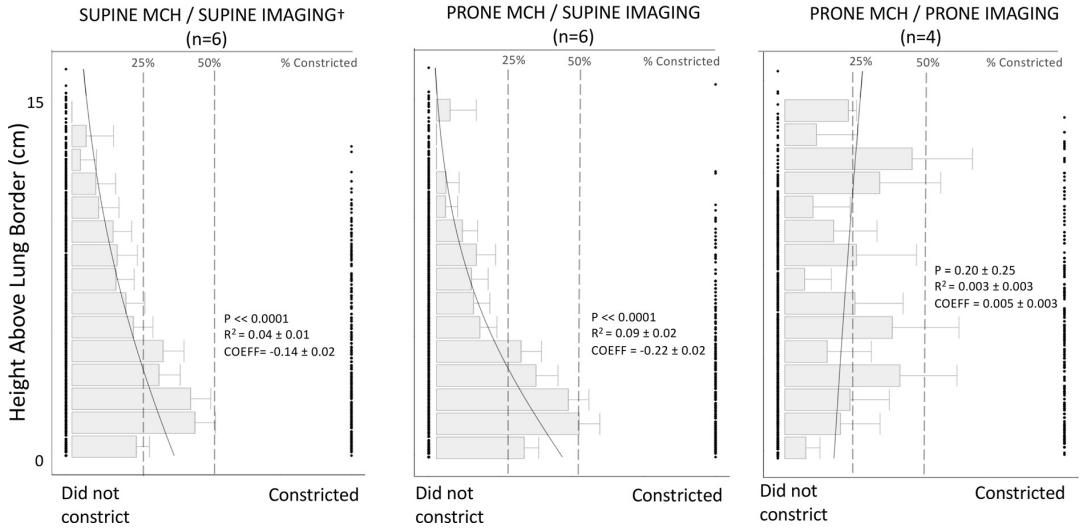

Fig. 3. For supine Mch/supine imaging (*left*), prone Mch/supine imaging (*middle*), and prone Mch/prone imaging (*right*), the constricted/nonconstricted binary outcome variable is shown as a function of height above the dependent lung border for each volume element in the study (each element is a point). A black solid line depicts the average best-fit logistic regression model, as detailed in the text. Average and standard deviations for the bootstrapped P values, McFadden's pseudo-R^2s, and fit coefficients (COEFF) are indicated next to the fit line. Also depicted as semishaded horizontal bars in each graph are the proportions of volume elements in each 1-cm bin that constricted following Mch, with error bars indicating the upper bound of the 95% confidence interval for each. The number (n) of subjects whose data was used to construct each logistic regression is indicated above each chart. †Data from our previously published study (8). Mch, methacholine.

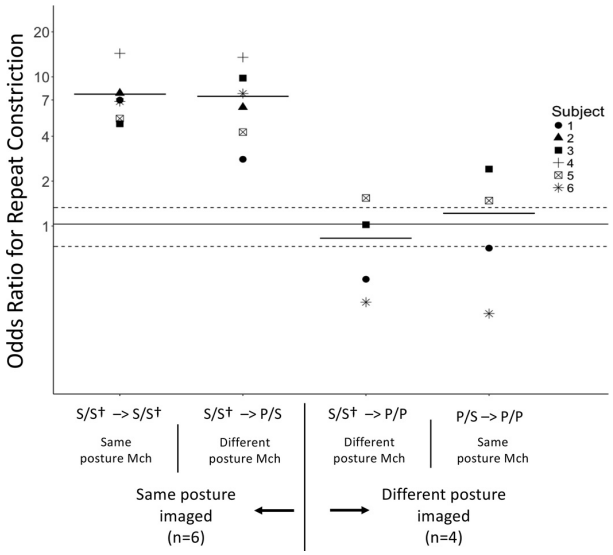

Fig. 4. Scatterplot of the odds ratios, on a log scale, for repeat constriction given a prior constriction in a previous study. The postures for each phase of the two studies in each pair are indicated on the *x*-axis; supine (S) and prone (P) for methacholine/imaging respectively, e.g., S/S refers to supine methacholine/supine imaging and S/S → P/S refers to the comparison between the supine methacholine supine imaging condition and the prone methacholine/supine imaging condition. Intrapair differences in posture during methacholine and/or imaging are indicated below the *x*-axis. A linear mixed effects model showed a significant fixed effect of experiment pair ($P < 0.001$) on the odds ratio for repeat constriction. Subjects are given unique symbols, and short solid lines represent group averages for each pair of studies. The solid horizontal line spanning the plot at 0.023 represents the mean log(odds) for 1,000 bootstrap samples with spatially random constriction, and the dashed lines represent two standard deviations of the bootstrapped means in each direction. Previous constriction was predictive of subsequent constriction for the leftmost two pairs [ln(odds) of data was greater than ln(odds) of spatially random model, $P = 0.004$ for S/S → S/S and $P = 0.006$ for S/S → P/S (Bonferroni-corrected)] but not for the rightmost two pairs [ln(odds) of data was not greater than ln(odds) of spatially random model, $P > 0.99$ for S/S → P/P and $P > 0.99$ for P/S → P/P (Bonferroni-corrected)]. The number (*n*) of subjects whose data was used in each comparison is indicated below the *x*-axis. †Data from our previously published study (8).

(3, 4). To help interpret the odds ratios for repeat constriction, we modeled the null hypothesis that constriction in the first condition does not predict constriction in a subsequent condition. To do this, we computed the odds ratio for repeat constriction between the first condition, supine methacholine/supine imaging, and 1,000 modeled data sets in which all subjects had randomly allocated (but proportionally representative, as defined by each subject's average fraction of constricted lung between the subsequent two conditions) constriction. The average of these 1,000 modeled study pairs was taken to represent the odds ratio for repeat constriction, assuming no spatial specificity for constriction in the second condition. A bootstrap randomization test with 1,000 iterations was used to determine if the observed ln(odds) for repeat constriction were statistically different from the null model for each pair of studies. Because four comparisons were performed (one for each pair of studies), the *P* values from these bootstrap tests were Bonferroni-corrected.

Similarly, we modeled a first-order hypothesis that constriction is predicted only by the effect of height above the dependent lung border as characterized by our best-fit logistic regression models (Fig. 3). For this, 1,000 modeled data sets for each postural condition were computed in which each lung element's likelihood of constriction was determined by its height above the dependent lung. The odds ratio for constriction in the model data, given constriction in the observed data, was then computed for each of the 1,000 repeats for each comparison of interest. The mean and standard deviation of these 1,000 odds ratios were taken to be representative of the odds ratio for repeat constriction within/between postural conditions, given the predisposing factor of height above the dependent lung alone.

Throughout the text, results are presented as mean (standard deviation).

RESULTS

Baseline Measurements

At baseline neither FEV_1, nor the full width half maximum of the SV distribution, nor the thoracic cage volume varied between the prone and supine postures ($P = 0.89$, $P = 0.47$, and $P = 0.21$, respectively, two-tailed paired *t*-tests). Mean SV at baseline was lower while prone than while supine ($P = 0.02$).

Lung-Wide Metrics of Constriction

FEV_1 decreased for all subjects following methacholine (as imposed by the study design), and the heterogeneity of SV increased on average (Table 3). Linear mixed effects models showed that posture during methacholine inhalation and/or imaging had no significant fixed effect on the methacholine-induced fall in FEV1 ($P = 0.96$) and no significant fixed effect on the increase in SV heterogeneity as measured by the change in the full width half maximum of the subjects' SV distributions ($P = 0.09$). The percent change in mean SV did not differ significantly based on the subjects' posture during methacholine delivery and/or imaging ($P = 0.18$), nor did the change in thoracic cage volume ($P = 0.17$).

On average, 29% (SD 7) of the lung (by volume) constricted following supine methacholine inhalation when the subject was imaged supine, 27% (SD 6) of the lung constricted following prone methacholine inhalation when the subject was imaged supine, and 26% (SD 14) of the lung constricted following prone methacholine inhalation when the subject was imaged prone (Table 3). A linear mixed effects model showed no significant fixed effect of this metric on posture during methacholine and/or imaging ($P = 0.80$).

Height from the Dependent Lung Border as a Predictor of Constriction

Figure 3 shows the binary outcome variable, constriction/nonconstriction, as a function of height above the dependent lung border, along with the corresponding best fit logistic regression model. Bar graphs of the fraction of lung that constricted in each 1-cm bin of height are superimposed. A volume element's height from the dependent lung border was a significant predictor of constriction in the two conditions in which imaging was performed supine (supine methacholine/supine imaging and prone methacholine/prone imaging) but not when imaging was performed prone (prone methacholine/prone imaging). The coefficient of the logistic regression was larger (more negative), and the predictive value of height (measured by McFadden's pseudo-R^2) was stronger in the prone methacholine/supine imaging condition than in the supine methacholine/supine imaging condition. The coefficient of a logistic regression, which is somewhat analogous to the slope of a linear regression, quantifies the rate by which the

ln(odds) of an outcome (in this case, constriction vs. nonconstriction) changes as a function of the independent variable (in this case, height above the dependent lung).

Odds Ratio for Recurrent Constriction of a Volume Element

In our previously published study (8) we showed that a lung volume element that had previously constricted was 7.7 times more likely [odds ratio 7.7 (SD 3.5)] to constrict during a subsequent study in which posture was the same both during methacholine inhalation and while imaging. In this study, we computed the odds ratios for repeat constriction between data from the first imaging session of our previously published study, in which supine methacholine administration was followed by supine imaging, and the new data acquired during two altered experimental conditions, prone methacholine administration followed by supine imaging, and prone methacholine administration followed by prone imaging (Fig. 4). Furthermore, we computed the odds ratio for repeat constriction between the two new conditions in this study, prone methacholine/supine imaging and prone methacholine/prone imaging, to determine the effect of solely modifying posture during imaging. We found that the odds ratio for repeat constriction between supine methacholine/supine imaging and prone methacholine/supine imaging was 7.4 (SD 3.9), the odds ratio for repeat constriction between the supine methacholine/supine imaging condition and the prone methacholine/prone imaging condition was 0.8 (SD 0.6), and the odds ratio for repeat constriction between the prone methacholine/supine imaging and prone methacholine/prone imaging conditions was 1.2 (SD 0.9) (Fig. 4).

A linear mixed effects model showed that the log-transformed odds ratios for repeat constriction varied between study pairs ($P < 0.001$). One thousand iterations of a model of our experiment with random (but proportionally representative) patterns of constriction showed that completely random constriction in the second condition (for all subjects) would result in an average odds ratio of 1.0 (SD 0.2). For the two study pairs in which the posture during imaging was the same (supine), a previous constriction event in a lung element was a strong predictor for a subsequent constriction event; the ln(odds) of the data was greater than the than ln(odds) of the spatially random model, $P = 0.004$ for supine methacholine/supine imaging $\rightarrow$ supine methacholine/supine imaging and $P = 0.006$ for supine methacholine/supine imaging $\rightarrow$ prone methacholine/supine imaging (Bonferroni-corrected). For the two study pairs in which the posture during imaging was different (prone vs. supine) a previous constriction event in a lung element did not predict a subsequent constriction event; the ln(odds) of the data was not different than the than ln(odds) of the spatially random model, $P > 0.99$ for supine methacholine/supine imaging $\rightarrow$ prone methacholine/prone imaging, and $P > 0.99$ for prone methacholine/supine imaging $\rightarrow$ prone methacholine/prone imaging [Bonferroni-corrected]).

First-order models of constriction, which incorporated the logistic regressions depicted in Fig. 3, allowed us to calculate the expected odds ratio for recurrent constriction given the effect of height above the dependent lung. These models showed that the height dependence alone would result in an odds ratio of 1.3 (SD 0.4) for repeat constriction between two subsequent supine methacholine/supine imaging challenges, an odds ratio of 1.4 (SD 0.5) for repeat constriction between the supine methacholine/supine imaging and prone methacholine/supine imaging condition, and an odds ratio of 1.0 (SD 0.3) for repeat constriction between prone methacholine/supine imaging and prone methacholine/prone imaging condition.

DISCUSSION

In brief, our data lead to two main inferences: *1*) administering methacholine while prone as opposed to while supine neither dampens the nondependent-dependent gradient of constriction nor diminishes the likelihood of a volume element recurrently constricting if imaging is still performed supine, and *2*) the prone posture while imaging eliminates the nondependent-dependent gradient of constriction and greatly diminishes the likelihood of a volume element recurrently constricting when compared with a previous supine imaging session.

Constriction in the supine methacholine/supine imaging study was a strong predictor of constriction in the prone methacholine/supine imaging condition, even though methacholine was administered in a different posture. In contrast, a volume element that constricted in the prone methacholine/supine imaging session has a no better than random chance of constricting in the prone methacholine/prone imaging session [odds ratio 1.2 (SD 0.9) vs. 1.0 (SD 0.2) for the random model, $P > 0.99$]. This suggests that the spatial pattern of methacholine bronchoconstriction is mostly independent of posture during drug inhalation, yet it is profoundly influenced by posture at the time of measurement. Because drug action peaked and reached a plateau in the same posture as methacholine was administered, we can further infer that posture during the peak of methacholine action has little effect on the spatial pattern of methacholine constriction if posture is subsequently changed.

It has been shown that methacholine distributes heterogeneously throughout the lung and that changing posture from seated to supine alters the deposition pattern of the drug (28). Furthermore, it has been shown that heterogeneity of deposition affects the potency of methacholine (20). However, our data make it clear that the pattern of methacholine deposition in the prone versus supine posture does not affect the degree to which regions of lung recurrently constrict, which means that the drug itself or the mechanisms by which it becomes spatially selective must be somehow distributed throughout the lung.

The pattern of methacholine deposition may, however, affect the gravitational pattern of constriction in a paradoxical way. The skew toward constriction in the dependent lung was stronger (larger effect size measured by McFadden's R^2) and steeper (more negative fit coefficient) in the prone methacholine/supine imaging condition than it was in the supine methacholine/supine imaging condition. It is unclear why this would be the case but one explanation may be that more uniform distribution of methacholine in the prone posture causes more uniform smooth muscle activation, which in turn allows for underlying physiological processes to manifest more clearly.

The dependent skew in constriction evident in our two supine imaging conditions has been reported previously in subjects with asthma (10, 11, 19, 30) and may be driven by gravitational influence on regional lung inflation. The dependent lung is compressed by the weight of the lung above it (13) and thus is likely to be less inflated than tissue in the nonde-

pendent lung. One of several predictions made by modeling studies is that the decrease in expansion-mediated parenchymal forces characteristic of less inflated regions leads to easier airway closure and therefore, a predisposition toward constriction under stress (31–33). The skew toward constriction in the dependent lung in our data is consistent with this prediction. The less significant dependent skew in the prone imaging condition may also be consistent with a model of expansion-mediated parenchymal forces predisposing a region toward bronchoconstriction, because studies have shown that lung density is more vertically homogeneous while prone than while supine (13, 23), and at least one study (16) suggests that alveolar stress is more uniform while prone than while supine.

Furthermore, the less significant dependent skew while prone echoes part of a previous report by Harris et al. (11). Utilizing ^{13}NN-saline positron emission tomography, Harris showed that the vertical gradient in lung fractional gas content changed following methacholine in the supine posture but not in the prone posture. Thus, the gravitational effect of methacholine constriction on lung fractional gas content was stronger while supine than while prone, just as the gravitational effect on likelihood of constriction was stronger in our study while supine than while prone. Another finding of the Harris study [that ventilation defects were smaller in the prone posture than in the supine posture (25% vs. 41%)] is visible as a very small effect in our study that was not statistically significant; the volume fraction of constriction in our subjects was less while prone [26% (SD 13)] than while supine [27% (SD 6) for prone methacholine, 29% (SD 7) for supine methacholine]. However, at least one finding of the Harris study (that ventilation defects were, by and large, dependent even while prone) is not evident in our study. The best-fit logistic regression model to the prone methacholine/prone imaging condition did not find a significant nondependent-dependent trend ($P = 0.20$) (Fig. 3). This may be because of the inherent difference in our definition of constriction versus the definition of a ventilation defect (see *Identification of bronchoconstricted regions* above).

However, only part of the overall spatially repeatable pattern of bronchoconstriction can be explained by gravitational height alone. By using first-order models, we predicted that the odds ratio for repeat constriction given the effect of height alone should be 1.3 (SD 0.4) for repeated supine methacholine/supine imaging sessions and 1.4 (SD 0.5) for recurrent constriction between supine methacholine/supine imaging and prone methacholine/supping imaging. These predictions based on gravitational tendency are much less than the observed odds ratios: 7.7 (SD 3.5) for repeat supine methacholine/supine imaging sessions and 7.4 (SD 3.9) for repeat constriction between supine methacholine/supine imaging and prone methacholine/supine imaging, which suggests that one or more additional factors must be at play. Furthermore, the relatively modest effect sizes of the height-based logistic regressions [Fig. 3, McFadden's $R^2 = 0.04$ (SD 0.01) for supine methacholine/supine imaging and McFadden's $R^2 = 0.09$ (SD 0.02) for prone methacholine/supine imaging] make it clear that gravitational height alone cannot account for the markedly recurrent pattern of bronchoconstriction.

In healthy subjects without anatomical remodeling because of disease, gravitational compression of lung tissue may act in concert with other factors to enforce a spatially recurrent pattern of bronchoconstriction. Leary et al. (21) have shown that recurrent constriction can also be caused by the innate asymmetry of the airway tree. Although airway asymmetry alone cannot be responsible for spatially recurrent bronchoconstriction (or else the pattern would have been at least partially recurrent between the supine and prone postures), it may play a significant role in conjunction with gravity. It is likely that innate anatomical features, superimposed upon by gravitational compressive/expansive forces, form a topography that accounts for the predisposition of some regions toward constriction. In subjects with asthma, one might speculate that structural pathology and inflammation could add yet more layers of to the topography.

It is also interesting to note that in Fig. 1, some voxels paradoxically experienced an increase in SV following methacholine or else remained close to their baseline value of SV. Modeling of bronchoconstriction in an airway tree has predicted that ventilation can be redistributed away from ventilation defects to other regions of the lung to maintain adequate overall ventilation (32). In our study, the between-subjects average fractional SV (methacholine SV/baseline SV) in lung units that were not classified as constricted was 1.29 (0.15). This means that there was a relative increase (postnormalization) in SV outside of the constricted regions, which is consistent with the previous model prediction.

Limitations. Our study is limited by the fact that we used a binary definition of constriction that is based on a change between baseline SVI and methacholine SVI. The marked similarity between the group average constriction fraction in each postural condition could hint that a particular percentage of lung will always be classified as constricted because of the method alone. However, there is a large degree of variability in constriction fraction between different days in the same subject (maximum intrasubject variability for this study was 0.06–0.32). Furthermore, the choice to use a PC_{20} dose of methacholine was made to elicit bronchoconstriction that was as consistent as possible between study days and between subjects, so this similarity in group average constricted fraction may be a result of this choice.

Another limitation is that the SVI measurement takes 18 min and 20 s to complete, although the bronchoconstriction in our study is due to a drug with a transient effect. Although methacholine action, on average, plateaus for 75 min after drug administration, the effect is variable between subjects (5). Thus, it is possible that bronchoconstriction ebbed during the SVI measurement because of metabolism of the drug. The SVI technique, as implemented, cannot capture this dynamic effect. Instead, it would report the time-averaged SV for each voxel. To avoid this complication, we imaged 15–35 min after methacholine administration, while drug action was as steady state as possible.

Our study is also limited because of a small sample size, especially for the prone methacholine/prone imaging condition in which data from two subjects had to be excluded. There is potential for sampling bias, especially when making comparisons between conditions. However, in Fig. 4, all four subjects who had acceptable data for each condition saw the same effect of changing posture during imaging—a decrease in the odds ratio for repeat constriction. In Fig. 3, the prone methacholine/prone imaging logistic regression was using data from 4 subjects instead of 6, but still encompassed 1,113 total lung regions. To test for differences between conditions in each of

our metrics, we used a linear mixed-effects model to account for the difference in sample size.

A further limitation of our study is that the imaged volume encompassed only 80% of one lung. The absence of the most medial and most lateral aspects of the right lung in our analysis is unlikely to affect our results, as our previous study showed a lack of difference in the spatial pattern of constriction between the medial and lateral slices (8). However, any systematic differences in the effect of posture on bronchoconstriction in the left versus right lung will not have been captured by this study.

Conclusion

The results of our study suggest that height above the dependent lung is a predictor of bronchoconstriction following methacholine when a subject lies supine but is not a predictor when a subject lies prone. This may suggest that differences in regional lung inflation play a role in determining the spatial pattern of methacholine bronchoconstriction, because lung inflation is more homogeneous while prone than while supine (13, 23). Furthermore, we have shown that changing posture during methacholine administration from supine to prone neither affects the spatial repeatability of constriction nor decreases the dependent (posterior) skew in constriction if imaging is subsequently performed supine. This suggests that the effects of the methacholine deposition pattern on the spatial pattern of bronchoconstriction, if they exist, can be overwhelmed by mechanical and/or anatomical factors.

ACKNOWLEDGMENTS

The authors thank Dr. Laura Crotty-Alexander for acting as medical advisor and Katie Kinninger for help with the methacholine challenge tests. This study relied upon algorithms developed by Amran K. Asadi and Ian Neuhart. Fred Cook developed hardware that made our protocol more streamlined and robust. A. Kizhakke Puliyakote provided help during data collection. We are extremely grateful to our subjects, who were each kind enough to come back for these follow-up studies.

GRANTS

Eric Geier's work was funded by NHLBI F30 HL-127980-3. The work was also funded by NHLBI R01 HL-119263.

DISCLOSURES

No conflicts of interest, financial or otherwise, are declared by the authors.

AUTHOR CONTRIBUTIONS

E.T.G., R.J.T., G.K.P., and R.C.S. conceived and designed research; E.T.G., K.K., and R.C.S. performed experiments; E.T.G., K.K., and R.C.S. analyzed data; E.T.G., K.K., R.J.T., G.K.P., and R.C.S. interpreted results of experiments; E.T.G. and G.K.P. prepared figures; E.T.G. drafted manuscript; E.T.G., K.K., R.J.T., G.K.P., and R.C.S. edited and revised manuscript; E.T.G., K.K., R.J.T., G.K.P., and R.C.S. approved final version of manuscript.

REFERENCES

1. **Arai TJ, Villongco CT, Villongco MT, Hopkins SR, Theilmann RJ.** Affine transformation registers small scale lung deformation. *Conf Proc IEEE Eng Med Biol Soc* 2012: 5298–5301, 2012. doi:10.1109/EMBC.2012.6347190.
2. **Bates D, Mächler M, Bolker B, Walker S.** Fitting linear mixed-effects models using lme4. *J Stat Softw* 67: 1–48, 2015. doi:10.18637/jss.v067.i01.
3. **Bland JM, Altman DG.** Transforming data. *BMJ* 312: 770, 1996. doi:10.1136/bmj.312.7033.770.
4. **Bland JM, Altman DG.** Statistics notes. The odds ratio. *BMJ* 320: 1468, 2000. doi:10.1136/bmj.320.7247.1468.
5. **Cartier A, Malo JL, Bégin P, Sestier M, Martin RR.** Time course of the bronchoconstriction induced by inhaled histamine and methacholine. *J Appl Physiol Respir Environ Exerc Physiol* 54: 821–826, 1983. doi:10.1152/jappl.1983.54.3.821.
6. **Cook FR, Geier ET, Asadi AK, Sá RC, Prisk GK.** Rapid prototyping of inspired gas delivery system for pulmonary MRI research. *3D Print Addit Manuf* 2: 196–203, 2015.
7. **Dunnill MS.** The pathology of asthma, with special reference to changes in the bronchial mucosa. *J Clin Pathol* 13: 27–33, 1960. doi:10.1136/jcp.13.1.27.
8. **Geier ETT, Neuhart I, Theilmann RJJ, Prisk GKK, Sá RCC.** Spatial persistence of reduced specific ventilation following methacholine challenge in the healthy human lung. *J Appl Physiol (1985)* 124: 1222–1232, 2018. doi:10.1152/japplphysiol.01032.2017.
9. **Hankinson JL, Odencrantz JR, Fedan KB.** Spirometric reference values from a sample of the general U.S. population. *Am J Respir Crit Care Med* 159: 179–187, 1999. doi:10.1164/ajrccm.159.1.9712108.
10. **Harris RS, Fujii-Rios H, Winkler T, Musch G, Vidal Melo MF, Venegas JG.** Ventilation defect formation in healthy and asthma subjects is determined by lung inflation. *PLoS One* 7: e53216, 2012. [Erratum in PLoS One 9: 2014.] doi:10.1371/journal.pone.0053216.
11. **Harris RS, Winkler T, Musch G, Vidal Melo MF, Schroeder T, Tgavalekos N, Venegas JG.** The prone position results in smaller ventilation defects during bronchoconstriction in asthma. *J Appl Physiol (1985)* 107: 266–274, 2009. doi:10.1152/japplphysiol.91386.2008.
12. **Harris RS, Winkler T, Tgavalekos N, Musch G, Melo MF, Schroeder T, Chang Y, Venegas JG.** Regional pulmonary perfusion, inflation, and ventilation defects in bronchoconstricted patients with asthma. *Am J Respir Crit Care Med* 174: 245–253, 2006. doi:10.1164/rccm.200510-1634OC.
13. **Hopkins SR, Henderson AC, Levin DL, Yamada K, Arai T, Buxton RB, Prisk GK.** Vertical gradients in regional lung density and perfusion in the supine human lung: the Slinky effect. *J Appl Physiol (1985)* 103: 240–248, 2007. doi:10.1152/japplphysiol.01289.2006.
14. **Hu B, Shao J, Palta M.** Pseudo-R2 in logistic regression model. *Stat Sin* 16: 847–860, 2006.
15. **Hughes PJC, Horn FC, Collier GJ, Biancardi A, Marshall H, Wild JM.** Spatial fuzzy c-means thresholding for semiautomated calculation of percentage lung ventilated volume from hyperpolarized gas and ^{1}H MRI. *J Magn Reson Imaging* 47: 640–646, 2018. doi:10.1002/jmri.25804.
16. **Johnson NJ, Luks AM, Glenny RW.** Gas exchange in the prone posture. *Respir Care* 62: 1097–1110, 2017. doi:10.4187/respcare.05512.
17. **King GG, Eberl S, Salome CM, Meikle SR, Woolcock AJ.** Airway closure measured by a technegas bolus and SPECT. *Am J Respir Crit Care Med* 155: 682–688, 1997. doi:10.1164/ajrccm.155.2.9032213.
18. **Kirby M, Heydarian M, Svenningsen S, Wheatley A, McCormack DG, Etemad-Rezai R, Parraga G.** Hyperpolarized 3He magnetic resonance functional imaging semiautomated segmentation. *Acad Radiol* 19: 141–152, 2012. doi:10.1016/j.acra.2011.10.007.
19. **Kruger SJ, Niles DJ, Dardzinski B, Harman A, Jarjour NN, Ruddy M, Nagle SK, Francois CJ, Sorkness RL, Burton RM, Munoz del Rio A, Fain SB.** Hyperpolarized helium-3 MRI of exercise-induced bronchoconstriction during challenge and therapy. *J Magn Reson Imaging* 39: 1230–1237, 2014. doi:10.1002/jmri.24272.
20. **Laube BL, Norman PS, Adams GK III.** The effect of aerosol distribution on airway responsiveness to inhaled methacholine in patients with asthma. *J Allergy Clin Immunol* 89: 510–518, 1992. doi:10.1016/0091-6749(92)90317-U.
21. **Leary D, Winkler T, Braune A, Maksym GN.** Effects of airway tree asymmetry on the emergence and spatial persistence of ventilation defects. *J Appl Physiol (1985)* 117: 353–362, 2014. doi:10.1152/japplphysiol.00881.2013.
22. **McFadden D.** Conditional logit analysis of qualitative choice behavior, edited by Zarembka P. In: *Frontiers in Econometrics*. New York: Academic, p. 105–142, 1973.
23. **Petersson J, Rohdin M, Sánchez-Crespo A, Nyrén S, Jacobsson H, Larsson SA, Lindahl SGE, Linnarsson D, Neradilek B, Polissar NL, Glenny RW, Mure M.** Posture primarily affects lung tissue distribution with minor effect on blood flow and ventilation. *Respir Physiol Neurobiol* 156: 293–303, 2007. doi:10.1016/j.resp.2006.11.001.
24. **Popa V.** ATS guidelines for methacholine and exercise challenge testing. *Am J Respir Crit Care Med* 163: 292–293, 2001. doi:10.1164/ajrccm.163.1.16310b.
25. **R Development Core Team.** R: a language and environment for statistical computing. Vienna, Austria: R Foundation for Statistical Computing. https://www.r-project.org/, 2016.

26. **Sá RC, Asadi AK, Theilmann RJ, Hopkins SR, Prisk GK, Darquenne C.** Validating the distribution of specific ventilation in healthy humans measured using proton MR imaging. *J Appl Physiol (1985)* 116: 1048–1056, 2014. doi:10.1152/japplphysiol.00982.2013.
27. **Sá RC, Cronin MV, Henderson AC, Holverda S, Theilmann RJ, Arai TJ, Dubowitz DJ, Hopkins SR, Buxton RB, Prisk GK.** Vertical distribution of specific ventilation in normal supine humans measured by oxygen-enhanced proton MRI. *J Appl Physiol (1985)* 109: 1950–1959, 2010. doi:10.1152/japplphysiol.00220.2010.
28. **Sá RC, Zeman KL, Bennett WD, Prisk GK, Darquenne C.** Effect of posture on regional deposition of coarse particles in the healthy human lung. *J Aerosol Med Pulm Drug Deliv* 28: 423–431, 2015. doi:10.1089/jamp.2014.1189.
29. **Simon BA, Kaczka DW, Bankier AA, Parraga G.** What can computed tomography and magnetic resonance imaging tell us about ventilation? *J Appl Physiol (1985)* 113: 647–657, 2012. doi:10.1152/japplphysiol.00353.2012.
30. **Svenningsen S, Guo F, Kirby M, Choy S, Wheatley A, McCormack DG, Parraga G.** Pulmonary functional magnetic resonance imaging: asthma temporal-spatial maps. *Acad Radiol* 21: 1402–1410, 2014. doi:10.1016/j.acra.2014.08.002.
31. **Venegas JG, Winkler T, Musch G, Vidal Melo MF, Layfield D, Tgavalekos N, Fischman AJ, Callahan RJ, Bellani G, Harris RS.** Self-organized patchiness in asthma as a prelude to catastrophic shifts. *Nature* 434: 777–782, 2005. doi:10.1038/nature03490.
32. **Winkler T, Venegas JG.** Complex airway behavior and paradoxical responses to bronchoprovocation. *J Appl Physiol (1985)* 103: 655–663, 2007. doi:10.1152/japplphysiol.00041.2007.
33. **Winkler T, Venegas JG, Harris RS.** Mathematical modeling of ventilation defects in asthma. *Drug Discov Today Dis Models* 15: 3–8, 2015. doi:10.1016/j.ddmod.2014.02.008.
34. **Yang G, Stewart CV, Sofka M, Tsai CL.** Registration of challenging image pairs: initialization, estimation, and decision. *IEEE Trans Pattern Anal Mach Intell* 29: 1973–1989, 2007. doi:10.1109/TPAMI.2007.1116.

Chapter 3, in full, is a reprint of *The spatial pattern of methacholine bronchoconstriction recurs when supine, independently of posture during provocation, but does not recur between postures*, Geier ET, Kubo K, Theilmann RJ, Prisk GK, Sá RC. This article was published online, Sept. 6 2018, ahead of print. The dissertation author was the primary investigator and author of this paper.

CHAPTER FOUR

Regions of methacholine-challenged lung remain bronchoconstricted after albuterol administration, yet go undetected by spirometry in healthy individuals

Regions of methacholine-challenged lung remain bronchoconstricted after albuterol administration, yet go undetected by spirometry, in healthy individuals

Authors

E.T Geier1, R.J. Theilmann2, G.K. Prisk1, R.C. Sá1

1Department of Medicine, University of California – San Diego, San Diego, California, USA

2Department of Radiology University of California – San Diego, San Diego, California, USA

Running head

Rescue of induced bronchoconstriction with albuterol in healthy individuals

Contact Information

Eric Geier
UCSD Department of Medicine
9500 Gilman Drive
La Jolla, CA 92093
egeier@ucsd.edu
Phone 1 765 661 9069

Abstract

While some asthmatic subjects exhibit ventilation defects that are resistant to bronchodilator therapy, it is unclear whether constriction due to bronchospasm alone in the normal lung fully recovers following bronchodilator. Six young, healthy subjects – in whom inflammation was assumed to be absent – were bronchoconstricted with a PC20 dose of methacholine and then bronchodilated with a standard dose of albuterol on three separate occasions. Spirometry and specific ventilation imaging were performed at baseline, during each methacholine bronchoconstriction, and following each subsequent albuterol administration. Specific ventilation imaging – a proton MRI technique – was used to spatially map specific ventilation across 80% of each subject's right lung. The ratio between regional specific ventilation at baseline and after intervention was used to classify areas that had constricted. Following methacholine inhalation, FEV1 fell by >20% and 28% (11%) of the lung was classified as constricted. Following subsequent albuterol inhalation, FEV1 recovered to above its baseline value, yet 12% (9%) of the lung was still classified as constricted. Of the 12% of lung units that were classified as constricted post-albuterol, approximately half [7% (7%)] had constricted after methacholine and failed to recover, while half [6% (4%)] had remained unconstricted after methacholine but paradoxically emerged as constricted after albuterol. Both the regions that failed to recover and the regions that emerged as constricted had higher specific ventilation values at baseline than the rest of the lung and thus likely received a higher dose of methacholine than their counterparts.

New and Noteworthy

In normal subjects bronchoconstricted with methacholine and subsequently treated with albuterol, not all regions of the healthy lung returned to their pre-bronchoconstricted specific ventilation after albuterol, despite full recovery of integrative lung indices (FEV1 and specific ventilation heterogeneity). The regions that remained bronchoconstricted following albuterol were those with the highest specific ventilation at baseline, which suggests that they may have received the highest methacholine dose.

Keywords

Methacholine, albuterol, ventilation defects, specific ventilation, bronchoconstriction

Introduction

Albuterol (salbutamol in some other parts of the world) is a first-line rescue therapy for asthma due to its rapid onset of action (3, 8). Albuterol is used to alleviate acute airflow obstruction and its frequency of use is an indicator of disease control (34). A recent hyperpolarized gas MRI study reported that subjects with ongoing inflammation due to poor asthma control have a diminished response to albuterol (23). This study showed that the percentage of unventilated lung, the ventilation defect percentage (VDP), was higher post-albuterol in patients with >3% sputum eosinophilia than in it was in those with <3% (23). Thus, not only do poorly-controlled asthmatics need their inhaler more often, but their inhaler provides them less benefit.

Airflow obstruction in asthma is known to have more than one etiology (28). Among the known causes are smooth muscle activation, thickening of the airway wall due to inflammation

(4, 27), and the presence of plasma and/or cellular infiltrate in the airways (25). Albuterol directly relaxes airway smooth muscle but does not decrease airway inflammation. Thus, it makes sense that ventilation defects related to ongoing inflammation – such as those reported in the above study (23) – might be expected to be resistant to albuterol rescue.

Studies of albuterol responsiveness have thus far been performed in asthmatic and COPD populations, because they are the primary recipients of the drug. However, we have shown in a previous proton functional MR imaging study that healthy individuals given methacholine can mimic an asthma-like spatial phenotype of bronchoconstriction that is recurrent over long time scales (weeks to months) (10). As we assume that healthy subjects do not have ongoing pulmonary inflammation, we infer that this provoked pattern of constriction is due to cholinergic smooth muscle activation. A priori, we expect that this type of bronchoconstriction would be reversed with inhaled beta-agonist therapy.

To test this hypothesis, we performed oxygen-enhanced proton imaging in six subjects at baseline to establish their normal function, three times following methacholine to identify areas of bronchoconstriction, and then three times following subsequent albuterol to characterize their recovery from the methacholine-induced constriction. The data from the baseline and methacholine conditions have been published in a study of the spatial recurrence of bronchoconstriction (10), and in a related study of the influence of posture on bronchoconstriction (9). The data from the albuterol condition are being presented here for the first time.

Methods

Human Subjects

The protocol for this study was approved by the Institutional Review Board of the University of California, San Diego. Eight subjects were recruited by word of mouth and each provided written, informed consent to participate. One subject withdrew from the study due to time constraints and one subject was excluded from participating after we discovered that their methacholine PC20 fell within the range characteristic of asthma. The six remaining subjects, each of whom finished the study, were young [age 29 (7) years], had normal FEV1 values [101% (6%) predicted], and were sex-balanced (three females, three males). All six denied having a history of cardiopulmonary disease. Individual subject data and methacholine challenge results for these six subjects, the same as studied in (10), are shown in Table 1. FEV1 was measured using an Easyone ™ diagnostic spirometer (ndd Medical Technologies, Andover, MA) and % predicted values were obtained from the National Health and Nutrition Examination Survey III (NHANES III) (12).

Study Sessions

Each of the six subjects completed four study sessions. The contents of each session and the time between sessions are shown in Table 2. Methacholine PC20 determination (see below) occurred during the first study session. The contents of each of the three following sessions are shown along a timeline in Figure 4-1. The baseline and post-methacholine specific ventilation imaging were the topic of a previous publication (10). The post-albuterol specific ventilation imaging scans are being presented for the first time here.

Methacholine Dose Determination

Methacholine challenge tests were performed according to standard procedures established by the American Thoracic Society (17), with the sole exception that all aspects of the tests were performed supine to mimic the scan position. Provocholine ® (methacholine chloride USP, Methapharm, Inc., Brantford, Ontario) was administered via a Koko ® Dosimeter (nSpire Health Inc., Longmont, CO) in doubling concentrations, starting from 0.03125 mg/ml and ending when a 20% drop in FEV1 was achieved. The final concentration administered in the stepwise regime was used for the remainder of the study, as a single dose, to elicit bronchoconstriction. Each subject's PC20 was calculated by interpolation from his or her dose response curve. Both PC20 and concentration for single-dose administration are shown for each subject in Table 1.

Imaging Drug Action

Specific ventilation imaging (SVI), a proton functional MRI technique (19, 20), was used to spatially sample specific ventilation (SV) across each subject's right lung. SVI was performed at baseline, after methacholine inhalation, and after albuterol inhalation to characterize how these drugs affected regional specific ventilation in each subject's right lung.

A single dose of methacholine, the concentration of which was determined for each subject by their challenge results (Table 1), was administered prior to imaging. Methacholine action peaks 1-4 minutes after drug inhalation and then plateaus for 75 minutes, on average (5). SVI data acquisition occurred over 220 breaths and took 18 minutes and 20 seconds to complete. Imaging began approximately 15 minutes after drug administration in order to acquire data during the steady-state plateau.

After methacholine imaging, 180 mcg of albuterol sulfate (ProAir HFA) was administered to each subject via a metered dose inhaler attached to a valve holding chamber

(OptiChamber Diamond, Philips Health). Albuterol acts rapidly; 63% of the total drug-induced change in specific airways conductance occurs in the first minute after inhalation (8). We began imaging ~2 minutes after the drug was administered and continued for 320 breaths (26 minutes and 40 seconds). For this study, the last 220 breaths (18 minutes and 20 seconds) were used to create SV maps. This choice was made so that SV maps from each condition (baseline, methacholine, albuterol) were created with an equal amount of information, 220 images.

Specific Ventilation Imaging

Specific Ventilation Imaging was first described in detail in Sá et al. 2010 (20). It relies on the fact that changes in tissue oxygen concentration manifest as changes in T1-weighted lung signal, and that alveolar oxygen rapidly diffuses into tissue. By abruptly changing FiO2, we cause a rise or fall in tissue oxygen content that depends on the rate at which resident gas is being replaced by inspired gas. Expressed as a ratio of volumes, this $\Delta V/Vo$ is termed specific ventilation. Thus, the rate of change of T1-weighted signal after a stepwise change in FiO2 is a measurement of SV.

Abrupt changes in FiO2 between 21% oxygen (room air) to 100% oxygen were achieved with a custom flow-bypass system attached to a tank of medical oxygen (6). Nine switches in FiO2 occurred to build signal for the SV measurement. Forty breaths were given for the subject to equilibrate after the first switch, and 20 breaths were given for the subject to equilibrate after each of the eight subsequent switches. The 40-breath block enhanced sensitivity to low-SV units, while the 20-breath blocks were optimized for SV values within the normal range (0.08-0.4).

Subjects were instructed to return to a relaxed lung volume after every breath and to breathe between the noises made by the scanner so that images could be acquired at a

reproducible lung volume as close to FRC as possible. During each short, FRC breath hold, a 1.5T EXCITE HDx TwinSpeed MRI system (General Electric Medical Systems, Milwaukee, WI) with an eight-element torso coil was used to collect single-shot fast spin echo (SSFSE) images of 4 abutting sagittal slices of each subject's right lung. The inversion recovery times for each slice were 1100, 1335, 1570, and 1805 ms, respectively. Each slice was acquired using a 40cm x 40cm field of view and was 1.5cm thick. Images were acquired at 128 x 128 and were reconstructed by the scanner onto a 256 x 256 matrix. The locations of the slices were chosen so that the most medial slice was just lateral of the major pulmonary vessels. The location of the imaging field with respect to each subject's thoracic spine was recorded and used to ensure that the lung volume being imaged was the same in each study session.

To correct for small differences in lung volume between successive FRC images, a generalized dual-bootstrap iterative closest point algorithm, in affine transformation mode, was used to register our images (33). Our previous work has shown that lung deformations resulting in an in-plane area change of up to 10% can be reliably registered with an affine transformation (2). All images with an in-plane area change of > 10% were removed from the time series and treated as missing data.

For each voxel in the image, a time course of 220 signal intensity values was created. Each voxel's time course was then correlated with a library of modeled responses to the air/oxygen FiO2 stimulus. The modeled time courses were for SV values equally spaced in log10 from 0.01-10, and the maximum correlation was taken as the voxel's SV value. Spatial smoothing of log transformed data was performed with a Gaussian kernel of size 1.1 cm x 1.1 cm (7 x 7 voxels) so that the smoothed resolution was approximately 1.8 cm3.

Recovery of bronchoconstricted lung regions

In our previous work (10), we compared baseline and post-methacholine SV maps to identify areas that had bronchoconstricted. To do this, we first normalized the maps between conditions based on their total specific ventilation. Next, we resampled each slice onto a 12 x 12 grid of lung regions and compared the average specific ventilation values of corresponding regions in each map. A volume element "i" was considered to have constricted if:

$$SV^{i}_{challenge} < 0.5 * SV^{i}_{baseline} \quad \text{and} \quad SV^{i}_{challenge} < \overline{SV}_{baseline} \qquad (1)$$

where $\overline{(SV)}$ represented the center of the SV distribution.

In the current study, we performed the same comparisons between the baseline and albuterol conditions to identify which areas remained constricted or emerged as constricted after albuterol administration (Figure 4-2). We recorded the volume fraction of the lung which fell into the following groups: 1) unconstricted with methacholine or albuterol, 2) constricted with methacholine and recovered with albuterol, 3) constricted with methacholine and did not recover with albuterol, 4) did not constrict with methacholine but emerged as constricted following albuterol. These fractions are shown in Table 3. Specific ventilation values for each group of the four groups of voxels are shown for each condition in Figure 4-3.

Global metrics of constriction and recovery

From each multi-slice map of specific ventilation, a histogram of SV values was created and fit a log(Gaussian) distribution . The full-width-half-maximum of the fit (FWHM) is taken in this study, as it been in past studies (9, 10, 19, 26), to be a measurement of specific ventilation heterogeneity. We used this metric, along with FEV1, to observe how global ventilatory function changed in response to methacholine and albuterol (Figure 4-4).

Statistics

The full-width-half maximum of the log(Gaussian) fit to each SV histograms was used as a measurement of ventilatory heterogeneity and compared between conditions using a linear mixed effects model, with condition (baseline, methacholine, albuterol) taken as a fixed effect and subject and session taken as random effects. A linear mixed model was chosen as the appropriate statistical test because the number of measurements for each subject varied between conditions (1 for baseline and 3 for post-methacholine and post-albuterol). FEV1 was also compared between conditions by using a linear mixed effects model, with condition taken as a fixed effect and subject and session taken as random effects. For FWHM and FEV1, P-values for the linear mixed effect models were obtained via a likelihood ratio test between the model with the fixed effect and a null model with no fixed effect. Significant fixed effects were investigated using post-hoc paired t-tests. For the two conditions in which subjects had multiple measurements (methacholine and albuterol) each subject's mean value of FWHM and FEV1 were averaged for the purpose of the post-hoc t-test.

The specific ventilation values of different groups of voxels – as defined above in table 3 – were averaged in each condition. The difference in SV between these groups, at baseline, was investigated with a one-way repeated measures ANOVA. Post-hoc testing was then performed with one-sided, paired t-tests.

Results

In these six subjects, regional ventilation did not fully recover within 30 minutes of albuterol rescue from methacholine bronchoconstriction. On average, 12% (9%) of the lung was

classified as constricted 10-30 minutes after albuterol inhalation (Table 3). Slightly more than half of these lung units – 7% (7%) of the total lung – constricted after methacholine and failed to recover after albuterol. Slightly less than half – 6 % (4%) of the total lung – did not constrict after methacholine but emerged as constricted after albuterol.

Whether a lung element was constricted after albuterol depended on its specific ventilation at baseline (P=0.016). In general, lung regions which were constricted after albuterol had a higher SV at baseline than did those that returned to normal after albuterol (Figure 4-3).

Figure 4-4 shows the FWHM of the SV distributions as a function of condition for each subject. Each subject had three measurements for post-methacholine and three measurements for post-albuterol, but only one baseline measurement. FWHM varied significantly as a function of condition (P<0.001). One-sided paired t-tests showed that FWHM was significantly higher after methacholine than it was at baseline (P=0.007), and significantly lower after albuterol than it was after methacholine (P<0.001). A two-sided paired t-test showed no difference between FWHM at baseline and after albuterol (P=0.78).

Figure 4-4 also shows FEV1 as a function of condition for each subject. A linear mixed effects model showed a significant fixed effect of condition on FEV1 (P<0.001). One-sided, paired t-tests showed that FEV1 varied significantly between baseline and methacholine conditions (P<0.001), and between methacholine and albuterol (P<0.001). A two-sided, paired t-test showed that FEV1 did not vary between baseline and albuterol (P=0.97).

Discussion

These data show that, even though FEV1 and the full-width-half-maximum of the SV distribution returned to normal after albuterol rescue, some regions of the lung did not recover

and some regions of the lung paradoxically emerged as constricted after albuterol administration. Maps from the subject with the most dramatic and reproducible lack of recovery, subject S3, are shown in Figure 4-5. Almost half of his lung regions classified that were classified as constricted following methacholine did not recover following albuterol. The other five subjects recovered more than S3, but none did so fully. Across all subjects, approximately one quarter of lung units that were classified as constricted following methacholine failed to recover with albuterol (Table 3).

The specific ventilation of both the unrecovered and the emerged lung units was higher, at baseline, than their counterparts (Figure 4-3), and it might be that this higher SV at baseline caused these units to end up as constricted after albuterol. High-SV regions likely received proportionally more methacholine than the rest of the lung, because the spatial pattern of aerosol deposition depends on the spatial pattern of ventilation (7, 11, 16, 21, 30). This higher dose of methacholine might create a higher cholinergic barrier that must be overcome by albuterol in order to relax the airway smooth muscle.

However, it is also evident that the greater dose of methacholine these units received did not result in a greater reduction in SV during constriction (Figure 4-3). This may not be surprising. Our recent MR study showed that the effect of the spatial pattern of methacholine deposition (which we modified by changing posture during inhalation) on the resulting spatial pattern of bronchoconstriction was minor compared to the effects of lung inflation and airway asymmetry (9). We posited that, at a PC20 dose, all lung regions receive sufficient drug to saturate airway smooth muscle tone, and thus the tendency to collapse is determined by other factors (9).

Thus, while excess methacholine did not cause more smooth muscle contraction, it did present a pharmaceutical barrier that had to be overcome by the adrenergic action of albuterol. In other words, the likelihood of a unit being constricted after albuterol may depend on the balance between the doses of methacholine and albuterol that unit received. This would explain the existence of lung regions that did not constrict with methacholine but emerged as constricted after albuterol. These units could have received a relative excess of methacholine but remained in their open state (1) due to the protective effect of inflation-mediated parenchymal forces and/or relatively increased flow due to upstream airway asymmetry (9, 15, 18, 29, 31, 32). However, once albuterol was administered, the higher cholinergic barrier in these units relative to their patent neighbors resulted in relatively greater post-albuterol smooth muscle tone. This increased smooth muscle tone could have caused them to paradoxically constrict after bronchodilator administration.

It is also possible that the relationship between increased SV at baseline and constriction after albuterol was not causative but correlative. Elements of the dependent lung are known to have both a higher specific ventilation (14) and a tendency to bronchoconstrict due to relative hypo-inflation at FRC (9, 13, 29, 31, 32). Thus, the fact that unrecovered and emerged voxels had a higher specific ventilation at baseline could be the result of this shared factor.

We tested for this by computing the centers of mass of the recovered, unrecovered, and emerged lung units with respect to the center of mass of the whole lung. While the centers of mass (COM) of both the unrecovered and recovered regions were in the posterior/dependent lung [COM displaced 1.4cm (1.7cm) towards the dependent lung for unrecovered regions and COM displaced 1.2cm (1.0cm) towards the dependent lung for recovered regions], there was no significant difference between these measurements ($P=0.68$, two-sided paired t-test). This

indicates that the dependent-nondependent position of a lung element predisposed it towards bronchoconstriction – as we reported in (9) – but did not determine whether or not it would recover following albuterol.

Further, the average center of mass of the emerged units was almost exactly coincident with the center of mass of the entire lung [COM displaced 0.03cm (2.3cm) towards the nondependent lung]. Thus, the dependent-nondependent location of a lung element did not play a role in whether it emerged as constricted after albuterol.

Our data rule out another hypothesis: that regions with more profound constriction, in terms of SV, are less likely to recover. SV during bronchoconstriction was not lower in the unrecovered vs recovered voxels (P=0.98, one-sided paired t-test, Figure 4-3). If there is an SV threshold below which albuterol cannot reach the affected lung tissue and thus recovery does not occur, we could not resolve it in this study.

In general, detection of albuterol-resistant ventilation defects is an application of functional imaging that has potential clinical importance. Imaging studies have demonstrated that patients with ongoing inflammation have ventilation defects that persist after bronchodilator administration, while patients with adequate inflammatory control do not (22). Another study showed ventilation defects that did not respond to albuterol improved after anti-Th2 therapy (24). While it is unlikely that our healthy subjects had ongoing pulmonary inflammation, they still had lung regions that failed to fully recover within 30 minutes of albuterol administration. These regions were likely transient and due to lingering effects of methacholine. Their detection with SVI, however, shows that perturbations in regional lung function persist after metrics of global lung function – such as FEV1 and ventilation heterogeneity – have returned to normal.

Limitations

Our study is limited by the fact that we have no repeat baseline measurements for these subjects. Thus, it is uncertain how much of each subject's lung would be classified as constricted without any intervention. To address this, we have quantified the volume fraction of imaged lung that would be classified as constricted without any drug intervention by using data from a previous repeatability study (19). In the twelve subjects for whom data was available (of 13), the fraction of lung that constricted between repeat studies was 0.01 (0.01). The fraction of lung classified as constricted during the methacholine and albuterol scans was 0.28 (0.11) and 0.12 (0.09), respectively. The difference implies that it is implausible that the amount of lung classified as constricted during these two interventions was enforced by the measurement, as opposed to by the drug interventions.

A second limitation of our study is that we are imaging with a "long exposure" technique, which means that any dynamic SV values will be reported as their average value over the 20-minute imaging window. A previous study has shown that methacholine action plateaus for 75 (54) minutes and that subsequent recovery takes 57 (38) minutes (5). We timed our methacholine imaging so that it occurred 15-35 minutes after drug administration, within that plateau. However, the inter-subject variability suggests that some subjects may have left the plateau during methacholine imaging, so their SV may have been changing and thus subject to being temporally averaged by the measurement.

Likewise, our albuterol imaging took place during a period in which SV was likely dynamic. While albuterol acts within minutes (3, 8), maximum change in FEV1 following albuterol occurs nearly an hour after administration (8). Thus, it is probable that SV changed while it was being imaged, 10-30 minutes after drug administration. Furthermore, while our

albuterol imaging took place in the theoretical plateau of methacholine action, the variability in the length of that plateau suggests that some of our subjects may have begun to recover without albuterol. Thus, the recovery we saw, in some cases, was likely a combined effect of methacholine metabolism and albuterol action.

Another limitation of our study was that our 4 imaging slices encompassed ~80% of the right lung and none of the left lung. Any systematic differences in albuterol recovery between the right and the left lung would not have been captured. Our previous study (10) showed no systematic effect of medial-lateral position on the likelihood of constriction, so within the right lung it is unlikely that we biased our results by excluding the most medial and most lateral portions of the lung.

Conclusion

While global metrics of ventilatory function (FEV1, SV heterogeneity) returned to baseline within 30 minutes of albuterol rescue from methacholine bronchoconstriction, not all regions of the recovered from being constricted. Furthermore, some units emerged as constricted after albuterol administration even though they were not constricted after methacholine. Both the units that did not recover and those that emerged as constricted tended to have higher SV at baseline than did the rest of the lung, which suggests that the correspondingly higher dose of methacholine they received prevented recovery following albuterol. These results show that regional measurements of change in SV is more sensitive to subtle physiological changes than are whole-lung measurements of ventilatory function.

References

1. **Anafi RC**, **Wilson TA**. Airway stability and heterogeneity in the constricted lung. *J Appl Physiol* 91: 1185–1192, 2001.

2. **Arai TJ**, **Villongco CT**, **Villongco MT**, **Hopkins SR**, **Theilmann RJ**. Affine transformation registers small scale lung deformation. In: *Proceedings of the Annual International Conference of the IEEE Engineering in Medicine and Biology Society, EMBS*. 2012, p. 5298–5301.

3. **Beach JR**, **Young CL**, **Stenton SC**, **Avery AJ**, **Walters EH**, **Hendrick DJ**. A comparison of the speeds of action of salmeterol and salbutamol in reversing methacholine-induced bronchoconstriction. *Pulm Pharmacol* 5: 133–135, 1992.

4. **Brewster CEP**, **Howarth PH**, **Djukanovic R**, **Wilson J**, **Holgate ST**, **Roche WR**. Myofibroblasts and Subepithelial Fibrosis in Bronchial Asthma. *Am J Respir Cell Mol Biol* 3: 507–511, 1990.

5. **Cartier A**, **Malo JL**, **Begin P**, **Sestier M**, **Martin RR**. Time course of the bronchoconstriction induced by inhaled histamine and methacholine. *J Appl Physiol* 54: 821–826, 1983.

6. **Cook FR**, **Geier ET**, **Asadi AK**, **Sá RC**, **Prisk GK**. Rapid prototyping of inspired gas delivery system for pulmonary MRI research. *3D Print Addit Manuf* 2, 2015.

7. **Darquenne C**, **van Ertbruggen C**, **Prisk GK**. Convective flow dominates aerosol delivery to the lung segments. *J Appl Physiol* 111: 48–54, 2011.

8. **Derom EY**, **Pauwels RA**. Time course of bronchodilating effect of inhaled formoterol, a potent and long acting sympathomimetic. *Thorax* 47: 30–33, 1992.

9. **Geier ET**, **Kubo K**, **Theilmann RJ**, **Prisk GK**, **Sá RC**. The spatial pattern of methacholine bronchoconstriction recurs when supine, independently of posture during provocation, but does not recur between postures. *J. Appl. Physiol.* (September 6, 2018). doi: 10.1152/japplphysiol.00487.2018.

10. **Geier ETT**, **Neuhart I**, **Theilmann RJJ**, **Prisk GKK**, **Sá RCC**. Spatial persistence of reduced specific ventilation following methacholine challenge in the healthy human lung. *J Appl Physiol* 110179187: 1222–1232, 2018.

11. **Greenblatt EE**, **Winkler T**, **Harris RS**, **Kelly VJ**, **Kone M**, **Katz I**, **Martin AR**, **Caillibotte G**, **Venegas J**. What Causes Uneven Aerosol Deposition in the

Bronchoconstricted Lung? A Quantitative Imaging Study. *J Aerosol Med Pulm Drug Deliv* 29: 57–75, 2015.

12. **Hankinson JL**, **Odencrantz JR**, **Fedan KB**. Spirometric reference values from a sample of the general U.S. Population. *Am J Respir Crit Care Med* 159: 179–187, 1999.

13. **Harris RS**, **Fujii-Rios H**, **Winkler T**, **Musch G**, **Vidal Melo MF**, **Venegas JG**. Ventilation Defect Formation in Healthy and Asthma Subjects Is Determined by Lung Inflation. *PLoS One* (2012). doi: 10.1371/journal.pone.0053216.

14. **Hopkins SR**, **Henderson AC**, **Levin DL**, **Yamada K**, **Arai T**, **Buxton RB**, **Prisk GK**. Vertical gradients in regional lung density and perfusion in the supine human lung: the Slinky effect. *J Appl Physiol* 103: 240–248, 2007.

15. **Leary D**, **Winkler T**, **Braune A**, **Maksym GN**. Effects of airway tree asymmetry on the emergence and spatial persistence of ventilation defects. *J Appl Physiol* 117: 353–362, 2014.

16. **Möller W**, **Meyer G**, **Scheuch G**, **Kreyling WG**, **Bennett WD**. Left-to-Right Asymmetry of Aerosol Deposition after Shallow Bolus Inhalation Depends on Lung Ventilation. *J Aerosol Med Pulm Drug Deliv* 22: 333–339, 2009.

17. **Popa V**. ATS guidelines for methacholine and exercise challenge testing. *Am J Respir Crit Care Med* 163: 292–293, 2001.

18. **Richter T**, **Bellani G**, **Scott Harris R**, **Vidal Melo MF**, **Winkler T**, **Venegas JG**, **Musch G**. Effect of prone position on regional shunt, aeration, and perfusion in experimental acute lung injury. *Am J Respir Crit Care Med* 172: 480–7, 2005.

19. **Sá RC**, **Asadi AK**, **Theilmann RJ**, **Hopkins SR**, **Prisk GK**, **Darquenne C**. Validating the distribution of specific ventilation in healthy humans measured using proton MR imaging. *J Appl Physiol* 116: 1048–1056, 2014.

20. **Sá RC**, **Cronin M V.**, **Cortney Henderson A**, **Holverda S**, **Theilmann RJ**, **Arai TJ**, **Dubowitz DJ**, **Hopkins SR**, **Buxton RB**, **Kim Prisk G**. Vertical distribution of specific ventilation in normal supine humans measured by oxygen-enhanced proton MRI. *J Appl Physiol* 109: 1950–1959, 2010.

21. **Sá RC**, **Zeman KL**, **Bennett WD**, **Prisk GK**, **Darquenne C**. Regional Ventilation Is the Main Determinant of Alveolar Deposition of Coarse Particles in the Supine Healthy Human Lung During Tidal Breathing. *J Aerosol Med Pulm Drug Deliv* 30: 322–331, 2017.

22. **Svenningsen S**, **Eddy RL**, **Lim H**, **Nair P**, **Parraga G**. Inflammatory and non-inflammatory contributions to ventilation heterogeneity in severe poorly-controlled asthmatics. *Am J Respir Crit Care Med* 195, 2017.

23. **Svenningsen S**, **Eddy RL**, **Lim HF**, **Cox PG**, **Nair P**, **Parraga G**. Sputum Eosinophilia and Magnetic Resonance Imaging Ventilation Heterogeneity in Severe Asthma. *Am J Respir Crit Care Med* 197: 876–884, 2018.

24. **Svenningsen SL**, **Eddy R**, **Capaldi DP**, **Kjarsgaard M**, **Radford K**, **Parraga G**, **Nair P**. Effect of Anti-Th2 Therapy on MRI Ventilation Heterogeneity in Prednisone-Dependent Asthma. *Am J Respir Crit Care Med* 197: A6393, 2018.

25. **Synek M**, **Beasley R**, **Frew AJ**, **Goulding D**, **Holloway L**, **Lampe FC**, **Roche WR**, **Holgate ST**. Cellular infiltration of the airways in asthma of varying severity. *Am J Respir Crit Care Med* 154: 224–30, 1996.

26. **Tedjasaputra V**, **Sa RC**, **Arai TJ**, **Holverda S**, **Theilmann RJ**, **Chen WT**, **Wagner PD**, **Davis CK**, **Kim Prisk G**, **Hopkins SR**. The heterogeneity of regional specific ventilation is unchanged following heavy exercise in athletes. *J Appl Physiol* 115: 126–135, 2013.

27. **Tiddens HA**, **Paré PD**, **Hogg JC**, **Hop WC**, **Lambert R**, **de Jongste JC**. Cartilaginous airway dimensions and airflow obstruction in human lungs. *Am J Respir Crit Care Med* 152: 260–266, 1995.

28. **Tiddens HAWM**, **de Jongste JC**. Airflow Obstruction in Asthma: There is More than Smooth Muscle. In: *Intensive Care in Childhood: A Challenge to the Future*, p. 337–343.

29. **Venegas JG**, **Winkler T**, **Musch G**, **Melo MFV**, **Layfield D**, **Tgavalekos N**, **Fischman AJ**, **Callahan RJ**, **Bellani G**, **Harris RS**. Self-organized patchiness in asthma as a prelude to catastrophic shifts. *Nature* 434: 777–782, 2005.

30. **Verbanck S**, **Ghorbaniasl G**, **Biddiscombe MF**, **Dragojlovic D**, **Ricks N**, **Lacor C**, **Ilsen B**, **de Mey J**, **Schuermans D**, **Underwood SR**, **Barnes PJ**, **Vincken W**, **Usmani OS**. Inhaled Aerosol Distribution in Human Airways: A Scintigraphy-Guided Study in a 3D Printed Model. *J Aerosol Med Pulm Drug Deliv* 29: 525–533, 2016.

31. **Winkler T**, **Venegas JG**. Complex airway behavior and paradoxical responses to bronchoprovocation. *J Appl Physiol* 103: 655–663, 2007.

32. **Winkler T**, **Venegas JG**, **Harris RS**. Mathematical modeling of ventilation defects in asthma. *Drug Discov Today Dis Model* 15: 3–8, 2015.

33. **Yang G**, **Stewart C V.**, **Sofka M**, **Tsai CL**. Registration of challenging image pairs: Initialization, estimation, and decision. *IEEE Trans Pattern Anal Mach Intell* 29: 1973–1989, 2007.

34. National Heart, Lung, and Blood Institute National Asthma Education and Prevention Program Expert Panel Report 3: Guidelines for the Diagnosis and Management of Asthma Full Report 2007 [Online]. https://www.nhlbi.nih.gov/files/docs/guidelines/asthgdln.pdf

Figures and Tables

Table 4-1: Six young subjects with normal FEV_1 values were recruited to be part of this study. Methacholine PC_{20} was determined per ATS guidelines (16), with the exception it was performed in the supine posture. The final dose in the stepwise challenge, the smallest that elicited a > 20% drop in FEV_1, was chosen as the methacholine dose for the remainder of the study. FEV_1 = forced expiratory volume in one second. PC_{20} = concentration of methacholine that elicits 20% drop in FEV_1, determined by interpolation from an empirically determined dose response curve. †Indicates data reported in our previous publication (9).

Subject	*Sex*	*Age, yr†*	*Height, m†*	*Weight, kg†*	*Seated FEV_1, liters (% predicted)†*	*Methacholine $PC20^{\dagger}$, mg/ml†*	*Methacholine dose, mg/ml†*
S1	M	21	1.60	59	3.82 (100)	2.8	4
S2	F	27	1.57	45	3.05 (101)	6.3	8
S3	M	27	1.88	96	5.59 (110)	10.0	16
S4	F	28	1.70	77	3.54 (101)	5.2	8
S5	M	41	1.78	83	3.87 (92)	10.9	16
S6	F	27	1.64	66	3.25 (99)	3.3	4
Mean (SD)		29 (7)	1.70 ± 0.12	71 ± 18	3.85 (0.91) [101 (6)]	6.4 (3.4)	9 (5)

Table 4-2: Each subject underwent 4 study sessions on separate days. The time elapsed since study enrollment for each study session are shown as group mean (standard deviation). The specific contents of each study session are shown in the rightmost column. †Indicates data that has been part of a prior publication (9).

Study Session	*Days since Study enrollment [Mean (SD)]*	*Contents of Study Session*
1	0	Methacholine Challenge†
2	115 (225)	Baseline Imaging†, Methacholine Imaging†, Albuterol Imaging
3	124 (124)	Methacholine Imaging†, Albuterol Imaging
4	212 (125)	Methacholine Imaging†, Albuterol Imaging

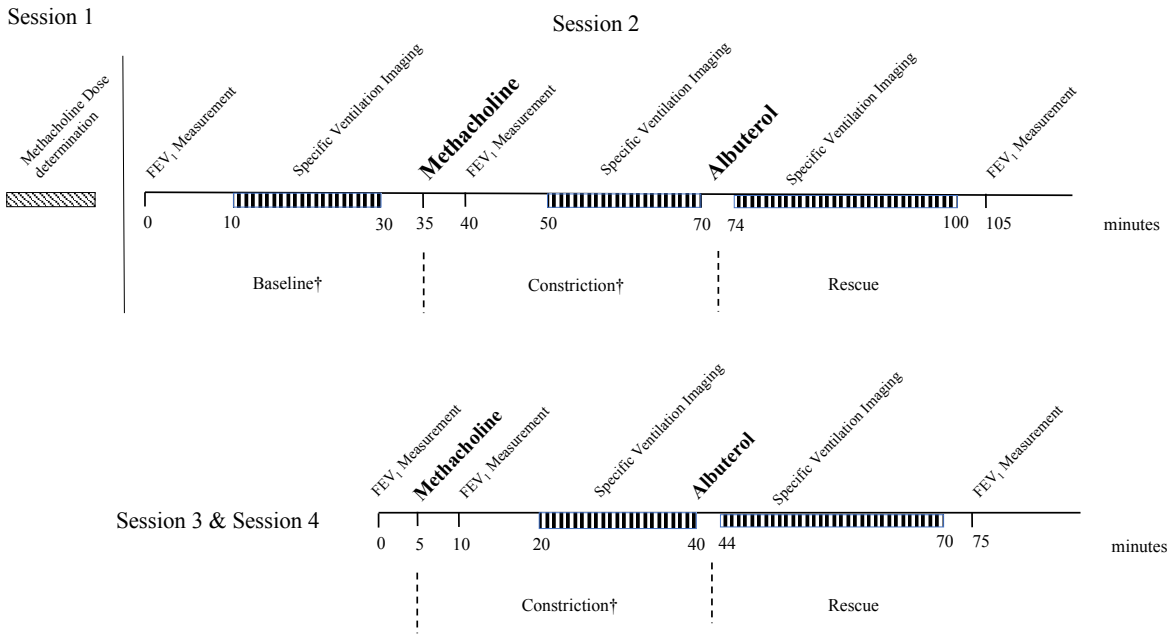

Figure 4-1: The contents of each study day, shown along an approximate timeline. Sessions 3 and 4 were identical to each other, and only differ from session 2 in that they did not contain a baseline SVI measurement prior to bronchoconstriction. †Indicates conditions that have been the subject of a prior publication (9).

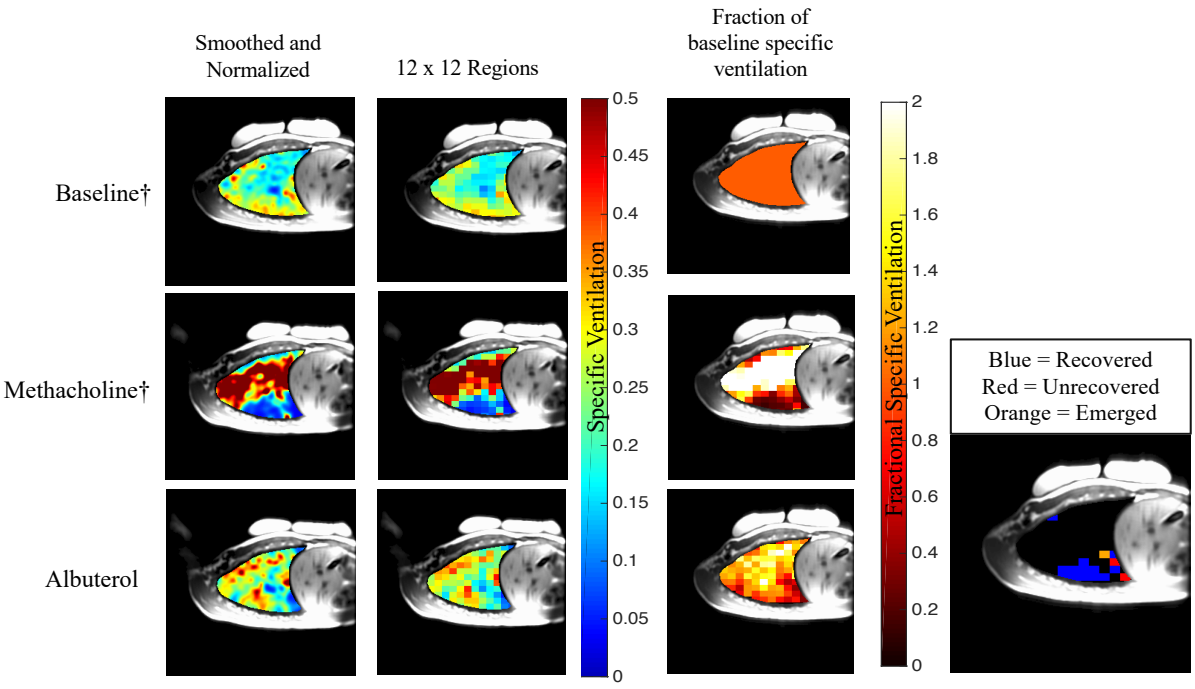

Figure 4-2: The method by which we quantified constricted lung regions is shown above for one slice of Subject S1's lung. Each SVI slice was smoothed, normalized, and divided into 12 x 12 regions based on the lung size. The average SV in each 12 x 12 lung region was compared between conditions to determine the fractional specific ventilation, compared to baseline. Regions which had a fractional SV < 0.5 and fell below the baseline mean SV were classified as constricted (see Methods). Lung regions which remained constricted following administration of albuterol were quantified by volume. These regions are shown in red in the far-right column. †Indicates data that have been the subject of a previous publication (9).

Table 4-3: Three measurements of each metric above were made in each subject at time points spread weeks to months apart. The mean and standard deviation for each subject is shown, and the mean and standard deviation of all measurements is shown in the bottom row. Each measurement refers to the fraction of the imaged right lung. For example: 29% of Subject 1's right lung constricted following methacholine, on average. The majority of these lung elements (23% of the total lung) recovered following albuterol. However, a portion of these units (6 % of the total lung) did not. In addition, 7% of Subject 1's lung was not constricted following methacholine but *became* constricted following albuterol, which meant that a total of 13% of his lung units were constricted after albuterol inhalation.

Subject	*Fraction of right lung constricted after methacholine (SD)*	*Fraction of right lung Recovered (SD)*	*Fraction of right lung unrecovered (SD)*	*Fraction of right lung emerged as constricted (SD)*	*Fraction of right lung constricted after albuterol (SD)*
S1	0.29 (0.02)	0.23 (0.01)	0.06 (0.03)	0.07 (0.04)	0.13 (0.06)
S2	0.22 (0.07)	0.21 (0.07)	0.01 (0.01)	0.09 (0.07)	0.10 (0.06)
S3	0.45 (0.09)	0.24 (0.09)	0.22 (0.05)	0.08 (0.05)	0.30 (0.03)
S4	0.26 (0.08)	0.23 (0.08)	0.03 (0.004)	0.02 (0.02)	0.05 (0.02)
S5	0.22 (0.14)	0.16 (0.14)	0.06 (0.02)	0.06 (0.001)	0.12 (0.02)
S6	0.21 (0.07)	0.18 (0.07)	0.03 (0.003)	0.03 (0.02)	0.06 (0.02)
Mean (SD)	0.28 (0.11)	0.21 (0.08)	0.07 (0.07)	0.06 (0.04)	0.12 (0.09)

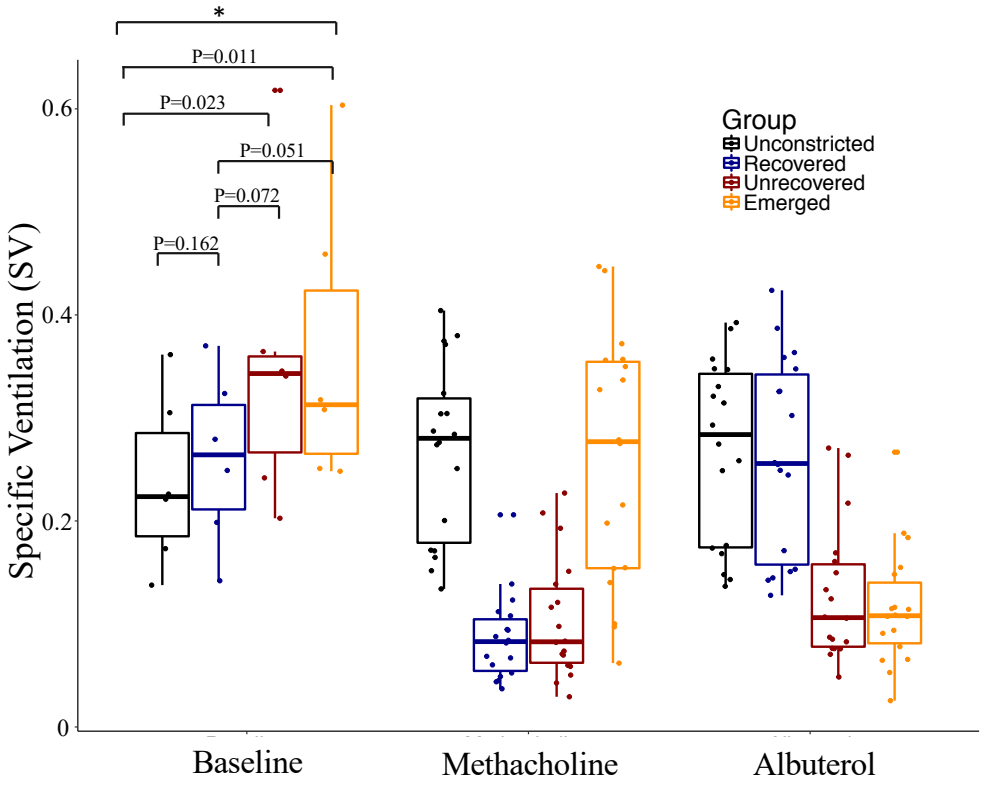

Figure 4-3: Boxplots for each group of lung units – those that never constricted (unconstricted), those that constricted with methacholine and subsequently recovered with albuterol (recovered), those that constricted with methacholine but did not recover with albuterol (unrecovered), and those that did not constrict with methacholine but emerged as constricted after albuterol (emerged) – are shown for each condition. Each point represents the average SV within each group of voxels for a certain session in a certain subject, and the boxplots represent the median, first, and third quartiles of all measurements. A one-way repeated measures ANOVA showed a significant effect of group on baseline SV (*, P=0.016). Post-hoc paired t-tests confirmed that both unrecovered and emerged regions had a significantly higher SV than unconstructed voxels at baseline (P=0.023 and P=0.011 respectively). No P-values are indicated for the methacholine and albuterol conditions, because the differences in SV are enforced by the group classifications.

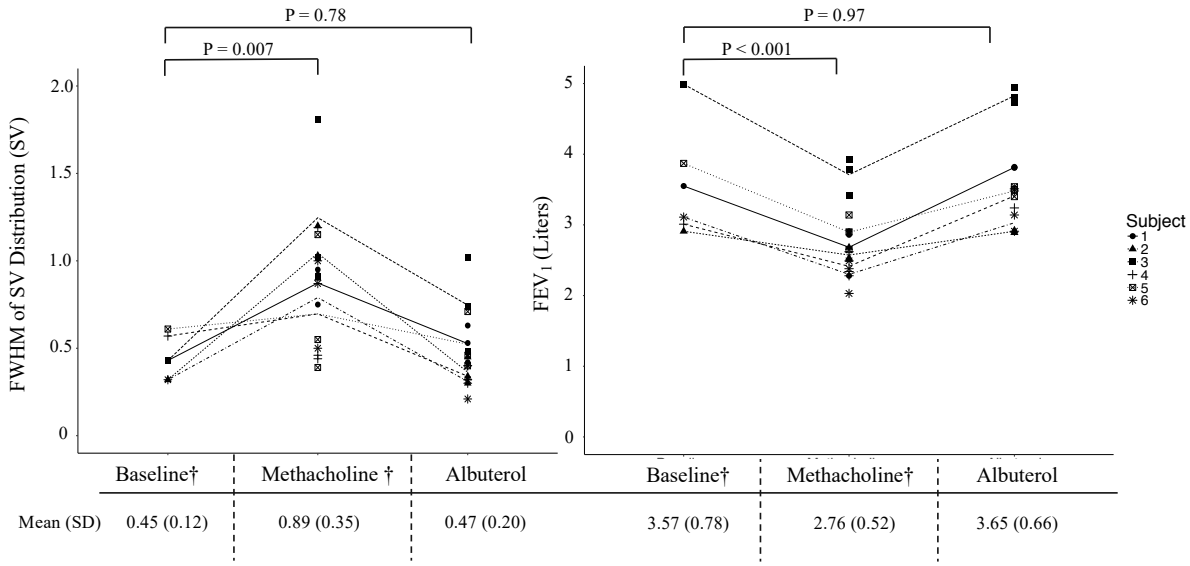

Figure 4-4: The full-width-half-maximum (FWHM) of the SV distribution and the forced expiratory volume in 1 second (FEV_1) are shown as a function of imaging condition for each of the 6 subjects. Each measurement is displayed as a subject-specific marker and intra-subject averages are shown as a subject-specific line. Overall means and standard deviations for each condition, for both FWHM and FEV_1, are shown below the x axes. Subject 2 and Subject 6 are each missing one albuterol FEV_1 measurement, so for those two subjects the post-albuterol FEV_1 average is between only two measurements each. †Indicates measurement that has been previously reported (9).

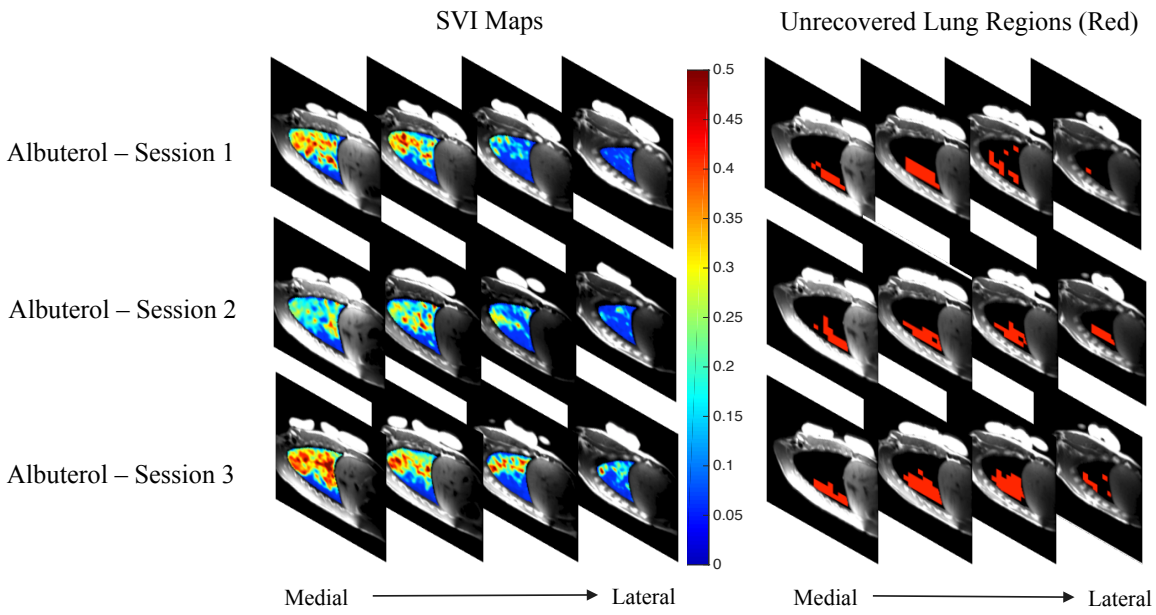

Figure 4-5: Subject S3 had reproducibly incomplete recovery from methacholine bronchoconstriction 10-30 minutes after albuterol rescue. The left group of maps shows the smoothed specific ventilation values for this subject in each post-albuterol imaging session. The right group of maps shows, in red, the lung regions that constricted following methacholine and did not subsequently recover (e.g. were still classified as constricted) with albuterol. On average, 22% -- nearly half of the 45% of his lung that constricted – did not recover with albuterol (see Table 3). In addition, 8% of his lung was not classified as constricted following methacholine but emerged as constricted following albuterol. These emerged units are not highlighted in this figure.

Chapter 4, in full, is a reprint of *Regions of methacholine-challenged lung remain bronchoconstricted after albuterol administration, yet go undetected by spirometry in healthy individuals*, Geier ET, Theilmann RJ, Prisk GK, Sá RC. This article was submitted to the Journal of Applied Physiology on October 15, 2018. The dissertation author was the primary investigator and author of this paper.

CHAPTER FIVE

Discussion

Summary of the results chapters

The goal of the study described in Chapter 2 was to find empirical data to support or refute a result of modeling studies: that smooth muscle action alone in an asymmetric airway tree can cause a highly spatially recurrent pattern of bronchoconstriction. Our finding, that regions of the lung that constricted were almost 8 times more likely than their counterparts to do so again, provided support for this prediction.

But our data also showed that regions in the posterior/dependent lung were more likely to constrict. Ours was not the only imaging study to show that tendency (11, 12, 15). Was the recurrent pattern of constriction, then, a result of asymmetrically airways, as Leary predicted (18)? Or was it instead a consequence of a general posterior or dependent tendency?

To answer this question, we first had to pry apart the posterior and the dependent lung. Since all parts of the Chapter 2 study were performed in the supine posture, it was impossible to tell whether the lung tended to constrict in the regions closest to the spine (posterior) or in the regions that were gravitationally lowest (dependent). The two possibilities had very different implications. If the lung tends to constrict in the posterior regions, there must be something inherent to the posterior airways that primes them for constriction. If, instead, the gravitationally

dependent regions tend to constrict, gravity must play a role in predisposing certain lung units towards constriction.

Two known effects of gravity could cause this predisposition: its influence on the pattern of drug deposition and/or the fact that the lung distorts under its own weight.

The gravitationally dependent lung ventilates more than the nondependent lung (23), and aerosolized particles like methacholine are distributed in greater quantities to areas with higher ventilation (24). Thus, it is likely that the methacholine our subjects inhaled was preferentially deposited in the dependent lung. More regional drug delivery could result in preferential bronchoconstriction in those regions.

Alternatively, the preferential constriction in the dependent lung could be due to deformable nature of the lung. The lung is known to distort under its own weight (14). Since the dependent lung is compressed by the weight of the lung above it, it is relatively less inflated at functional residual capacity (FRC) than the nondependent lung. The Venegas and Winkler model predicts that less inflated regions are more likely to constrict than their counterparts, because the less-expanded parenchyma exerts less outward force on the airway during smooth muscle activation (31, 34). In 2012, a PET imaging study corroborated this prediction by showing that less expanded regions constricted more in response to methacholine challenge than did their more inflated counterparts (11).

Thus the goals of our second study (Chapter 3) were twofold: First, determine whether the tendency towards constriction is in the posterior or the dependent lung, and second (if the tendency is dependent), determine whether the tendency is caused by preferential methacholine deposition or by lower inflation in the dependent lung due to gravitational compression of tissue.

The fact that the posterior lung was not more likely to constrict in the prone position (because it was nondependent in that posture) was clear evidence that the constriction is more likely to occur in the dependent, as opposed to the posterior, lung. The only time the posterior lung is more likely to constrict is when it happens to also be dependent.

The fact that administering methacholine while prone, as opposed while supine, did not affect the resulting pattern of bronchoconstriction provided evidence that the dependent tendency was caused by gravitational compression of tissue, not gravitational influence on methacholine deposition. Furthermore, these results indicated that changing gravitational orientation *while constricted* changes the spatial pattern of bronchoconstriction. Put differently, we discovered that, by flipping a person from prone to supine during bronchoconstriction, some airways that were closed will open and vice versa.

****

We also sought to understand how the lung recovers from methacholine constriction when albuterol is administered. Since methacholine provocation in healthy individuals causes bronchoconstriction that is entirely due to smooth muscle action, we hypothesized that administration of a smooth muscle dilator (like albuterol) should result in complete recovery from bronchoconstriction.

Chapter 4 presents our test of this hypothesis. We performed SVI again in our 6 healthy subjects after albuterol rescue subsequent to methacholine bronchoconstriction. The data did not support our original hypothesis; none of the six healthy subjects fully recovered from methacholine bronchoconstriction within 30 minutes of bronchodilator therapy.

This result might have been expected in asthmatics, because some of them have a diminished response to albuterol. This reduced sensitivity can be due to drug tolerance (9), age

(32), ongoing inflammation (27), or even certain genetic phenotypes (10). The genetic variability in albuterol response recently entered the gestalt when a single-nucleotide polymorphism implicated in albuterol subsensitivity was found to be specific to the African American community (10).

In our healthy subjects, however, these mechanisms of albuterol resistance are assumed to be absent. Yet the subjects did not fully recover. Furthermore, their lack of recovery was not detected by the classical measurement of pulmonary function, forced expiratory volume in 1 second (FEV_1), nor was it detectable by our own whole-lung functional imaging metric - heterogeneity of specific ventilation. Only by studying specific ventilation on a regional basis were we able to identify regions of the lung function had been compromised.

This finding, in itself, shows that regional measurements of specific ventilation are sensitive to subtle changes in lung function that escape whole-lung metrics such as FEV_1. This higher sensitivity makes functional imaging of SV a potential attractive biomarker for selecting treatment candidates or evaluating treatment response in those with recalcitrant asthma.

Why is bronchoconstriction not *completely* spatially recurrent?

At least one major point has been left undiscussed in the three data chapters of this dissertation: Why is the spatial pattern of bronchoconstriction not *completely* recurrent?

In our first article, we reported that 53% of lung units which constricted during one provocation did so again in the next. This fell within the range reported by previous studies, 20-67% (16, 17, 21). However, if regions of lung are predisposed towards constriction by their upstream/downstream airway geometry and their relative level of inflation, both of which are assumed stable over time in healthy subjects, the pattern of constriction should be essentially

invariable. The model put forth by Leary and colleagues, which was based on an anatomically-realistic lung, predicted only 3% variation in regional ventilation between repeat constriction events (18).

Since the variability between sessions we observed was much greater than the variability Leary predicted, and the between-sessions variability in the Leary model is due to perturbations in initial conditions, it is likely that the true variability in initial conditions *in vivo* is much higher than the 1% that Leary modeled. This variability in initial conditions is present in the lungs of young, healthy subjects, in whom inflammation is assumed to be absent.

The most likely mechanism, other than inflammation, that could cause heterogeneity in airway caliber that changes with time is smooth muscle tone. And the scale of this fluctuation in smooth muscle tone is significant (on the order of the fixed effects of gravity and airway geometry), as it accounts for ~50% of the areas that bronchoconstrict after methacholine.

Why would healthy individuals have spatially heterogeneous smooth muscle activation that varies with time? If Wayne Mitzner is correct that airway smooth muscle is "the appendix of the lung", then we must concede that this process takes place without a purpose. And, since blood flow is actively regulated within the lung to match ventilation (at least to some degree), that would mean that the lung devotes resources to account for meaningless heterogeneity. If true, this would mean that airway smooth muscle is even more of a liability than the appendix, because we must compensate for it even when it isn't afflicted.

An alternative explanation for this phenomenon exists, though it has been a contentious hypothesis for decades. Severinghaus and associates, in a seminal study, showed that occlusion of one pulmonary artery results in a doubling of airway resistance and a 25% decrease in compliance in the ipsilateral (same) lung of a dog (25). This meant that the smooth muscle of

the lung was acting to redistribute ventilation away from areas of the lung that were no longer perfused. Severinghaus and colleagues gathered that this process was mediated by a decrease in CO_2, because when hypercapnic gas was given during the experiment the changes in resistance and compliance did not occur (25).

Later, another group showed that airway smooth muscle contracts in response to hyperoxic conditions (26), and it was thought that this occurred to help maintain regional balance between ventilation and perfusion. This seemed to be corroborated by a later finding, that blockade of vagal tone to airway smooth muscle resulted in more ventilatory heterogeneity (6).

The idea that ventilation is actively regulated to help match perfusion is not universally accepted. Mitzner points out that the change in respiratory mechanics observed by Severinghaus are relatively minor (only a 25% reduction in compliance in response to total blockage of blood flow) and only occur at levels of CO_2 that are much less than what we typically observe *in vivo* (20).

We know, however, that the spatial pattern of pulmonary perfusion changes fluctuates over time (1) . Thus, if ventilation is actively regulated via airway smooth muscle to match perfusion, we might expect a spatial pattern of airway smooth muscle action that varies as well. If true, this might explain the variability in initial conditions evident in our experiment, which ultimately results in a more variable than expected pattern of bronchoconstriction with methacholine.

Potential future studies in asthmatics

The fact that we studied bronchoconstriction in healthy individuals but not in asthmatics is a limitation of this dissertation. The approach was reductionist; by excluding some aspects of

the disease - inflammation and remodeling - we are able to focus on just one - smooth muscle constriction. But how does what we learned apply to people with asthma?

It is likely that asthmatics have a spatial response to methacholine that is much different than what we observed in healthy subjects. In healthy subjects, the force generated by airway smooth muscle in response to methacholine quickly reaches a plateau (35). The dose we gave our healthy subjects, we believe, was enough to elicit a plateau response in nearly every region of the lung. Since tone was saturated everywhere, tone did not determine which areas of the lung constricted. Instead, the underlying forces that predispose an airway to either constrict or stay open - inflation and upstream/downstream anatomy - determined the pattern. In healthy subjects these effects are fixed, so the pattern was recurrent.

Asthmatics, on the other hand, lack this plateau of airway smooth muscle action (35). Thus we cannot infer that every area of the lung is experiencing maximum (plateau) smooth muscle stress. So the pattern of methacholine bronchoconstriction, in these individuals, could depend more on local drug dose and drug responsiveness than it does in healthy individuals.

Local drug dose depends on local ventilation (24). Thus, this aspect of an asthmatic's spatial pattern of constriction may be influenced by his or her pattern of ventilation - which, in turn, is influenced by a variety of factors both fixed (i.e. gravity) and variable (i.e. upstream occlusion due to ongoing inflammation).

Drug responsiveness in asthmatics is also, most likely, spatially heterogeneous. It is known that inflammatory cytokines lead to bronchial hyperresponsiveness (2), so local prevalence of these mediators could lead to locally more or less responsive smooth muscle. This would lead to a pattern of constriction that is also influenced by the underlying heterogeneity of inflammation.

Thus, we would hypothesize that the spatial pattern of bronchoconstriction in asthmatics will be subject to two forms of heterogeneity related to methacholine that were not present in healthy subjects: heterogeneity in drug delivery and heterogeneity in drug responsiveness. We expect that these forms of heterogeneity would vary with time as the underlying spatial pattern of inflammation varies. In the setting of the Venegas and Winkler model, this temporally varying heterogeneity would be represented by relatively large perturbations in initial conditions. This would lead to a more spatially chaotic pattern of bronchoconstriction than what we see in healthy individuals.

However, it may be true that chronic asthmatics have structural changes that lead to regions of spatially recurrent constriction. Chronic asthma results in thickening of the airway wall, and areas in which this effect is especially prevalent could become foci of recurrent bronchoconstriction through the upstream/downstream feedback mechanisms proposed by Venegas and Winkler (31). As these areas accumulate over time, an asthmatic's spatial pattern of bronchoconstriction may become more recurrent.

Thus, asthma has characteristics that could both decrease and increase the recurrence of a subject's spatial pattern of bronchoconstriction. Critically, the temporally variable effects should be present in nearly every asthmatic, while the temporally fixed effect (caused by airway remodeling) is thought to be a characteristic of chronic, persistent asthma. Therefore, we hypothesize that young, short-term asthmatics will have a variable pattern of constriction that becomes more recurrent as the disease persists. So far, no data exists to support or refute this hypothesis.

Preliminary data from a mild asthmatic

While we did not originally intend to study methacholine bronchoconstriction in asthmatics as part of this dissertation work, the chance to do so (in a limited fashion) presented itself when one of our subjects was diagnosed with asthma during the course of our study.

We found that, in this young, asthmatic subject, the spatial pattern of bronchoconstriction was less recurrent than it was in healthy individuals. Only 24% of her lung units which constricted in one challenge did so again in a subsequent challenge (compared to an average of 53% in healthy individuals). Furthermore, 0% of her lung units which constricted in the first two sessions did so again in the third (compared to 68% in healthy individuals). She had no regions of lung which constricted in all three challenges.

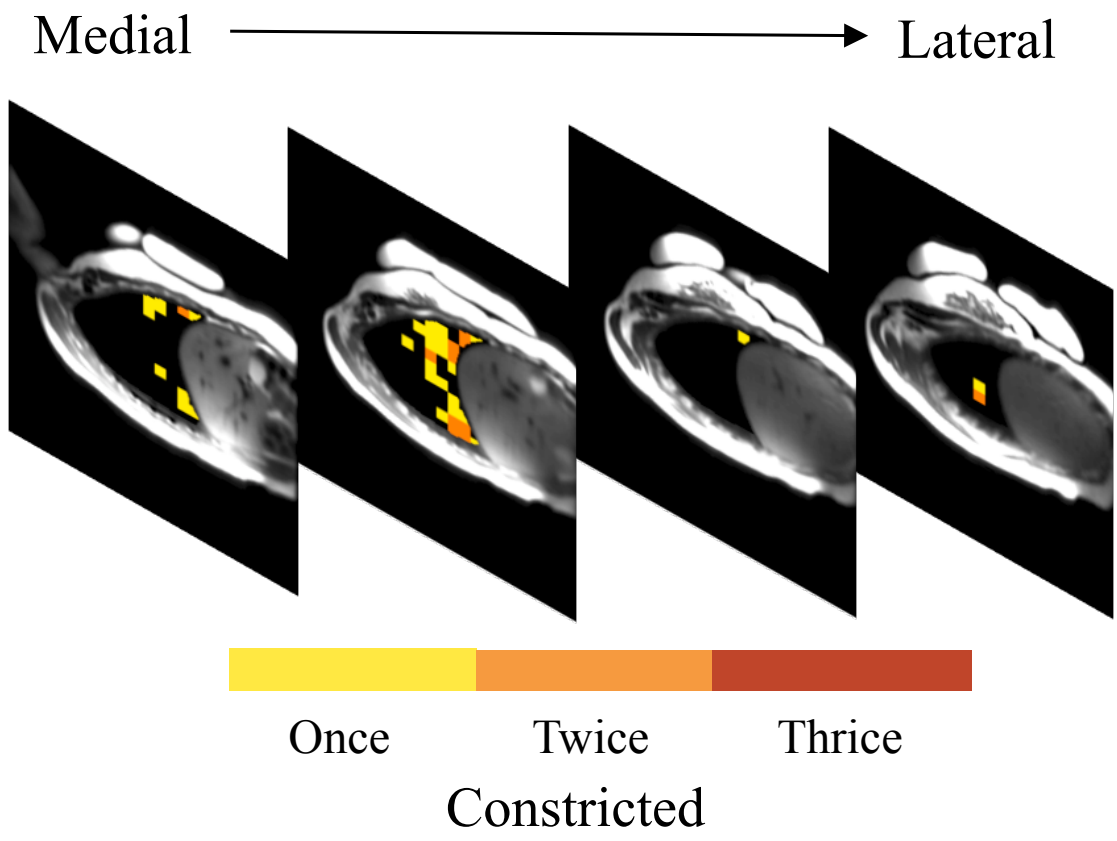

Figure 5-1: Spatial repeatability of bronchoconstriction in a young, recently-diagnosed asthmatic. No regions of her lung constricted in all three challenges (no thrice constrictors). The same data is displayed for 6 healthy, young subjects in Figure 3-6.

We acknowledge the risk in making inferences from the data of only one subject. But this trend, if it was borne out in a group of subjects similar to this one (young and recently diagnosed with asthma), would support our previous hypothesis - that asthmatics with a short disease duration have a highly variable pattern of methacholine bronchoconstriction that is due to relatively greater perturbations in initial conditions between subsequent challenges.

Towards a clinical biomarker

The results presented in Chapter 4 show that regional measurements of ventilation provide the resolution to detect subtle effects that would have escaped classical functional measurements such as FEV_1 or ventilation heterogeneity. This result fits in with others that have begun to make the case for functional imaging as a clinical biomarker.

One such result came recently from Svenningsen and her colleagues. This group showed that a certain subset of asthmatics had ventilation defects that were resistant to therapy with albuterol, but resolved after several weeks of treatment with an anti-Th2 monoclonal antibody (27, 29). These albuterol-resistant defects may be characteristic of an asthma phenotype in whom treatment with this drug is especially appropriate and/or efficacious.

Furthermore, a reduction in the percentage of defective lung may be useful clinical endpoint. It has been demonstrated that the percentage of an asthmatic's lung that is classified as a defect correlates with their overall quality of life (28). Thus, the ventilation defect percentage may be the ideal tool for clinical research studies, as it depicts the objective physiological characteristics of the disease while also correlating with the patient's subjective experience.

In order for functional ventilatory imaging to become a clinical biomarker, it must first become a widely accessible. Specific Ventilation Imaging is especially well situated in this

regard because it is relatively easy to perform and infinitely repeatable. Other MR functional imaging methods require the subject to inhale hyperpolarized gas to create contrast. The gas and the hyperpolarization process are expensive and the equipment required is highly specialized. SVI, on the other hand, requires only a clinical MR scanner, a bottle of medical oxygen, and a mask equipped with a plastic flow-bypass device. The first two are ubiquitous in the clinical environment, and the last can be cheaply obtained (4).

CT and PET are both, like SVI, capable of producing maps of ventilatory function using standard equipment. Both provide a higher signal-to-noise ratio than SVI, but the radiation exposure associated with CT and PET presents a problem for large studies, particularly those with repeat measurements. Since asthma is a chronic disease that progresses over decades, longitudinal studies with repeat measurements may be of interest. SVI is particularly well suited for these types of studies because it is based on proton MRI, an imaging technique with no known long-term effects.

Targeting treatment with functional imaging

Historically, one of the primary functions of imaging has been to tell surgeons which areas of the body they need to fix or cut out. Typically the area is an anatomical anomaly - a tumor, lesion, tear, etc. However, the emerging field of functional imaging carries with it the promise to guide medical intervention by maps of function instead of anatomy. This was realized first in the 1990s, when functional MRI of the brain was used to help surgeons stay away from the motor cortex while performing intracranial tumor resections (13).

There is at least one invasive treatment of asthma that might benefit from this kind functional guidance, bronchial thermoplasty. In bronchial thermoplasty (BTP), an expanding

basket of four electrodes is attached to a bronchoscope and used to thermally ablate airway smooth muscle (33). Following thermal ablation, epithelium and mucus glands regenerate but smooth muscle bulk is permanently reduced (3).

The decrease in smooth muscle bulk leads to an increase in flow through the ablated airways and a reduction in smooth muscle responsiveness. Together, these effects prevent airflow obstruction after exposure to asthmatic triggers. Further, the increased flow through the ablated airways may lead to a downstream cascade of airway reopening, which ultimately leads to healthier, less heterogeneous flow patterns (7).

As BTP is invasive, there is a reasonable urge to limit the procedure to the minimal beneficial dose. One ongoing clinical research trial seeks to minimize dose by targeting regions of impaired ventilation with functional MRI, and then restricting thermoplasty to those region (22). No articles or abstracts have been published for this study.

The benefit of targeted vs. global BTP is not obvious. If Wayne Mitzner is correct that the airway smooth muscle is the "appendix of the lung" and only exists to become pathologic, then the greatest benefit to patients may come from ablation of all accessible regions of smooth muscle.

Further, the benefit of BTP may lie in the fact that all areas of the lung are equally ablated. The effect of ablation is to prevent a particular segment of airway from constricting. When this happens, the upstream and downstream feedback predicted by Venegas and Winkler is interrupted at the level at which the ablation was performed. By treating only the unhealthy airways and not the healthy airways, surgeons might be simply forcing the previously healthy areas to now constrict under duress. The result would be recurrent bronchoconstriction in the

untreated areas, which would lead to damage and remodeling in the areas that were previously healthy.

Furthermore, guided bronchial thermoplasty is only justified if the adverse effects of guided treatment are less than those of whole-lung treatment. So far, evidence of severe adverse effects in whole-lung bronchial thermoplasty has been sparse. One of the original investigations of BTP reported no severe adverse effects of the treatment, and all minor effects happened within a week of the procedure (5). Later, a 5-year investigation found that none of 52 patients who underwent BTP experienced pneumothroax, intubation, mechanical ventilation, cardiac arrhythmias, or death related to the procedure (30). The rate of adverse events was not significantly higher between patients who underwent thermoplasty and those who underwent sham bronchoscopy (30). Patients undergo bronchoscopy whether or not BTP is targeted or global, so it is unlikely that targeted treatment will reduce side effects.

However, targeted therapy may have time and cost benefits. Typically, bronchial thermoplasty is performed in three sessions, each of which requires sedation and bronchoscopy. If the number of sessions could be reduced to one or two via image-based guidance, the total cost would likely decrease in tandem.

Conclusion

The purpose of this dissertation work was to learn about asthma by studying people who don't have the disease. In some sense, it was a control experiment. We showed that the spatially recurrent pattern of constriction that had previously been demonstrated in asthmatics (16, 17, 21) could also be elicited in healthy individuals, and that the spatial trends present in asthmatics (11,

12) were also present in healthy individuals. Bronchoconstriction is patchy and skewed towards the dependent lung, no inflammation or remodeling required.

But our results provided more than just points of comparison. They also produced new, surprising insight: the pattern of methacholine deposition does not determine the resulting pattern of bronchoconstriction, and the spatial pattern of bronchoconstriction in a given subject can be changed in the middle of an event by simply changing the subject's gravitational orientation. This second result paints smooth muscle-mediated bronchoconstriction in a new light, as a dynamic process that can shift and adjust to new conditions.

Our data also provided a convincing reason why SVI could be the method of choice in future studies of asthma. Functional imaging with SVI showed that healthy subjects did not recover from bronchoconstriction shortly after albuterol inhalation, even though their FEV_1, a current standard-of-care technique, and global ventilation heterogeneity, a relatively cutting-edge technique, both returned to normal. This showed that SVI is sensitive to subtle effects that these previous techniques would miss.

As asthma becomes more prevalent (19), and new, personalized treatments for recalcitrant asthma become approved (8), the need to precisely phenotype patients and monitor their response to treatment becomes more evident. Specific Ventilation Imaging may prove to be a useful tool for the job, as it is safe, sensitive, and can be adapted for use in any medical center with an MRI machine.

References

1. **Asadi AK**, **Cronin M V.**, **Sá RC**, **Theilmann RJ**, **Holverda S**, **Hopkins SR**, **Buxton RB**, **Prisk GK**. Spatial-temporal dynamics of pulmonary blood flow in the healthy human lung in response to altered F_{iO_2}. *J Appl Physiol* 114: 107–118, 2013.

2. **Barnes PJ**. New concepts in the pathogenesis of bronchial hyperresponsiveness and asthma. *J Allergy Clin Immunol* 83: 1013–1026, 1989.

3. **Barnes PJ**, **Drazen JM**, **Rennard SI**, **Thomson NC**, **Polkey MI**, **Shah PL**. Surgical and Other Mechanical Procedures. *Asthma COPD* (January 1, 2009). doi: 10.1016/B978-0-12-374001-4.00059-6.

4. **Cook FR**, **Geier ET**, **Asadi AK**, **Sá RC**, **Prisk GK**. Rapid prototyping of inspired gas delivery system for pulmonary MRI research. *3D Print Addit Manuf* 2, 2015.

5. **Cox G**, **Miller JD**, **McWilliams A**, **Fitzgerald JM**, **Lam S**. Bronchial thermoplasty for asthma. *Am J Respir Crit Care Med* 173: 965–9, 2006.

6. **Crawford AB**, **Makowska M**, **Engel LA**. Effect of bronchomotor tone on static mechanical properties of lung and ventilation distribution. *J Appl Physiol* 63: 2278–85, 1987.

7. **Donovan GM**, **Elliot JG**, **Green FHY**, **James AL**, **Noble PB**. Unraveling a Clinical Paradox: Why Does Bronchial Thermoplasty Work in Asthma? *Am J Respir Cell Mol Biol* 59: 355–362, 2018.

8. **Fajt ML**, **Wenzel SE**. Asthma phenotypes and the use of biologic medications in asthma and allergic disease: The next steps toward personalized care. *J Allergy Clin Immunol* 135: 299–310, 2015.

9. **Hancox RJ**, **Subbarao P**, **Kamada D**, **Watson RM**, **Hargreave FE**, **Inman MD**. β_2-Agonist Tolerance and Exercise-induced Bronchospasm. *Am J Respir Crit Care Med* 165: 1068–1070, 2002.

10. **Hardin M**, **Cho MH**, **McDonald M-L**, **Wan E**, **Lomas DA**, **Coxson HO**, **MacNee W**, **Vestbo J**, **Yates JC**, **Agusti A**, **Calverley PMA**, **Celli B**, **Crim C**, **Rennard S**, **Wouters E**, **Bakke P**, **Bhatt SP**, **Kim V**, **Ramsdell J**, **Regan EA**, **Make BJ**, **Hokanson JE**, **Crapo JD**, **Beaty TH**, **Hersh CP**, **Investigators on behalf of the E and Copdg**, **Crapo J**, **Silverman E**, **Make B**, **Regan E**, **Beaty T**, **Laird N**, **Lange C**, **Cho M**, **Santorico S**, **Hokanson J**, **DeMeo D**, **Hansel N**, **Hersh C**, **Castaldi P**, **McDonald M-L**, **Wan E**, **Hardin M**, **Hetmanski J**, **Parker M**, **Foreman M**, **Hobbs B**, **Busch R**, **El-Bouiez A**, **Castaldi P**, **Hardin M**, **Qiao D**, **Regan E**, **Halper-Stromberg E**, **Begum F**, **Won S**, **Fredericksen B**, **Lutz S**, **Lynch DA**, **Coxson HO**, **Han MK**, **Hoffman EA**, **Humphries S**, **Jacobson FL**, **Judy PF**, **Kazerooni EA**, **Newell JD**, **Regan E**, **Ross JC**, **Estepar RSJ**, **Stoel BC**, **Tschirren J**, **Rikxoort E van**, **Ginneken B van**, **Washko G**, **Wilson CG**,

Qaisi M Al, **Gray T**, **Kluiber A**, **Mann T**, **Sieren J**, **Stinson D**, **Schroeder J**, **Beek E Van**, **Jensen R**, **Everett D**, **Faino A**, **Strand M**, **Wilson C**, **Hokanson JE**, **Black-Shinn J**, **Kinney G**, **Lutz S**, **Pratte K**, **centers CopdgI**, **Curtis J**, **Martinez C**, **Pernicano PG**, **Hanania N**, **Alapat P**, **Bandi V**, **Atik M**, **Boriek A**, **Guntupalli K**, **Guy E**, **Parulekar A**, **Nachiappan A**, **DeMeo D**, **Hersh C**, **Washko G**, **Jacobson F**, **Barr RG**, **Thomashow B**, **Austin J**, **D'Souza B**, **Pearson GDN**, **Rozenshtein A**, **MacIntyre N**, **McAdams HP**, **McEvoy C**, **Tashjian J**, **Wise R**, **Hansel N**, **Brown R**, **Horton K**, **Putcha N**, **Casaburi R**, **Adami A**, **Porszasz J**, **Fischer H**, **Budoff M**, **Cannon D**, **Rossiter H**, **Sharafkhaneh A**, **Lan C**, **Wendt C**, **Bell B**, **Foreman M**, **Westney G**, **Berkowitz E**, **Bowler R**, **Lynch D**, **Rosiello R**, **Pace D**, **Criner G**, **Ciccolella D**, **Cordova F**, **Dass C**, **D'Alonzo R**, **Desai P**, **Jacobs M**, **Kelsen S**, **Kim V**, **Mamary AJ**, **Marchetti N**, **Satti A**, **Shenoy K**, **Steiner RM**, **Swift A**, **Swift I**, **Vega-Sanchez G**, **Nath H**, **Dransfield M**, **Bailey W**, **Wells JM**, **Bhatt S**, **Nath H**, **Ramsdell J**, **Friedman P**, **Soler X**, **Yen A**, **Cornellas A**, **Newell J**, **Thompson B**, **Han M**, **Kazerooni E**, **Martinez F**, **Billings J**, **Allen T**, **Sciurba F**, **Chandra D**, **Weissfeld J**, **Fuhrman C**, **Bon J**, **Anzueto A**, **Adams S**, **Maselli-Caceres D**, **Ruiz ME**, **Bourbeau J**, **Fitzgerald M**, **Hernández P**, **Killian K**, **Levy R**, **Maltais F**, **O'Donnell D**, **Krepelka J**, **Vestbo J**, **Wouters E**, **Quinn D**, **Bakke P**, **Kosnik M**, **Agusti A**, **Mallorca P de**, **Feschenko Y**, **Gavrisyuk V**, **Yashina L**, **Yashina L**, **MacNee W**, **Singh D**, **Wedzicha J**, **Anzueto A**, **Braman S**, **Casaburi R**, **Celli B**, **Giessel G**, **Gotfried M**, **Greenwald G**, **Hanania N**, **Mahler D**, **Make B**, **Rennard S**, **Rochester C**, **Scanlon P**, **Schuller D**, **Sciurba F**, **Sharafkhaneh A**, **Siler T**, **Silverman E**, **Wanner A**, **Wise R**, **Coxson H**, **Crim C**, **Edwards L**, **Lomas D**, **MacNee W**, **Silverman E**, **Singer RT**, **Vestbo J**, **Yates J**, **Agusti A**, **Calverley P**, **Celli B**, **Crim C**, **Miller B**, **MacNee W**, **Rennard S**, **Tal-Singer R**, **Wouters E**, **Yates J**. A genome-wide analysis of the response to inhaled β2-agonists in chronic obstructive pulmonary disease. *Pharmacogenomics J* 16: 326–335, 2016.

11. **Harris RS**, **Fujii-Rios H**, **Winkler T**, **Musch G**, **Vidal Melo MF**, **Venegas JG**. Ventilation Defect Formation in Healthy and Asthma Subjects Is Determined by Lung Inflation. *PLoS One* (2012). doi: 10.1371/journal.pone.0053216.

12. **Harris RS**, **Winkler T**, **Musch G**, **Vidal Melo MF**, **Schroeder T**, **Tgavalekos N**, **Venegas JG**. The prone position results in smaller ventilation defects during bronchoconstriction in asthma. *J Appl Physiol* 107: 266–74, 2009.

13. **Holodny AI**, **Schulder M**, **Liu W-C**, **Wolko J**, **Maldjian JA**, **Kalnin AJ**. The Effect of Brain Tumors on BOLD Functional MR Imaging Activation in the Adjacent Motor Cortex: Implications for Image-guided Neurosurgery [Online]. http://www.ajnr.org/content/ajnr/21/8/1415.full.pdf [9 Oct. 2018].

14. **Hopkins SR**, **Henderson AC**, **Levin DL**, **Yamada K**, **Arai T**, **Buxton RB**, **Prisk GK**. Vertical gradients in regional lung density and perfusion in the supine human lung: the Slinky effect. *J Appl Physiol* 103: 240–248, 2007.

15. **Kruger SJ**, **Niles DJ**, **Dardzinski B**, **Harman A**, **Jarjour NN**, **Ruddy M**, **Nagle SK**, **Francois CJ**, **Sorkness RL**, **Burton RM**, **Munoz del Rio A**, **Fain SB**. Hyperpolarized

Helium-3 MRI of exercise-induced bronchoconstriction during challenge and therapy. *J Magn Reson Imaging* 39: 1230–7, 2014.

16. **de Lange EE**, **Altes TA**, **Patrie JT**, **Battiston JJ**, **Juersivich AP**, **Mugler JP**, **Platts-Mills TA**. Changes in Regional Airflow Obstruction over Time in the Lungs of Patients with Asthma: Evaluation with ^{3} He MR Imaging. *Radiology* 250: 567–575, 2009.

17. **de Lange EE**, **Altes TA**, **Patrie JT**, **Parmar J**, **Brookeman JR**, **Mugler JP**, **Platts-Mills TAE**. The variability of regional airflow obstruction within the lungs of patients with asthma: Assessment with hyperpolarized helium-3 magnetic resonance imaging. *J. Allergy Clin. Immunol.* (2007). doi: 10.1016/j.jaci.2006.12.659.

18. **Leary D**, **Winkler T**, **Braune A**, **Maksym GN**. Effects of airway tree asymmetry on the emergence and spatial persistence of ventilation defects. *J Appl Physiol* 117: 353–362, 2014.

19. **Lundbäck B**, **Backman H**, **Lötvall J**, **Rönmark E**. Is asthma prevalence still increasing? *Expert Rev Respir Med* 10: 39–51, 2016.

20. **Mitzner W**. Airway Smooth Muscle. *Am J Respir Crit Care Med* 169: 787–790, 2004.

21. **Niles DJ**, **Kruger SJ**, **Dardzinski BJ**, **Harman A**, **Jarjour NN**, **Ruddy M**, **Nagle SK**, **François CJ**, **Fain SB**. He MR Imaging 1. *Radiol n Radiol* 266, 2013.

22. **Parraga G**. Hyperpolarized Magnetic Resonance Imaging in Asthma Pre- and Post-Bronchial Thermoplasty - [Online]. 2014. https://clinicaltrials.gov/ct2/show/NCT02263794.

23. **Sá RC**, **Cronin M V.**, **Cortney Henderson A**, **Holverda S**, **Theilmann RJ**, **Arai TJ**, **Dubowitz DJ**, **Hopkins SR**, **Buxton RB**, **Kim Prisk G**. Vertical distribution of specific ventilation in normal supine humans measured by oxygen-enhanced proton MRI. *J Appl Physiol* 109: 1950–1959, 2010.

24. **Sá RC**, **Zeman KL**, **Bennett WD**, **Prisk GK**, **Darquenne C**. Regional Ventilation Is the Main Determinant of Alveolar Deposition of Coarse Particles in the Supine Healthy Human Lung During Tidal Breathing. *J Aerosol Med Pulm Drug Deliv* 30: 322–331, 2017.

25. **Severinghaus JW**, **Swenson EW**, **Finley TN**, **Lategola MT**, **Williams J**. Unilateral hypoventilation produced in dogs by occluding one pulmonary artery. *J Appl Physiol* 16: 53–60, 1961.

26. **Stewart RM**, **Weir EK**, **Montgomery MR**, **Niewoehner DE**. Hydrogen peroxide contracts airway smooth muscle: a possible endogenous mechanism. [Online]. *Respir Physiol* 45: 333–42, 1981. http://www.ncbi.nlm.nih.gov/pubmed/7330488 [23 Oct. 2018].

27. **Svenningsen S**, **Eddy RL**, **Lim HF**, **Cox PG**, **Nair P**, **Parraga G**. Sputum Eosinophilia and Magnetic Resonance Imaging Ventilation Heterogeneity in Severe Asthma. *Am J Respir Crit Care Med* 197: 876–884, 2018.

28. **Svenningsen S**, **Nair P**, **Guo F**, **McCormack DG**, **Parraga G**. Is ventilation heterogeneity related to asthma control? *Eur. Respir. J.* (2016). doi: 10.1183/13993003.00393-2016.

29. **Svenningsen SL**, **Eddy R**, **Capaldi DP**, **Kjarsgaard M**, **Radford K**, **Parraga G**, **Nair P**. Effect of Anti-Th2 Therapy on MRI Ventilation Heterogeneity in Prednisone-Dependent Asthma. *Am J Respir Crit Care Med* 197: A6393, 2018.

30. **Thomson NC**, **Rubin AS**, **Niven RM**, **Corris PA**, **Siersted HC**, **Olivenstein R**, **Pavord ID**, **McCormack D**, **Laviolette M**, **Shargill NS**, **Cox G**. Long-term (5 year) safety of bronchial thermoplasty: Asthma Intervention Research (AIR) trial. BioMed Central.

31. **Venegas JG**, **Winkler T**, **Musch G**, **Melo MFV**, **Layfield D**, **Tgavalekos N**, **Fischman AJ**, **Callahan RJ**, **Bellani G**, **Harris RS**. Self-organized patchiness in asthma as a prelude to catastrophic shifts. *Nature* 434: 777–782, 2005.

32. **Vestal RE**, **Wood AJJ**, **Shand DG**. Reduced β-adrenoceptor sensitivity in the elderly. *Clin Pharmacol Ther* 26: 181–186, 1979.

33. **Wahidi MM**, **Kraft M**. Bronchial Thermoplasty for Severe Asthma. *Am J Respir Crit Care Med* 185: 709–714, 2012.

34. **Winkler T**, **Venegas JG**. Complex airway behavior and paradoxical responses to bronchoprovocation. *J Appl Physiol* 103: 655–663, 2007.

35. **Woolcock AJ**, **Salome CM**, **Yan K**. The shape of the dose-response curve to histamine in asthmatic and normal subjects. *Am Rev Respir Dis* 130: 71–5, 1984.

APPENDIX A

Specific Ventilation Imaging: using oxygen-enhanced proton MRI to quantify specific ventilation in the human lung

Specific Ventilation Imaging: using oxygen-enhanced proton MRI to quantify specific ventilation in the human lung

Eric T. Geier[1], Rebecca J. Theilmann[2], Chantal Darquenne[1], G. Kim Prisk[1], Rui C. Sá[1]

Pulmonary Imaging Laboratory

Departments of Medicine[1] and Radiology[2] ,

University of California, San Diego, La Jolla, California, USA

Running tittle: Specific Ventilation Imaging, video methods

Keywords:

Respiration, Lung, Specific Ventilation, functional Magnetic Resonance Imaging, oxygen enhanced Magnetic Resonance Imaging

Address for correspondence: Rui Carlos Sá

rcsa@ucsd.edu

Abstract

Specific ventilation Imaging is a functional Magnetic Resonance Imaging technique capable of quantifying specific ventilation - the ratio of the fresh gas entering a lung region divided by the end-expiratory volume of that region - in the human lung, using only inhaled oxygen as a contrast agent. Regional quantification of specific ventilation has the potential to help identify areas of pathologic lung function.

Oxygen in solution in a tissue shortens the tissue's longitudinal relaxation time (T_1), and thus a change in tissue oxygenation can be detected as a change in T_1-weighted signal in an inversion recovery image. Following an abrupt change between two concentrations of inspired oxygen, the rate at which a lung voxel equilibrates to a new steady-state T_1 reflects the rate at which resident gas is being replaced by inhaled gas. This rate is the voxel's specific ventilation.

To elicit this sudden change in oxygenation, our subjects alternately breathe 20-breath blocks of air and 100% oxygen while in the MR scanner. The stepwise change in inspired gas is achieved during a single end-expiratory breath hold through use of a custom 3D printed flow bypass system (6). To detect the corresponding change in T_1, we use a global inversion pulse followed by a single shot fast spin echo sequence to acquire two-dimensional T_1-weighted images in a 1.5 T MRI (General Electric Medical Systems, Milwaukee,WI) scanner with an attached eight-element torso coil. Both single slice and multi-slice imaging are possible, with slightly different imaging parameters. Quantification of specific ventilation is achieved by correlating the time-course of signal intensity for each lung voxel with a library of simulated SV responses to the air/oxygen stimulus. The technique has been validated in healthy subjects, by comparing it to Multiple Breath Washout, and proved to accurately determine the heterogeneity of the specific ventilation distribution.

Introduction

Specific Ventilation Imaging (SVI) is a proton Magnetic Resonance Imaging technique capable of quantitatively mapping specific ventilation in the human lung, using oxygen as a contrast agent. Specific ventilation is the ratio of fresh gas delivered to a lung region in one breath divided by the end expiratory volume of the same lung region. In conjunction with measurements of local lung density, specific ventilation can be used to compute regional ventilation. Measurements of local ventilation and ventilation heterogeneity that are provided by SVI have the potential to enrich our understanding of how the lung functions, both normally and abnormally.

Specific Ventilation Imaging is an extension of the classical physiology test Multiple Breath Washout (MBW), a technique first introduced in the 1950's (7, 17) Both techniques use gas washin/washout to measure heterogeneity of specific ventilation, but SVI provides spatially-localized information while MBW provides only global measures of heterogeneity. In MBW, we use a mass spectrometer to measure the mixed expired concentration of an inert gas (nitrogen, helium, sulfur hexafluoride, etc) over many breaths during a washout of that gas. Along with the expired volume per breath during the washout period, this information can be used to compute the overall distribution of specific ventilation in the lung. In SVI, we use an MR scanner to measure T_1-weighted signal – which is a surrogate for the amount of oxygen in solution in tissues, a direct indicator of local oxygen concentration – in each lung voxel over many breaths during several washin/washouts of oxygen. In a way that is directly analogous to MBW, this information allows us to compute the SV *of each lung voxel*. In other words, we are performing thousands of parallel MBW-like experiments, one for each voxel, during an SVI experiment. Indeed, the spatial maps of SV thus produced can be compiled to recover the SV heterogeneity

output of MBW. A validation study performed by our lab (18) showed that the two methodologies produced similar results when performed in series on the same subjects.

Other imaging modalities exist that, like SVI, provide spatial measures of ventilation heterogeneity. PET (16, 22), SPECT (), and hyperpolarized gas MRI (10, 13) techniques have been used to create a substantial body of literature regarding the spatial pattern of ventilation in healthy and abnormal subjects. In general, these techniques have at least one distinct advantage over SVI, in that their signal-to-noise ratio is characteristically higher. However, each technique also has a characteristic disadvantage: PET and SPECT involve exposure to ionizing radiation, and hyperpolarized MRI requires the use of highly specialized hyperpolarized gas and a dedicated MR scanner.

SVI, a proton-MRI technique, uses 1.5 Tesla MR hardware with inhaled oxygen as a contrast agent (both elements are readily available in healthcare), making it potentially more generalizable to the clinical environment. Furthermore, as SVI involves no ionizing radiation, it has no contraindications for longitudinal and interventional studies that follow patients over time. Thus, it is ideally suited for studying disease progression or evaluating how individual patients responds to treatment. Due to its relative ease and safe repeatability, specific ventilation imaging is, in general, an ideal technique for those who wish to study large effects and/or a large number of people over time or in several different clinical locations.

Following the original publication describing the technique (19), Specific Ventilation Imaging has been used in studies focused on the effect of rapid saline infusion, posture, exercise, and bronchoconstriction (8, 9, 11, 12, 20). The technique has been compared in validation studies with the well-established multiple-breath washout test (18) and more recently with hyperpolarized gas multiple breath specific ventilation imaging (1). This validated, reliable, and

readily deployable technique, capable of quantitatively mapping specific ventilation in the human lung has the potential to significantly contribute to early detection and diagnosis of respiratory disease. It also presents new opportunities to quantify regional lung abnormalities and follow changes induced by therapy. These changes in region-specific lung function, which SVI enables us to measure for the first time, have the potential to become biomarkers for assessing the impact of drugs and inhaled therapies, and could be an extremely useful tool in clinical trials.

Protocol

The University of California, San Diego Human Research Protection Program has approved this protocol.

1. Subject safety and training

1.1) Obtain written, informed consent from the subject. Describe the potential risks presented by exposure to rapidly changing magnetic fields, and the potential discomfort of using facial mask and breathing dry gas.

1.2) Ensure that the subject can safely undergo MR scanning, utilizing the MRI safety screening questionnaire that has been approved by your institution.

1.3) If the subject is a female of childbearing age, and uncertain of her pregnancy status, ask her to self-administer an over-the-counter pregnancy test. If the subject is pregnant, she must be excluded from the remainder of the study.

1.4) Measure the subject's weight. Scanner safety parameters that limit the amount of radio frequency (RF) energy delivered to the subject require input of this characteristic.

1.5) Train the subject to breathe in time with the MR scan sequence. Preferably, play an audio recording of a previous scan and instruct the subject to breathe in and out fully between

the noises made by image acquisition (which occur every 5 seconds), performing the exercise along with them.

1.6) Determine the size of Hans-Rudolph face mask (sizes range from petite – XL) that best fits the subject by measuring the subject's nose-to-chin dimensions. An appropriately-sized mask will fit comfortably yet will prevent air from leaking in between the mask and the subject's skin at any point. Try on other sizes if necessary.

2. Preparation of the MRI environment

2.1) Only persons who have been trained in MRI safety, to the standards of your institution, should be allowed to enter the scanner room or assist in performing this experiment.

2.2) Configure the MR scanner for use with a torso coil.

2.3) Prepare the scanner table with sheets, pads, and pillows so that the subject will be comfortable for at least 20 minutes during imaging.

2.4) Assemble oxygen delivery system

2.4.1) Place a two/three-way switching valve within reach of the scanner operator or person performing the SVI experiment.

2.4.2) Connect a tank of medical oxygen to one inlet of the switching valve using ¼" plastic tubing.

2.4.3) Connect the outlet of the switch valve located in the control room to the 8 meter (or sufficient length for your scanner) plastic tubing. Feed this length of tubing through the pass-through, from the control room to the scanner room, and ensure that it will reach the middle of the scanner bore.

2.4.4) Connect the end of the long length of tubing to the flow-bypass attachment.

2.4.5) Secure the flow-bypass attachment to the Hans-Rudolph face mask that was fit to the subject in step 1.6.

2.4.6) Verify that the pressure on the gas tank regulator is set to ~70 psi.

2.4.7) Test the switch valve by activating the flow of oxygen, making sure adequate flow is present at the outlet of the flow-bypass attachment and that no leaks are present in the plastic tubing.

3. Instrumenting the subject and preparing him or her for imaging

3.1) Have the subject lie on the MRI table, feet towards the scanner bore. Make sure the top lower-coil element provide adequate coverage of the lung apices, by making sure the top of the lower-coil element is higher than the subject's shoulders.

3.2) Have the subject insert earplugs and verify that sound is being blocked.

3.3) Tape the squeeze ball (or alternate safety mechanism) to the subject's wrist so that it can be easily accessed.

3.4) Attach the mask and flow-bypass system to the subject's face. Briefly occlude the expiratory side of the flow-bypass attachment and ask the subject to attempt a normal inspiration and expiration to check for leaks.

3.5) Place the subject into the scanner, using the laser centering tool to make sure that the torso coil occupies the center of the bore.

3.6) Connect the flow bypass line to the 3D printed flow-bypass mask attachment using the tight-fitting brass nut to the inlet.

4. MRI Imaging

4.1) Select the anatomical location for imaging slices.

4.1.1) Acquire a localizer sequence to obtain an anatomical map that will be used to prescribe the rest of the exam.

4.1.2) Select up to 4 sagittal lung slices to be studied. Typically, the field of view is set to 40x40cm and slice thickness to 1.5cm. Slices are chosen to minimize the intrusion of large pulmonary vessels medially and chest wall laterally. Slice selection can be done in any plane; up to 4 slices can be selected. For the purpose of demonstration, one slice will be acquired.

4.2) Specific Ventilation Imaging

4.2.1) Specific Ventilation Imaging is a type of Inversion Recovery (IR) imaging. The inversion time for the most medial slice should be set to 1100ms (maximizing air-oxygen contrast (5)). Each additional slice is acquired after the first, at intervals of 235 ms (1335 ms, 1570ms, 1805ms).

4.2.2) Following the inversion recovery pulse and a time interval (described by the inversion time), each slice image is acquired using a half-Fourier single-shot turbo spin-echo (HASTE), at 128x128 resolution (70-lines of k-space sampled); images are reconstructed to 256x256 resolution.

4.2.3) Repeat 4.2.1 and 4.2.2 for a total of 220 consecutive breaths. The subject is asked to voluntarily gate, such that each of the 220 iterations, typically acquired 5s apart, should be acquired at the end of a normal expiration in a short voluntary breathing interruption at Functional Residual Capacity (FRC). It is important that a similar lung volume is reached consistently during each of these consecutive acquisitions.

4.2.4) Monitor the consistency of the subject's lung volume (end expiration) during subsequent acquisitions and provide feedback to improve quality if necessary. Increase TR (the time interval between successive acquisitions) if the subject finds it difficult to reach a consistent lung volume every 5 seconds.

4.2.5) Switch the subject's inspired gas mixture every 20 breaths (during the acquisition breath hold for the subject's comfort), alternating between room air and medical oxygen. Make note of when the switches occurred, and the intervals during which the subject was breathing each gas. Allow the subject to breath 100% oxygen for 40 breaths at some point in the experiment (typically for breaths 20-60 or 180-220).

4.2.6) Regularly verify heart rate (40-80 for normal subjects at rest) and oxygen saturation (typically 98-100%), as deviations from the norm can signal distress or anxiety.

4.2.7) Talk to the subject frequently, giving regular updates of time remaining.

4.2.8) After breath 220, imaging is complete. Return the subject to room air and remove him or her from the scanner.

5. Creating a specific ventilation map from a time series of images

5.1) Verify that you have a stack of 220 consecutive MR images for each lung slice acquired, obtained during 6 oxygen wash-ins and 5 oxygen wash-outs. One oxygen wash-in should be 40 breaths long, while all other wash-ins/wash-outs should be 20 breaths long.

5.2) Import the registered images to Matlab (the Mathworks, Natick, MA).

5.3) Of the 220 images, choose one that you think best represents functional residual capacity. This should be the "mode" of lung volumes in the stack.

5.4) Using the "mode" image as reference, use projective registration to register all images to the functional residual capacity reference. Our group uses either an algorithm developed in house (available here (3)) or a publicly-available generalized-dual bootstrap iterative closest point algorithm (GDB-ICP (23)).

5.5) Use the output of the registration algorithm to compute the area change of each image. Images whose registration step required > 10% area change are discarded from your image stack and treated as missing data (4).

5.6) Quantify specific ventilation in the lung from the registered stack using an algorithm developed in house (18, 19), implemented in Matlab. Quantification is made by comparing the time response of each voxel to the consecutive oxygen washin and washout series, to a library of 50 simulated, noise free, responses, corresponding to specific ventilations ranging from 0.01 to 10, in 15% increments. Each voxel is assigned a value of specific ventilation corresponding to the SV of the simulated ideal presenting maximal correlation with each voxel's time series.

5.7) The output of the previous step is a map of specific ventilation for an image slice. A histogram of the distribution is often created at this stage. One variable of interest is the width of the SV distribution, as it is a measure of the SV heterogeneity, independently of tidal volume.

6) Combining SV and density maps to compute regional alveolar ventilation

6.1) In addition to SVI, you may choose to acquire lung proton density images (21), as previously described in JoVE (2) sections 4.4 and 5.1. If so, obtain the proton density images in the same lung slice(s), at the same lung volume (FRC, end of a normal expiration), at a resolution of 64x64, corresponding to a voxel size of ~6.3x6.3x15mm (~0.6cm^3).

6.2) Aligning SV and proton density:

6.2.1) Smooth both the SV and proton density images using a gaussian filter with a kernel size of ~1 cm^3.

6.2.2) Perform a rigid registration (translation and rotation) between the map of SV and the map of density using a mutual information-based algorithm.

6.3) Compute alveolar ventilation from co-registered SV and proton density data:

6.3.1) Under the assumption that the lung is composed of air and tissue and that tissue density is ~1 g/cm^3, lung density is a measure of the tissue fraction in the sampled volume. Hence (1-Density) is a measure of the fraction of air in the sampled volume at the end of a normal expiration.

6.3.2) For each lung region SV = $\Delta V / V_0$ and (1 – Density) $\approx V_0$. Thus, the product (1-Density) x SV = regional ventilation, expressed in natural units. Multiplying this product by the volume of a voxel (or other region of interest) and the breathing frequency (imposed, typically 12 breaths/min), produces a map of ventilation in the more familiar units of ml/min.

Representative Results:

Single slice SVI in a healthy subject

Specific Ventilation Imaging produces quantitative maps of specific ventilation similar to Figure A-1, which depicts a single slice in the right lung of a 39-year-old healthy female. Note the presence of the expected vertical gradient in specific ventilation; the dependent portion of the lung presents higher specific ventilation than the non-dependent portion of the lung. A histogram of the mapped specific ventilation values is presented (Figure A-1, filled circles) along with a best-fit log-normal probability distribution function (dotted line). The width of the best-fit distribution can be used as a metric of specific ventilation heterogeneity (15, 18). Specific ventilation heterogeneity thus measured has been compared to SV heterogeneity measured by the well-established MBW technique in the same subjects, and the difference in the metric between the two methods was found to be less than the MBW inter-test variability (18). Further, a spatial comparison with a hyperpolarized gas multiple breath specific ventilation imaging (1) showed reliable group estimates of SV-heterogeneity, despite higher than expected intra-subject variability.

Specific ventilation maps can also be used in conjunction with lung density maps to compute regional alveolar ventilation. Figure A-2 depicts a map of alveolar ventilation for the same lung slice as picture in Figure A-1. To generate maps of alveolar ventilation, SV and density images must be spatially smoothed to minimize the potential minor misalignments between the two modalities.

Response to methacholine challenge in an asthmatic subject.

SVI can be used to measure both lung-wide and regional responses to interventions such as exercise (20), posture (12), or medication (8). As an example, Figure A-3 depicts single-slice maps from the lung of a mild asthmatic female subject at baseline (panel A), following bronchoconstriction with methacholine (panel B), and after albuterol-assisted recovery (panel C). Note the increased SV heterogeneity during the induced asthma event, and the presence of large patches of little to no specific ventilation (dark blue regions in the dependent portion of the lung). Also note that some regions paradoxically increase ventilation during bronchoconstriction (green-red regions).

Multi-slice SVI

Up to four, 15mm lung slices can be simultaneously imaged with SVI. Figure A-3 depicts four contiguous right lung slices, covering ~70% of the right lung, in a moderate asthmatic male subject who had been withdrawn from his asthma medications for 24 hours.

Discussion

Specific ventilation imaging (SVI) allows quantitative mapping of the spatial distribution of specific ventilation in the human lung. Alternatives to SVI exist but are limited in some manner: Multiple Breath Washout provides a measure of heterogeneity, but lacks spatial information (15). Alternative imaging methods expose patients to ionizing radiation (e.g. SPECT, PET, CT, gamma scintigraphy) or are not readily available nor translatable (hyperpolarized gas imaging using MRI). Specific Ventilation Imaging provides spatial information and can be performed using a standard clinical scanner and inhaled oxygen as the contrast source, and thus can be translated to nearly any clinical research setting. The fact that SVI does not require the use of radiation or contrast agents makes it well-suited for repeat or longitudinal studies that quantitatively evaluate regional responses to medication, therapy or interventions. This type of regional quantitative information on the impact of therapy may be especially useful in the context of inhaled drug delivery.

The disadvantages of SVI are that it has a relatively low signal-to-noise ratio (typically 4-7), it requires ~18minutes to acquire and that it is somewhat laborious for the subject and the data analyst. Subject training is essential for acquisition of reliable specific ventilation data. The subject is typically trained, using a recorded soundtrack of the scanner noises, prior to the imaging session, so that he or she can reach a reproducible volume (FRC) for each of the 220 breath hold images. Ideally, this is achieved while breathing at a normal, comfortable tidal volume without hyperventilating. Imprecise breath holds must be accounted for in post-processing by the data analyst, who must use image registration software to account for differences in lung volume (section 5.3 above).

Since the technique's original publication (19), SVI has undergone a modification to streamline its implementation. We have developed and 3D-printed a flow-bypass system (6), compatible with Hans Rudolph series 7400 masks, that is MR-compatible and enables near-instantaneous switching between delivery of room air and oxygen to the subject. This system significantly diminishes the complexity of the original setup, which resembled the gas-delivery setup previously described in a JoVE paper relating to perfusion imaging (2).

Limitations of the technique

As presented here, Specific Ventilation Imaging has 2 main limitations: 1) the four slices of (typically) the right lung that are acquired represent only ~70% of the right lung; and 2) SVI takes ~18 minutes to acquire, and thus the map of SV reflects each voxel's time-averaged specific ventilation over this interval. However, full lung coverage can be attained by repeating the procedure or by degrading spatial resolution, and scan time can be reduced at the expense of resolution (accuracy) in SV. The technique is, in general, versatile and different acquisition compromises are possible, each optimal for different applications. For example, in a study of dynamic recovery from an asthma event (24), we analyzed SVI data at a higher temporal resolution (~7min vs. ~18min) and the same spatial resolution, at the cost of a ~ 30% increase in uncertainty of SV (estimated from Monte Carlo simulations). A recent modeling study (14) sought to quantify the impact of several minor limitations of the SVI technique, namely 1) that the imaged volume does not encompass the entire right lung, 2) that small misalignments between successive images may exist even after registration, and 3) that pulmonary veins, by transporting blood from elsewhere in the lung into an imaged region, may add confounding signal that reflects ventilation in the region where that blood was originally oxygenated and not

in the region in which it is being imaged. The study (14) found that 1) in healthy subjects, a single-slice image (which encompasses only 8% of the total lung) estimates the vertical gradient of SV within 10% of its true value, 2) SVI analysis performed on images that are misaligned, on average, by 9% (a worst case scenario) result in a ~20% underestimation of mean specific ventilation, and 3) pulmonary venous signal leads to systematic overestimation of the specific ventilation by less than 10%.

Future applications

The ability to produce functional images of the human lung – as opposed to inferring function from anatomical changes - has the potential to contribute to early diagnosis and increase our understanding of the lung in health and disease. In particular, the ability to produce repeatable and quantitative regional maps of ventilation permits longitudinal studies of disease progression and allows quantification of the effect of interventions, such as inhaled asthma medications. By combining Specific Ventilation Imaging with a MRI technique to measure pulmonary perfusion (previously presented in this journal (2)), maps of the ventilation-perfusion ratio in health and disease can be generated (12). As mismatch between ventilation and perfusion is a major cause of hypoxia and hypercapnia, regional information on the ventilation perfusion ratio in health and disease can provide further insight into the impact of lung disease.

Acknowledgements

Supported by National Heart, Lung and Blood Institute (NHLBI) grants R01 HL-080203, R01 HL-081171, R01 HL-104118, R01-HL119263 and the National Space Biomedical Research Institute through National Aeronautics and Space Administration grant NCC 9-58. E.T. Geier was supported by NHLBI grant F30 HL127980.

Disclosures

The authors declare that they have no competing financial interests.

References

1. **Arai TJ**, **Horn FC**, **Hart KA**, **Rao MR**, **Collier GJ**, **Theilmann RJ**, **Sá RC**, **Prisk GK**, **Wild JM**. Comparison of Quantitative Specific Ventilation Imaging in the Lung: Oxygen Enhanced 1H and 3He Multibreath MRI. Annual Scientific Meeting of the British Chapter of ISMRM, Edinburgh, Scotland, . Edinburgh, Scotland.: 2014.

2. **Arai TJ**, **Prisk GK**, **Holverda S**, **Sá RC**, **Theilmann RJ**, **Henderson AC**, **Cronin MV**, **Cronin MV**, **Buxton RB**. Magnetic Resonance Imaging Quantification of Pulmonary Perfusion using Calibrated Arterial Spin Labeling. *JoVE (Journal of Visualized Experiments)* : e2712–e2712, 2011.

3. **Arai TJ**, **Sá RC**. Deformator: Projective transformation to register small scale Lung deformation [Online]. 1st ed. Github. hhtps://github.com/UCSDPulmonaryImaging/Deforminator.

4. **Arai TJ**, **Villongco CT**, **Villongco MT**, **Hopkins SR**, **Theilmann RJ**. Affine transformation registers small scale lung deformation. *Conf Proc IEEE Eng Med Biol Soc* 2012: 5298–5301, 2012.

5. **Chen Q**, **Jakob PM**, **Griswold MA**, **Levin DL**, **Hatabu H**, **Edelman RR**. Oxygen enhanced MR ventilation imaging of the lung. *MAGMA* 7: 153–161, 1998.

6. **Cook FR**, **Geier ET**, **Asadi AK**, **Sá RC**, **Prisk GK**. Rapid Prototyping of Inspired Gas Delivery System for Pulmonary MRI Research. *3D Printing and Additive Manufacturing* 2: 196–203, 2015.

7. **Fowler WS**. Lung Function Studies. III. Uneven Pulmonary Ventilation in Normal Subjects and in Patients with Pulmonary Disease. *J Appl Physiol* 2: 283–299, 1949.

8. **Geier ET**, **Neuhart I**, **Theilmann RJ**, **Prisk GK**, **Sá RC**. Spatial persistence of reduced specific ventilation following methacholine challenge in the healthy human lung. *J Appl Physiol* 124: 1222–1232, 2018.

9. **Hall ET**, **Sá RC**, **Holverda S**, **Arai TJ**, **Dubowitz DJ**, **Theilmann RJ**, **Prisk GK**, **Hopkins SR**. The effect of supine exercise on the distribution of regional pulmonary blood flow measured using proton MRI. *J Appl Physiol* 116: 451–461, 2014.

10. **Hamedani H**, **Kadlecek S**, **Xin Y**, **Siddiqui S**, **Gatens H**, **Naji J**, **Ishii M**, **Cereda M**, **Rossman M**, **Rizi R**. A hybrid multibreath wash-in wash-out lung function quantification scheme in human subjects using hyperpolarized 3 He MRI for simultaneous assessment of

specific ventilation, alveolar oxygen tension, oxygen uptake, and air trapping. *Magn Reson Med* 78: 611–624, 2017.

11. **Henderson AC**, **Sá RC**, **Barash IA**, **Holverda S**, **Buxton RB**, **Prisk GK**. Rapid intravenous infusion of 20mL/kg saline alters the distribution of perfusion in healthy supine humans. *Respir Physiol Neurobiol* 180: 331–341, 2012.

12. **Henderson AC**, **Sá RC**, **Theilmann RJ**, **Buxton RB**, **Buxton RB**, **Prisk GK**, **Hopkins SR**, **Hopkins SR**. The gravitational distribution of ventilation-perfusion ratio is more uniform in prone than supine posture in the normal human lung. *J Appl Physiol* 115: 313–324, 2013.

13. **Horn FC**, **Deppe MH**, **Marshall H**, **Parra-Robles J**, **Wild JM**. Quantification of regional fractional ventilation in human subjects by measurement of hyperpolarized 3He washout with 2D and 3D MRI. *J Appl Physiol* 116: 129–139, 2014.

14. **Kang W**, **Tawhai MH**, **Clark AR**, **Sá RC**, **Geier ET**, **Prisk GK**, **Burrowes KS**. In silico modeling of oxygen-enhanced MRI of specific ventilation. *Physiol Rep* 6: e13659, 2018.

15. **Lewis SM**, **Evans JW**, **Jalowayski AA**. Continuous Distributions of Specific Ventilation Recovered From Inert-Gas Washout. *J Appl Physiol* 44: 416–423, 1978.

16. **Musch G**, **Layfield JDH**, **Harris RS**, **Melo MFV**, **Winkler T**, **Callahan RJ**, **Fischman AJ**, **Venegas JG**. Topographical distribution of pulmonary perfusion and ventilation, assessed by PET in supine and prone humans. *J Appl Physiol* 93: 1841–1851, 2002.

17. **Robertson JS**, **Siri WE**, **Jones HB**. Lung ventilation patterns determined by analysis of nitrogen elimination rates; use of mass spectrometer as a continuous gas analyzer. *J Clin Invest* 29: 577–590, 1950.

18. **Sá RC**, **Asadi AK**, **Theilmann RJ**, **Hopkins SR**, **Prisk GK**, **Darquenne C**. Validating the distribution of specific ventilation in healthy humans measured using proton MR imaging. *J Appl Physiol* 116: 1048–1056, 2014.

19. **Sá RC**, **Cronin MV**, **Henderson AC**, **Holverda S**, **Theilmann RJ**, **Arai TJ**, **Dubowitz DJ**, **Buxton RB**, **Prisk GK**. Vertical distribution of specific ventilation in normal supine humans measured by oxygen-enhanced proton MRI. *J Appl Physiol* 109: 1950–1959, 2010.

20. **Tedjasaputra V**, **Sá RC**, **Arai TJ**, **Holverda S**, **Theilmann RJ**, **Chen WT**, **Wagner PD**, **Davis CK**, **Prisk GK**. The heterogeneity of regional specific ventilation is unchanged following heavy exercise in athletes. *J Appl Physiol* 115: 126–135, 2013.

21. **Theilmann RJ**, **Arai TJ**, **Samiee A**, **Dubowitz DJ**, **Hopkins SR**, **Buxton RB**, **Prisk GK**. Quantitative MRI measurement of lung density must account for the change in T(2) (*) with lung inflation. *J Magn Reson Imaging* 30: 527–534, 2009.

22. **Venegas JG**, **Schroeder T**, **Harris RS**, **Winkler RT**, **Melo MFV**. The distribution of ventilation during bronchoconstriction is patchy and bimodal: a PET imaging study. *Respir Physiol Neurobiol* 148: 57–64, 2005.

23. **Yang G**, **Stewart CV**, **Sofka M**, **Tsai C-L**. Registration of Challenging Image Pairs: Initialization, Estimation, and Decision. *IEEE Trans Pattern Anal Machine Intell* 29: 1973–1989, [no date].

24. **Zapol WM**, **Charles HC**, **Martin AR**, **Sá RC**, **Yu B**, **Ichinose F**, **MacIntyre N**, **Mammarappallil J**, **Moon R**, **Chen JZ**, **Geier ET**, **Darquenne C**, **Prisk GK**, **Katz I**. Pulmonary Delivery of Therapeutic and Diagnostic Gases. *J Aerosol Med Pulm Drug Deliv* 31: 78–87, 2018.

Figures

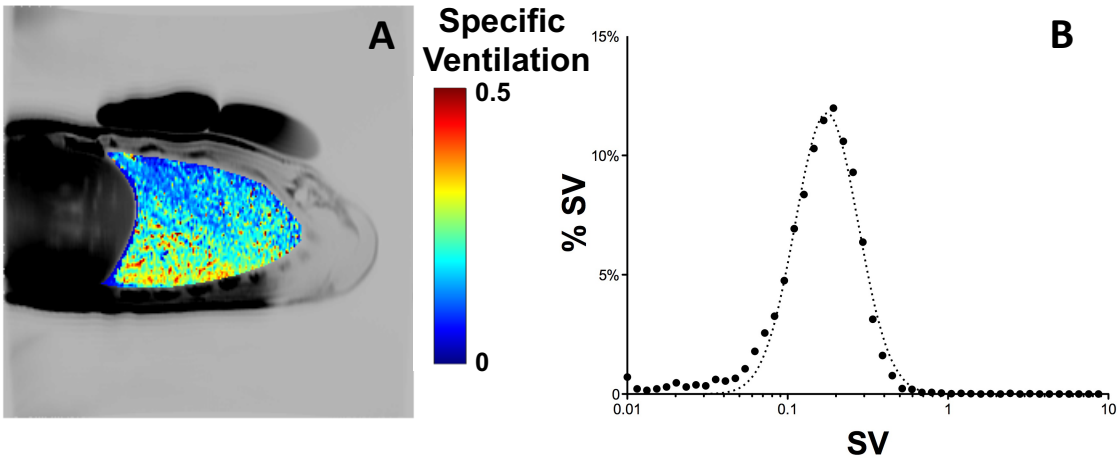

Figure A-1 – A) Typical map of specific ventilation (color), overlaid onto an anatomical MRI image of the same supine subject (gray scale). Specific ventilation ranges from very low values (blue) to SV=0.5 (red). The subject, a 39-year-old healthy volunteer, was imaged in the supine posture. Note the vertical gradient in specific ventilation. In this image, two phantoms of known MR characteristic, used for calibration of absolute density were placed in the anterior chest wall. These phantoms are not required for SVI quantification. B) Histogram of the distribution of specific ventilation (filled circles) compiled from the SV map. The width of the distribution represents the heterogeneity of specific ventilation in the lung slice studied. In this example, the distribution is unimodal and the width of the log Gaussian fitted distribution (dotted line) was 0.41, within the typical healthy range.

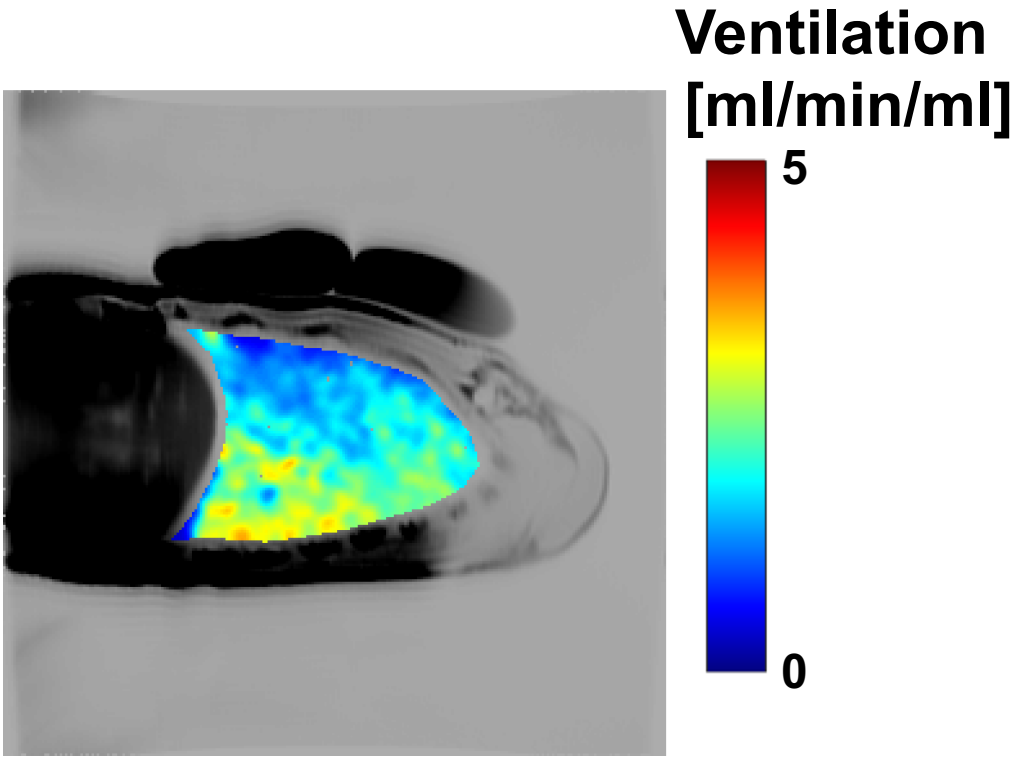

Figure A-2 –Ventilation map (ml/min) for the same subject and lung slice as Figure A-1. Ventilation maps are generated, as described in detail in section 6, using an SV map together with a map of lung proton density in the same slice. In this example, both the SV and density maps were smoothed using a log Gaussian kernel with a full width at half maximum of 5 voxels, resulting in a spatial scale of XX cm in plane.

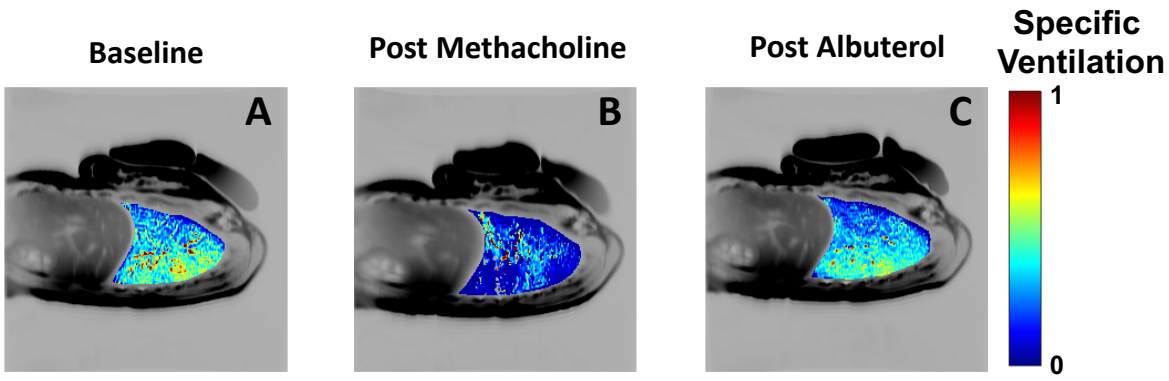

Figure A-3 – Specific ventilation measured in a mild asthmatic subject (female, age 23) at baseline (Panel A), following inhalation of methacholine (Panel B) and following inhalation of albuterol (Panel C). Note the significant changes in the distribution of specific ventilation following the induction of an asthma-like event using methacholine (Panel B), with large regions of the dependent lung showing little to no specific ventilation. Also note the subsequent return to baseline condition following bronchodilator administration (Panel C). As in Figure A-1, the specific ventilation maps have been overlaid into an anatomical MRI.

Lateral Medial

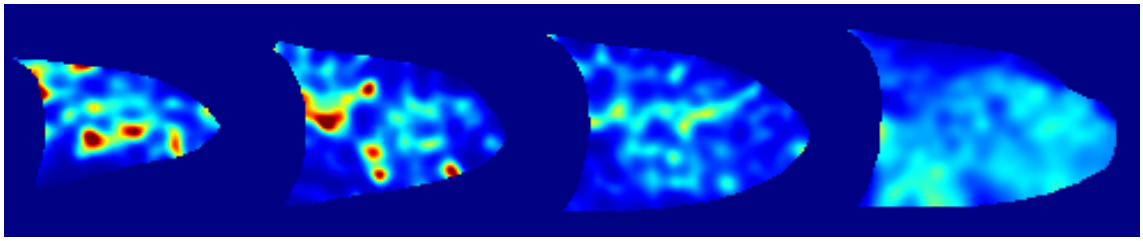

Figure A-4 – Specific ventilation map of 4 contiguous right lung slices, acquired in a 26-year-old male moderate asthmatic after 24-hour withdrawal of daily asthma medications. The 4 slices shown cover ~70% of the right lung,

Appendix A, in full, is a part of *Specific Ventilation Imaging: using oxygen-enhanced proton MRI to quantify specific ventilation in the human lung*, Geier ET, Theilmann RJ, Darquenne C, Prisk GK, Sá RC. This work, we anticipate, will be submitted to the Journal of Visualized Experiments in late 2018. The dissertation author was the author of this paper.

APPENDIX B

Rapid Prototyping of Inspired Gas Delivery System for Pulmonary MRI Research

3D PRINTING AND ADDITIVE MANUFACTURING
Volume 2, Number 4, 2015

DOI: 10.1089/3dp.2015.0027

ORIGINAL ARTICLE

Rapid Prototyping of Inspired Gas Delivery System for Pulmonary MRI Research

Fredrick Roscoe Cook,[1] Eric T. Geier,[1] Amran K. Asadi,[2] Rui Carlos Sá,[1] and G. Kim Prisk[1,2]

Abstract

Specific ventilation imaging (SVI) is a noninvasive magnetic resonance imaging (MRI)-based method for determining the regional distribution of inspired air in the lungs, useful for the assessment of pulmonary function in medical research. This technique works by monitoring the rate of magnetic resonance signal change in response to a series of imposed step changes in inspired oxygen concentration. The current SVI technique requires a complex system of tubes, valves, and electronics that are used to supply and rapidly switch inspired gases while subjects are imaged, which makes the technique difficult to translate into the clinical setting. This report discusses the design and implementation of custom three-dimensional (3D) printed hardware that greatly simplifies SVI measurement of lung function. Several hardware prototypes were modeled using computer-aided design software and printed for evaluation. After finalization of the design, the new delivery system was evaluated based on O_2 and N_2 concentration step responses and validated against the current SVI protocol. The design performed rapid switching of supplied gas within 250 ms and consistently supplied the desired concentration of O_2 during operation. It features a reduction in the number of commercial hardware components, from five to one, and a reduction in the number of gas lines between the operator's room and the scanner room, from four to one, as well as a substantially reduced preparation time from 25 to 5 min. 3D printing is well suited to the design of inexpensive custom MRI compatible hardware, making it particularly useful in imaging-based research.

Introduction

Specific ventilation (SV) is a dimensionless quantity that measures how efficiently a lung region is ventilated.[1] The Pulmonary Imaging Laboratory at UCSD pioneered specific ventilation imaging (SVI), a technique that measures this metric spatially in the human lung using proton magnetic resonance imaging (MRI).[2] This method quantifies SV by measuring the rate of change in the MRI signal of lung regions after the subject has undergone a step change in the fraction of inspired oxygen (FIO_2). During the imaging sequence, research subjects are supplied air (21% O_2) and 100% O_2 in alternating cycles of 20 breaths while images of their lung are acquired after each expiration. The original method for supplying the inspired gas involved a complicated plumbing system consisting of a facemask, gas reservoir bag, nonrebreathing T-shaped three-way valve, large-bore tubes, and a pneumatically operated remote-controlled valve to achieve rapid switching between gases.

Numerous safety and space restrictions governed the design and operation of this system. The hardware inside the MRI room is subject to multiple safety precautions to prevent injury to the subject. The MRI uses a powerful magnetic field, which is active at all times and attracts ferrous materials toward the bore of the scanner with considerable force. Additionally, there are space restrictions for hardware that is worn or in contact with the subject, such as facemasks and nonrebreathing valves, due to the narrow space available inside the scanner bore. To ensure safety in the MRI environment, hardware placed in the scanner room must be constructed of plastics and nonferrous metals. Components worn by the subject must be able to fit inside the scanner bore without interference.

In this report, we discuss the design of an improved method of delivering and rapidly switching inspired gases in the magnetic resonance (MR) environment. Using three-dimensional (3D) printing-assisted rapid prototyping, we developed custom hardware that performs gas delivery and rapid switching without the use of expensive commercial hardware or electronics. 3D printing enabled inexpensive and speedy design iteration compared with traditional machining or purchase and assembly of commercially available products and provided the

Departments of [1]Medicine and [2]Radiology, University of California, San Diego, La Jolla, California.

advantage of fabricating custom-designed hardware with MR safe materials. This resulted in a final design that is a simpler and more robust gas delivery method than the original plumbing system.

Materials and Methods

Original plumbing system

A diagram of the components of the original plumbing and improved systems for supplying inspired gas is displayed in Figure 1. A number of components are placed inside the operator's room due to MR compatibility restrictions. These include a compressed oxygen tank, compressed air tank, a flow meter (model 4830; Hans Rudolph, Inc., Shawnee, KS), and a pneumatic valve controller (model 4285; Hans Rudolph, Inc.). The components inside the MR scanner room include a gas reservoir bag (model 6170; Hans Rudolph, Inc.), a pneumatic switching valve (model 8500; Hans Rudolph, Inc.) placed outside the scanner bore, and finally a nonrebreathing T-shaped three-way valve (model 2600; Hans Rudolph, Inc.) connected to the facemask worn by the subject. The pneumatic switching valve has two inlets, one

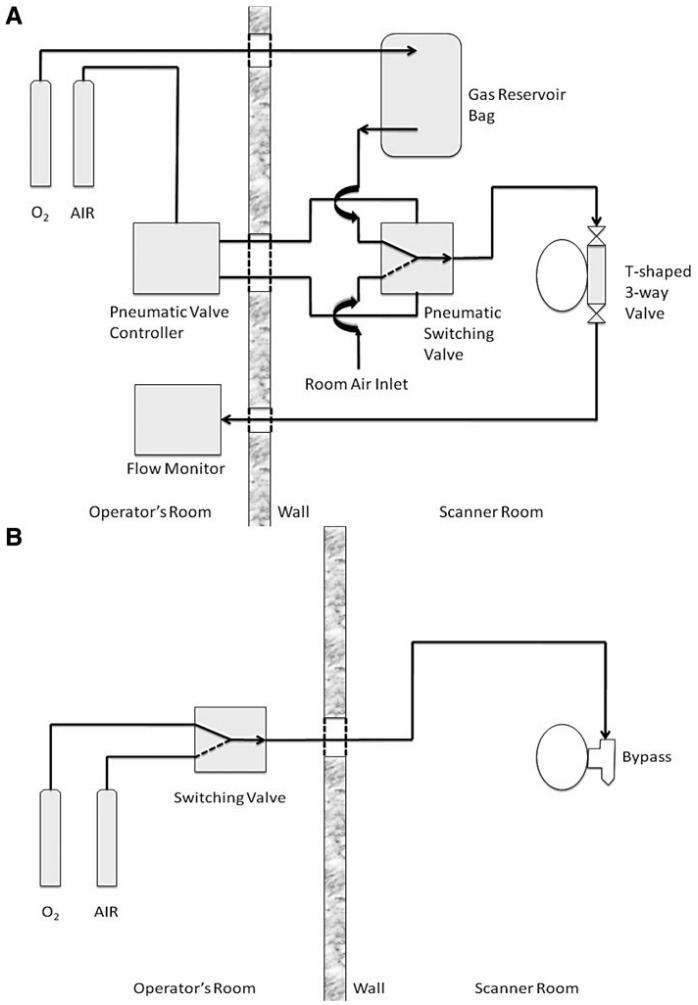

FIG. 1. **(A)** Diagram of original plumbing system components, including inspiratory and expiratory tubing, remotely operated switching valve, and T-shaped three-way valve. At least four lines of large-bore and small-bore tubing are passed through the wall of the MR scanner room. **(B)** Diagram of the improved system, which has reduced the components to one valve and one pass through line. MR, magnetic resonance.

connecting the valve to the gas reservoir bag and the other open to room air. The outlet of this valve connects to the inlet of the facemask valve through a large-bore tube. The connection lines between the operator's room and scanner room components include a 1/4 inch tube connecting the oxygen tank to the gas reservoir bag, two 1/4 inch tubes connecting the pneumatic switching valve to its operating module, and a large-bore tube from the expiratory side of the facemask valve to the flow monitor, making the gas lines a closed circuit. These connections are fed through a small porthole in the wall of the scanner room called a pass through.

During operation, the subject inspires the supplied gas at room pressure, either through a gas reservoir bag prefilled with oxygen or through a low-resistance large-bore tube open to the air in the scanner room. The pneumatic valve controller used supplied tank air to actuate the switching valve between the inlets to these two reservoirs. A flow monitor is placed at the outlet of the system to record the subject's tidal volume, or volume of expired gas, used later during the computation of SV to correct for an inherent plumbing delay imposed by the scanner's physical constraints. The limited space in the scanner bore is also the reason why the flow monitor is placed in the expiratory line. The new replacement method of gas delivery was designed to reduce complexity while performing similar function with the original plumbing system.

Design and construction of prototype

The new design utilizes bypass flow to supply a stream of gas for subjects to breathe from during operation. To our knowledge, there are no commercial components readily available that perform this specific function and are MR compatible. Figure 2 displays a schematic drawing of the featured bypass flow attachment, which inserts into a standard facemask. The outlet of the bypass flow attachment remains open to the atmosphere at all times regardless of whether it is connected to a source or supplied by flowing gas. This new fail-safe is an important advantage over the previous plumbing system that ensures that the subjects are not in danger of having their breathing occluded in the event of a failure in the gas supply.

The bypass flow attachment was modeled on SolidWorks (Dassault Systèmes S.A., Velizy, France) computer-aided design software and printed on a Makerbot Replicator 2 (Makerbot Industries, Brooklyn, NY) 3D printer in polylactic acid (PLA). The model was sliced and prepared in G-code through the MakerWare software available with the printer. The settings used for printing were 0.2 mm layer height, 15% internal fill, and a wall thickness of two shells (0.8 mm). The total material used is 45 g PLA and printing time is 3 h and 11 min.

The design has two modes of operation using one or two supplied gases. In the one-gas configuration, only 100% O_2 is

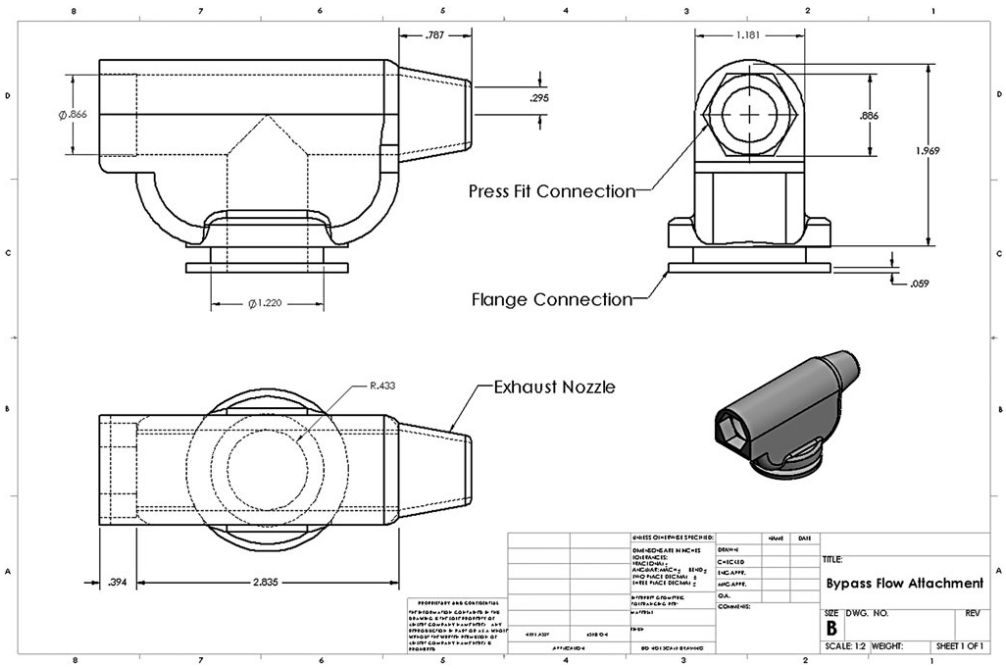

FIG. 2. A schematic of the bypass flow attachment with dimensions called out in inches. It outlines a press fit connection for the inspiratory line, a flange connection for the facemask, and exhaust nozzle open to the atmosphere.

supplied during operation, with the subject breathing room air when O_2 is not flowing. In the two-gas configuration, both O_2 and another gas mixture are connected to the switching valve such that the subject is supplied either inspired gas at all times during scanning. This also makes it possible to use in studies involving other inspired gas mixtures, such as hypoxic and hyperoxic gas (e.g., 12.5% and 30% O_2, respectively).

Polycarbonate 1/4 inch diameter tubing connects each tank to the inlets of the switching valve, which is clamped onto the edge of the operator's desk. The tubing connecting the switching valve outlet to the prototype was assembled from 30 ft of 1/4 inch, 6 ft of 3/8 inch, and 3 ft of 1/2 inch diameter tubing connected with brass tube fittings. This provided adequate length to reach the subject from the console room and reduced noise due to gas flow. A converging nozzle is attached to the exhaust outlet of the bypass flow attachment to reduce noise and increase outlet flow to prevent inspiration of outside gases. The combination of expanding tube diameter and nozzle reduced noise due to gas flow from 123 to 98 dB, a level at which the subjects could still hear verbal instructions from the operator during scanning.

Figure 3 displays the featured hardware of the improved gas delivery system. A length of tubing connects the bypass flow attachment to the outlet of a Swagelok (Swagelok, Solon, OH) three-way switching valve in the console room. The inlets of this switching valve are then connected to up to two compressed gas tanks.

After each use, the 3D printed hardware was submerged in Cidex (Advanced Sterilization Products, Irvine, CA) cleaning solution for 20 min for sterilization, rinsed with soap and water, then soaked in clean water overnight. While there is no direct contact between the part and the subject during operation, parts such as this are routinely sterilized either by high-level liquid disinfectant or gas sterilization. It was previously shown that PLA components can be cleaned with common disinfectants, although not by autoclaving as the PLA will become soft at temperatures of 60°C or higher.[3] While no damage to the component surfaces or leaking was observed, the wall thickness and internal fill may be adjusted in subsequent prints to increase strength.

Evaluation of step function

The functional requirement of the design can be described as providing a step function with fast rise time and low steady-state error. For the experiment to be performed properly, the switch between inspired O_2 levels must occur rapidly such that the FIO_2 presents a step change to the subject. The rise time is considered to be the time taken for the oxygen concentration to change from 0% to 90% of its final value (from 21% to 92% O_2, respectively).

The previous plumbing system switched inspired gases with a significant delay due to the large volume (600 mL) of the inspiratory line between the switching valve and the facemask. After switching, subsequent inspirations were of a mixture of gases until the line was cleared of the previous gas and filled with the new supplied gas. This hardware arrangement created a delay in the switching of FIO_2 in the subject that had to be corrected for computationally after scanning. By supplying a bypass flow through small-bore tubing across the subject's airway, the inspired gas can be switched rapidly between breaths and the subject will experience a step change in FIO_2 with fast rise time at the next inspiration.

The desired behavior of the design is to supply the subject with a steady state of the desired O_2 concentration during operation. If the subject's inspiratory flow exceeds the bypass flow, outside gases will be inspired and create a steady-state error in O_2 concentration. This leads to unreliable signal acquisition in the resulting images. A bypass flow was chosen to exceed the peak inspiratory flow of the subject to prevent inspiration of outside gases.

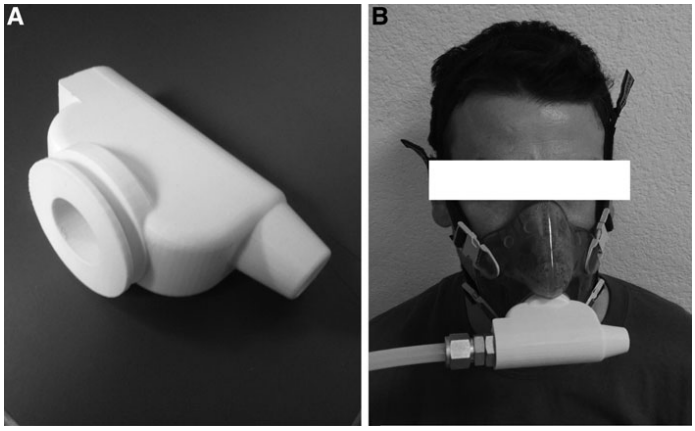

FIG. 3. **(A)** The bypass flow attachment printed in PLA. **(B)** The facemask and bypass flow attachment worn by a subject. The supplied gas flows across the facemask for the subject to breathe from and exhausts into the environment. PLA, polylactic acid.

Reinspiration and dead space

Instrumental dead space refers to a volume enclosed in hardware where expired gases may be reinspired. A high volume of dead space can lead to undesired gas mixing that contributes to signal delay and steady-state error. The internal volume of the bypass flow attachment was kept small enough to prevent reinspiration, but still allow subjects to breathe comfortably. During operation, the bypass flow partially fills the internal volume of the attachment with the supplied gas, further reducing instrumental dead space.

Multiple breath washout testing

The multiple breath inert gas washout is used to analyze pulmonary function. During the nitrogen multiple breath washout, the subject breathes air initially, then the inspired gas switches to 100% oxygen (0% nitrogen).[1] Flow and the expired gas concentrations of N_2 and O_2 are recorded for a certain number of breaths, typically until the concentration of N_2 falls below 2%. The expired N_2 concentration decreases, while the expired O_2 concentration rises as the residual N_2 in the lungs is diluted in each successive breath.

To evaluate the functionality of the design, multiple breath washouts were performed according to the procedure described in Singer *et al.*[4] using the improved gas delivery system to observe the step response of the inspired gas switching. A successful washout of N_2 indicates stability of the supplied O_2 concentration, and rise time was observed visually after switching the inspired gas between breaths.

Subjects performed the washout while seated with the flow meter positioned between the facemask and bypass flow attachment. A sampling line for a medical gas analyzer (Perkin-Elmer, Waltham, MA) was placed at the mouth of the facemask. The washout was completed when the expiratory N_2 concentration was at 2% or lower for multiple breaths, at which time the inspired gas switched back to air. The gas concentration signals were recorded using data acquisition tools in LabVIEW (National Instruments, Austin, TX) at a sampling rate of 500 Hz. The data were then processed in Matlab (Mathworks, Natick, MA).

Specific ventilation imaging

Functionally, the SVI procedure is comparable with performing a series of multiple breath washouts done in succession where N_2 is alternately washed out and washed in, depending on the supplied gas. After achieving the desired performance, the improved gas delivery system was integrated into the SVI protocol and tested. Images were acquired for each breath and analyzed in MATLAB (Mathworks) using the methods described in Sá *et al.*[2] The resulting map of SV values was then compared with an SV map for the same subject using the original plumbing system. Statistical analyses were performed using Prism (GraphPad, San Diego, CA).

Results

A bypass flow of 2.0 L/s was used to exceed subjects' peak inspiratory flow during the SVI procedure. At this rate, the supplied gas will physically clear the inspiratory line of the previous gas in 100 ms after switching, a significant improvement over the original plumbing system.

The bypass flow attachment has an instrumental dead space of 41 mL in addition to the standard facemask (73–113 mL depending on size). At this low volume, the effects of reinspiration of gases were negligible.

Figure 4 displays the flow and gas concentrations recorded during the nitrogen multiple breath washout. The rise time, the time taken for the inspired O_2 concentration to reach at least 92%, was 150 ms (Fig. 4A). The figure also shows stability in the supplied gas concentration as the inspired O_2 remains at $\sim$100% during operation. The curve of expired O_2 and N_2 concentrations follows the expected quasiexponential behavior for multiple breath washouts as the O_2 concentration rises, while N_2 is gradually diluted out of the lung (Fig. 4B).

Figure 5 displays SV maps for the same subject obtained using the original plumbing system (Fig. 5A) and the improved gas delivery system (Fig. 5B). Figure 5C presents a histogram of the SV distribution of the original map and two separate maps using the improved system obtained 7 days apart. The average values for the SVI distribution, assuming a

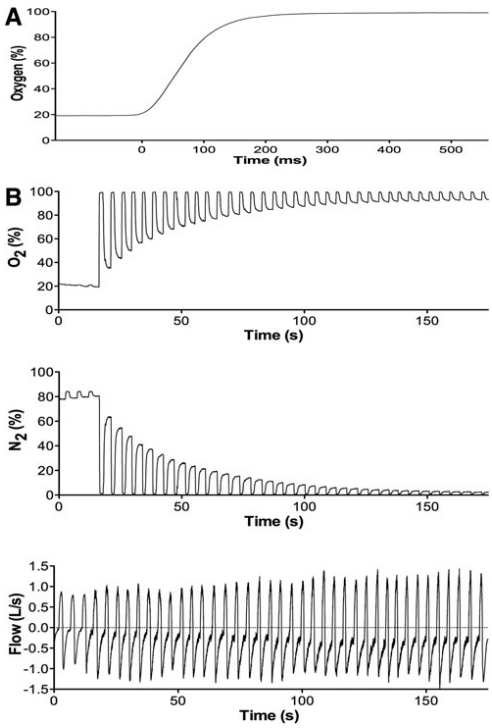

FIG. 4. **(A)** The switch in supplied O_2 occurs with a 150-ms rise time (rise time measured as time to 92% oxygen). The delay associated with clearing the supply line ($\sim$100 ms) is not included in this plot. **(B)** Gas concentrations of O_2 (*top*) and N_2 (*middle*), as well as flow (*bottom*), during nitrogen multiple breath washout of a healthy seated subject. The response in expired O_2 and N_2 to 100% supplied inspired O_2 presents a quasiexponential curve as O_2 is saturated and N_2 is diluted.

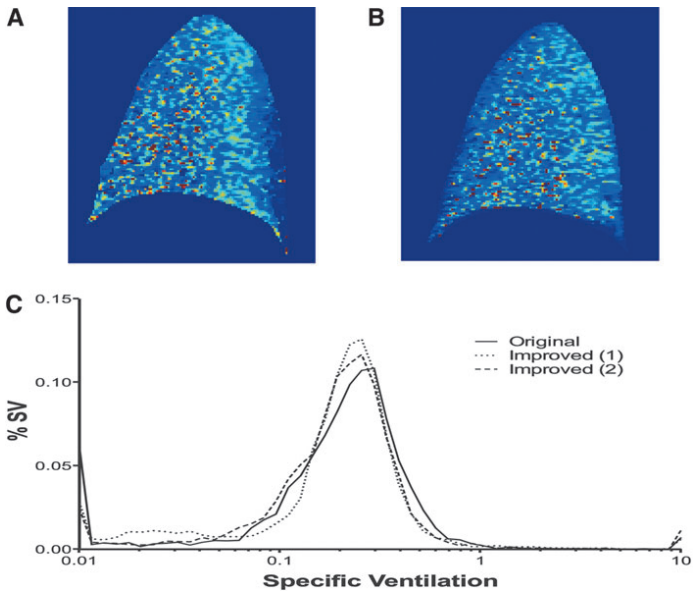

FIG. 5. Regional SV maps calculated using images acquired using **(A)** the original plumbing system and **(B)** the improved gas delivery method. **(C)** A histogram of SV distribution of an SV map produced using the previous plumbing system and two maps produced using the improved system. SV, specific ventilation. Color images available online at www.liebertpub.com/3dp

log (Gaussian), were as follows: original map, amplitude 0.10, center 0.24, and width 0.48; the average ± standard deviation values of the two improved gas delivery maps were amplitude 0.12 ± 0.01, center 0.23 ± 0.01, and width 0.41 ± 0.06. In a previous SVI validation study, the 95% confidence interval difference between repeated SVI measurements of heterogeneity (width) using the original plumbing system was found to be –0.127 and 0.141 (repeated measures in 13 subjects, confidence interval estimated using Student's *t*-distribution, df = 12).[5] When comparing the original plumbing system with the new gas delivery system, the individual differences in width were –0.113 and 0.034, falling within this range.

Discussion

The design was shown to deliver and rapidly switch inspired gases with fast rise time and reliable supplied O_2 concentration stability. It was successfully used in multiple breath washout and SV procedures. The average preparation time for an experiment was shortened from 25 to 5 min using the improved gas delivery system.

In the original plumbing system, due to the limited space within the MR scanner bore, the remotely operated valve was placed outside the bore away from the subject's mask and T-shaped three-way valve and connected through a large-bore tube. This introduced a delay in the abrupt switch of inspired gas concentrations as the volume of the inspiratory line had to be cleared of the previous supplied gas through subsequent breaths. This delay had to be corrected for by measuring the tidal volume, or volume of expired gas, of each of the subject's breaths to calculate when the supplied gases had completely switched. To measure tidal volume, large-bore tubing attached the outlet of the T-shaped valve to a flow meter placed in the console room, which also made the plumbing system a closed circuit and could possibly occlude breathing in the event of operational error. The signal delay had to be calculated for each individual subject and added complexity, time, and effort to the computation of SV.

The improved method eliminated this delay by placing the manually operated switching valve in the console room and connecting the small-bore inspiratory line directly to the bypass flow attachment on the subject's facemask, while leaving the outlet open to the environment. The constant bypass flow clears the inspiratory line of the previous gas such that the subject experiences a true step change in O_2 concentrations with a combined plumbing delay and rise time of 250 ms. This rapid switching reduced the inspired gas signal delay to negligible values and eliminated the need for tidal volume measurement and exhaust tubing, which allowed for an open circuit operation that ensures that the subject's breathing is in no danger of being occluded due to hardware failure or human error. These improvements not only reduced the hardware components and computational complexity for SV but also reduced the potential for experimental error.

The center and amplitude of the SV distributions obtained with the novel and the original plumbing (shown in Fig. 5) were of negligible average difference. The widths of distributions for the original and improved systems were shown to have individual difference values within the 95% confidence

interval for repeated measures obtained using the original plumbing system.[5] Therefore, we can conclude that the results obtained using the new gas delivery system are not significantly different from results obtained using the previous method. The improved system was shown to be similarly reliable in obtaining data for SV distribution maps.

The compatibility of PLA components to the MRI environment, as well as the advantages of 3D printing components over traditional fabrication methods, was previously discussed in Herrmann *et al.*[3] By comparison, to have the bypass flow attachment machined out of polyetheretherketone (PEEK), a medical grade plastic with high dimensional stability and chemical resistance, would cost an estimated $890 and take up to 2 weeks to deliver. With a locally available 3D printer, the design can be delivered overnight at a material cost of $2 based on a price of $45/kg of PLA filament.

The supplied flow used during operation is dependent on the subject's inspiratory flow. For example, while 2.0 L/s is used for adult subjects, pediatric subjects require less flow to supply 100% inspired gas. Pediatric subjects would also benefit from reduced dead space. For this case, the design may be printed in smaller, patient-tailored versions to accommodate the size or age of the subject. This adds to the versatility of the design when fabricated through 3D printing.

The inspired gas delivery system can be implemented in any research study involving rapid switching of inspired gasses while in the MRI. It is MR safe, being constructed from PLA and nonferrous metals, and is manually operated without pneumatic remote control valves or other electronic equipment. The new gas delivery system improves safety by allowing normal breathing with and without supplied gas flow, and also adds the ability to perform SVI and multiple breath washout procedures simultaneously in the MR scanner.

Conclusion

This report presented a replacement method of delivering inspired gas to research subjects in the MRI environment. The technology of 3D printing introduces many advantages for designing custom MR-compatible hardware cheaply and quickly, allowing the improved gas delivery system to overcome safety and space restrictions that hampered the previous method. The commercial availability of 3D printers makes this method readily available to be cheaply fabricated for any laboratory or clinic attempting to perform SVI or other MRI-based physiologic studies. The design can also be easily modified, using computer-aided design software, to fit different equipment, making the technique of 3D printing an advantageous alternative to fabrication by machining or purchase of commercial hardware.

Acknowledgments

This work benefited from the technical contributions of Janelle Fine for MBW hardware. This work was supported by the National Institutes of Health through National Heart, Lung, and Blood Institute Grants R01-HL104118, R01-HL119263, and F30-HL-110755.

Author Disclosure Statement

No competing financial interests exist.

References

1. Lewis SM, Evans JW, Jalowayski AA. Continuous distributions of specific ventilation recovered from inert gas washout. J Appl Physiol Respir Environ Exerc Physiol 1978; 44:416–423.
2. Sá RC, Cronin MV, Henderson AC, *et al*. Vertical distribution of specific ventilation in normal supine humans measured by oxygen-enhanced proton MRI. J Appl Physiol 2010;109: 1950–1959.
3. Herrmann K, Gärtner C, Güllmar D, *et al*. 3D printing of MRI compatible components: why every MRI research group should have a low-budget 3D printer. Med Eng Phys 2014; 36:1373–1380.
4. Singer F, Houltz B, Latzin P, *et al*. A realistic validation study of a new nitrogen multiple-breath washout system. PLoS One 2012;7:e36083.
5. Sá RC, Asadi AK, Theilmann RJ, *et al*. Validating the distribution of specific ventilation in healthy humans measured using proton MR imaging. J Appl Physiol 2014;116:1048–1056.

Address correspondence to:
G. Kim Prisk
Department of Medicine
University of California, San Diego
9500 Gilman Drive
La Jolla, CA 92093-0852

E-mail: kprisk@ucsd.edu

Appendix B, in full, is a part of *Rapid Prototyping of Inspired Gas Delivery System for Pulmonary MRI Research*, Cook FR, Geier ET, Asadi AK, Sá RC, Prisk GK. This article appeared in 3D Printing and Additive Manufacturing. vol 2(4), 2015. The dissertation author was the second author of this paper.